Experimental and Modeling Studies on Developing A Condensing-Frosting Performance Map for A Variable Speed Air Source Heat Pump Unit for Frosting Suppression

LIU Shengnan

PhD

The Hong Kong Polytechnic University

2023

The Hong Kong Polytechnic University

Department of Building Environment and Energy Engineering

Experimental and modeling studies on developing a condensing-frosting performance map for a variable speed air source heat pump unit for frosting suppression

LIU Shengnan

A thesis submitted in partial fulfillment of the requirements for the Degree of Doctor of Philosophy

December 2022

Certificate of Originality

I hereby declare that this thesis is my own work and that, to the best of my knowledge and belief, it reproduces no material previously published or written, nor material that has been accepted for the award of any other degree or diploma, except where due acknowledgement has been made in the text.

_____(Signed)

____LIU Shengnan____(Name of student)

Abstract

Air source heat pumps (ASHPs) can be used to help effectively achieve carbon emission reduction and alleviate the global energy crisis, and have been hence widely used in many parts of the world. However, for a space heating AHSP unit, frost may form on its outdoor coil surface at certain operating and ambient conditions. The accumulation of frost would adversely affect the normal operation of the ASHP unit, and regular defrosting was therefore required, leading to a low operating efficiency and poor indoor thermal comfort. Therefore, effective frosting suppression was crucial to the further wider applications of ASHPs. However, existing frosting suppression measures may not be applicable in practice due to their various inadequacies.

In addition, variable speed (VS) technology has been increasingly used in air conditioning (A/C) systems and ASHPs. Previous studies on the operating characteristics of a VS direct expansion (DX) A/C system and the development of its operating performance maps were reported. The study results suggested that simultaneously changing compressor speed and air fan speed of the VS DX A/C system could cause the changes in its evaporating temperature. Therefore, for a VS ASHP unit, likewise, changing both speeds of its compressor and outdoor air fan can also cause the changes in its evaporating temperature, thus changing its outdoor coil surface temperature that affects frosting performances directly. However, this would also impact the heating performances of the VS ASHP unit. At present, there have been no systematic studies on the effects of changing both speeds of compressor and outdoor air fan of a VS ASHP unit on its frosting and heating performances, so as to provide essential guidelines for the design, operation and control of VS ASHPs.

Therefore, in this Thesis, a study on developing, experimentally and by modeling, condensing-frosting performance maps for an experimental VS ASHP unit to comprehensively evaluate its frosting suppression and heating performances under different speed combinations of the compressor and outdoor air fan is presented. A novel control strategy that can be used to achieve effective frosting suppression while meeting the heating requirements, based on the developed performance maps, is also presented in the Thesis.

Firstly, an experimental setup is detailed. It included an experimental VS ASHP unit and an environmental chamber. The experimental VS ASHP unit was placed inside the environmental chamber, where there were a simulated indoor heated space and a simulated outdoor space. The experimental setup could provide different test conditions required for the intended experimental study. All operating parameters of the experimental VS ASHP unit and the environmental chamber could be real time monitored and recorded using high-precision measuring devices. With the availability of the experimental setup, the operating characteristics of the experimental VS ASHP unit could be experimentally studied, an established mathematical model for the experimental VS ASHP unit experimentally validated, and finally the developed novel control strategy for the experimental VS ASHP unit tested.

Secondly, an experimental study on the detailed relationships between frosting suppression performances and the total output heating capacities of the experimental VS ASHP unit under different speed combinations of its compressor and outdoor air fan is reported. The condensing-frosting performance maps obtained in the experimental study demonstrated that for the experimental VS ASHP unit, changing

the speeds of its compressor and outdoor air fan would result in not only different outdoor coil surface temperatures, but also different total output heating capacities. A higher outdoor coil surface temperature and thus a better frosting suppression performance may be achieved, but usually at the expenses of losing some of its total output heating capacity. Furthermore, the experimental results also suggested that when the experimental ASHP unit was operated at different speed combinations that can lead to the same or similar total output heating capacities, its operating characteristics in terms of outdoor coil surface states can be significantly different. The obtained condensing-frosting performance maps may be used as an essential guidance for the design, operation and control of ASHPs for frosting suppression operation.

Thirdly, a modeling study on developing a mathematical model for the experimental VS ASHP unit is presented. The model was developed by referring to previously published mathematical models for VS A/C systems and experimentally validated using the experimental data obtained in the experimental study. The average relative errors between the measured and predicted total output heating capacity and COP were at less than 4.0 %, and the average error between the measured and predicted outdoor coil surface temperature at 0.2 °C. A follow-up modeling study was then carried out using the validated model to obtain condensing-frosting performance maps for the experimental VS ASHP unit having different outdoor coil surface areas and at different outdoor operating conditions. The modeling study results suggested that by increasing outdoor coil surface area of the experimental VS ASHP unit from 50 % to 150 %, its surface temperature on average was increased by more than 1.37 °C, which was inducive to a better frost suppression performance, and the total output heating

capacity by more than 11.07 %, but at a higher initial manufacturing cost. Besides, at a fixed outdoor relative humidity, the maximum output heating capacity of the experimental VS ASHP unit under frost-free operation was significantly increased as the outdoor air temperature was increased. Furthermore, at a fixed outdoor air temperature, as the outdoor air relative humidity was decreased, the outdoor coil surface temperatures and total output heating capacities were slightly reduced, but the frost-free region on the condensing-frosting performance map was enlarged, mainly due to the change in outdoor air dew point temperature. The modeling study results also suggested that the developed model can be a useful tool in studying the characteristics of VS ASHPs during both frosting and frost-free operations.

Finally, the Thesis reports the development of a novel control strategy based on the obtained condensing-frosting performance maps for the experimental VS ASHP unit to achieve effective frosting suppression during operation. The developed novel control strategy was experimentally tested using the experimental VS ASHP unit. The test results suggested that the experimental VS ASHP unit under the developed novel control strategy could not only achieve effective frosting suppression, but also output the required heating capacity at high COP values whenever possible. By using the developed novel control strategy, the heating duration in one frosting-defrosting operation cycle could be increased by up to 157.68 %, and the daily defrosting frequency, duration and energy consumption reduced by up to 59.09 %, 36.30 % and 32.96 %, respectively. The proposed novel control strategy was straightforward and simple to implement, and could contribute to the further developments of frosting suppression technology for ASHPs.

Publications Arising from the Thesis

Journal Papers

- **Liu Shengnan**, Bai Xiaoxia, Zhang Long, Lin Yao, Deng Shiming, Wang Wei, Wei Minchen. Developing condensing-frosting performance maps for a variable speed air source heat pump (ASHP) for frosting suppression. Applied Thermal Engineering, 2022, 211: 118397. (Based on Chapter 5)

- **Liu Shengnan**, Bai Xiaoxia, Deng Shiming, Zhang Long, Wei Minchen. A modeling study on developing the condensing-frosting performance maps for a variable speed air source heat pump. Journal of Building Engineering, 2022, 58: 104990. (Based on Chapter 6)

- **Liu Shengnan**, Bai Xiaoxia, Deng Shiming, Zhang Long, Wei Minchen. Developing a novel control strategy for frosting suppression based on condensing-frosting performance maps for variable speed air source heat pumps. Energy and Buildings, 2023, 113049. (Based on Chapter 7)

Acknowledgements

First of all, I would like to give my sincere gratitude to my Chief Supervisor, Prof. Wei Minchen, and my Co-Supervisor, Dr. You Ruoyu, both from the Department of Building Environment and Energy Engineering, The Hong Kong Polytechnic University, for their continuous helps and valuable advice. Their enthusiasm and dedication to research always inspire me, and they are also my role models in my study and work.

Secondly, my special thanks must go to Prof. Deng Shiming, from Qatar University, for providing me with the precious opportunity to pursue my Ph.D. study and bringing me to HVAC research. His patient guidance and valuable suggestions greatly encouraged me throughout the course of my study. His rigorous work attitude, immense knowledge and plentiful experience are admirable. I would also like to express my gratitude to Dr. Zhang Long, from Beijing Institute of Technology, for generously sharing his professional knowledge and experience with me, which was of great help to my research.

Thirdly, I would like to thank my colleagues in Hong Kong, Dr. Yan Huaxia, Dr. Fang Guanyu, Dr. Yang Liu, Dr. Fang Yibo and Mr. Bai Xiaoxia for their supports to my Ph.D. study. I also wish to thank my friends, Ms. Yu Jingya, Ms. Wang Shuang, Ms. Wang Haitang, Ms. Liu Andi, Mr. Yu Tao, Ms. Yang Di and Mr. Huang Zheng for their encouragement and company, which made my research life more enjoyable.

Finally, I wish to express my deepest gratitude to my parents and grandmother for their unconditional love and supports. I would like to dedicate this Thesis to my beloved grandmother. I will keep going with love.

Table of Contents

List of Figures

Chapter 2 **Page**

Chapter 5

Chapter 6

Appendix

Photo images of the experimental setup

List of Tables

Chapter 7

Nomenclature

Variable	Description	Unit
d	moisture content	kg/kg
D	diameter	m
f	friction factor	
F	outdoor coil heat exchange surface area	m^2
h	specific enthalpy	kJ/kg
L	length	m
m	mass flow rate	kg/s
n	compressor speed	rps
P	pressure	Pa
Q	total output heating capacity	kW
$\overline{Q}$	average total output heating capacity	kW
RH	relative humidity	%
T	temperature	°C
t	time	s
u	velocity	m/s
V	compressor stroke volume	m^3/rev
v	mass flux	kg/(m^2·s)
W	power input	kW
x	dry fraction	
α	convective heat transfer coefficient	W/(m^2·°C)
δ	thickness	mm
λ	thermal conductivity	W/(m·K)

ρ	density	kg/m^3
ξ	heat leakage coefficient	
ζ	local loss coefficient	
Δ	difference	

Subscripts

a	air
c	indoor coil
d	dry-bulb
e	outdoor coil
f	frost
h	heating
i	inlet
o	outlet
r	refrigerant
sc	sub-cooling
sh	superheat
s	single phase
tp	two phases
w	wet-bulb

List of Abbreviations

A/C	air conditioning
ASHP	air source heat pump
CCD	charge-coupled device
COP	coefficient of performance
DX	direct expansion
EEV	electronic expansion valve
E SHR	equipment sensible heat ratio
LGU	load generating unit
PID	proportional-integral-derivative
VS	variable speed

Chapter 1

Introduction

With the increased problems of severe global energy shortage and environmental pollution, energy-efficient and environmentally friendly space heating technologies have been paid more and more attention. Among them, air source heat pumps (ASHPs) have been widely promoted and employed in many countries and regions due to their advantages of a wide application range, high efficiency, flexibility in installation and low cost. The United States, the European Union and China have successively classified ASHPs as energy-saving devices or renewable energy technologies that can be used to help reduce energy consumption in buildings, which is crucial to help achieve carbon emission reduction and mitigate global energy crisis. Therefore, it can be expected that ASHPs will have a broader market prospect worldwide.

However, for a space heating ASHP unit, frosting on its outdoor coil surface was still one of the main issues restricting its further development. When its outdoor coil surface temperature was below both the dew point of ambient air and the freezing point of water, frosting on the outdoor coil surface took place. As the frost formed and accumulated on the outdoor coil surface, the resistance of air flowing through the finned tubes in the outdoor coil was gradually increased and thus air flow rate decreased. This would cause serious negative impacts on the heating performance, energy efficiency and operational reliability of the ASHP unit. In addition, as the result of frosting, regular defrosting had to be implemented to ensure the normal operation of the ASHP unit, which would cause additional energy consumption and affect the indoor thermal environment. To address the negative effects caused by frosting and

defrosting, extensive measures for suppressing or delaying frosting on the outdoor coil surface in an ASHP unit have been proposed. However, most of these frosting suppression measures have not been successfully implemented in practice due to their own shortcomings, such as high costs, poor stability and durability, etc. Therefore, it was highly necessary to further develop the effective frosting suppression measure for both the efficient and stable operation of an ASHP unit and reducing the energy consumption for defrosting.

On the other hand, with technology advancements, variable speed (VS) technology has been widely applied to space heating ASHPs. For a VS ASHP unit, using different compressor and outdoor air fan speeds may result in different outdoor coil surface temperatures, thus leading to different frosting suppression performances. This may also result in different total output heating capacity from the unit. Hence, varying compressor and outdoor air fan speeds in a VS ASHP unit may be potentially adopted for frosting suppression. However, only scattered studies on applying VS technology to frosting suppression for ASHPs may be identified, and there have been a lack of systematic and comprehensive studies on the effects of varying compressor and outdoor air fan speeds on the frosting suppression and heating performances, which is very important for guiding the future frosting suppression operation of ASHPs.

Therefore, to comprehensively study and evaluate the frosting suppression and heating performances of a VS ASHP unit by varying its compressor and outdoor air fan speeds, a condensing-frosting performance map was proposed. The performance map could directly show the relationship between the total output heating capacity and outdoor coil surface status (dry, wet or condensing or frosting) of the unit under different speed

combinations of the compressor and outdoor air fan, and may therefore be used as a basis to guide the efficient and safe operation of the ASHP unit for frosting suppression while at the same time providing the required output heating capacity. Therefore, a research project to develop the proposed condensing-frosting performance map for an experimental VS ASHP unit for frosting suppression has been carried out by using experimental and modeling approaches, and the project results are reported in this Thesis.

Firstly, a comprehensive literature review on various issues related to frosting and its suppression for space heating ASHPs is reported in Chapter 2. The reviewed studies can be divided into four parts: frost formation process and its effects on the operating performances of ASHPs; existing frosting suppression measures for ASHPs; applying VS technology to air conditioning (A/C) units and ASHPs; and mathematical modeling of a VS ASHP unit. Based on the literature review, the current related research status is understood, and research gaps are identified.

In Chapter 3, a proposition for the research project reported in this Thesis, including the background, project title, aims and objectives, and research methodologies, is presented in detail based on the research gaps identified in Chapter 2.

Chapter 4 reports an experimental setup, which was specially established for carrying out the required experimental work of the research project reported in this Thesis. Firstly, two main parts of the experimental setup, i.e., an experimental VS ASHP unit and an environmental chamber, are separately presented in detail. This is followed by

presenting a detailed description of a computerized data monitoring and acquisition system built in the experimental setup.

Chapter 5 presents an experimental study on developing the condensing-frosting performance maps for the experimental VS ASHP unit. In this Chapter, experimental procedures and test operating conditions are firstly described in detail. This is followed by presenting an experimental investigation on the effects of changing the compressor and the outdoor air fan speeds of the experimental VS ASHP unit on its outdoor coil surface temperature and the total output heating capacity. Based on the obtained extensive experimental data, condensing-frosting performance maps for the experimental VS ASHP unit at three typical outdoor ambient air conditions were developed. To analyze the operational characteristics of the experimental ASHP unit when operated at three different outdoor coil surface statuses of condensing, condensing / frosting and frosting, but at almost the same total output heating capacity, a further comparative experiment was also carried out, and the experimental results is reported.

In Chapter 6, the development of a physical-based mathematical model for the experimental VS ASHP unit, which can be used to obtaining condensing-frosting performance maps at other non-experimental configurations and ambient conditions, is reported. The developed mathematical model was validated by using the experimental data reported in Chapter 5. Using the validated model, a follow-up modeling study is presented, where condensing-frosting performance maps for the experimental VS ASHP unit at non-experimental unit configurations and outdoor operating ambient conditions were obtained, and the influences of the unit

configurations and operating conditions on the frosting suppression and heating performances of the experimental VS ASHP unit were numerically investigated.

Based on the experimental and modeling studies reported in Chapters 5 and 6, Chapter 7 presents a novel control strategy for the experimental VS ASHP unit to achieve effective frosting suppression. This novel control strategy was proposed based on the obtained condensing-frosting performance maps. Extensive experimental tests at different outdoor ambient conditions were carried out to examine the controllability and effectiveness of the developed novel control strategy by using the experimental setup reported in Chapter 4, and the experimental results are reported in Chapter 7.

Finally, the conclusions of this Thesis and the proposed future work are presented in Chapter 8.

Chapter 2

Literature review

2.1 Introduction

With the increased problems of severe global energy shortage and environmental pollution, developing energy-efficient and environmentally friendly space heating technologies becomes increasingly critical [Carroll et al., 2020; Zhang et al., 2017]. Among the proposed efficient and clean heating technologies, ASHPs have been highly rated due to their advantages of wide application ranges, high efficiency, installation convenience and low capital cost [Amirirad et al., 2018; Zhang et al., 2018a; Chesser et al., 2021]. For a space heating ASHP unit, it extracts heat from outdoor ambient air as a heat source and transfers the extracted heat to a heated indoor space. At present, the European Union [2009] and China [2015] have actively promoted the application of ASHPs for building space heating in an attempt to effectively reduce building energy consumption.

However, frosting is still a problem that restricts the further development of air source heat pumps. For a space heating ASHP unit operated at low air temperature and high relative humidity, its outdoor coil surface was prone to be frosted, which was difficult to avoid [Zhu et al., 2015]. The accumulation of frost on outdoor coil surface can reduce the operating performances of ASHPs, in terms of coefficient of performance (COP) and output heating capacity, and even affect the operating stability and safety [Guo et al., 2008; Da Silva et al., 2011; Xu et al., 2020]. In order to avoid or mitigate the negative effects of frosting on ASHPs, a large number of studies has been carried

out to better understand the frosting mechanism on an outdoor coil surface and to develop effective frosting suppression measures for a space heating ASHP unit.

In this Chapter, a comprehensive review of the literature related to frosting and suppressing frosting for space heating ASHPs is presented. Firstly, the previous studies on frost formation process and its effects on the operating performances of ASHPs are reported. Secondly, existing frosting suppression measures for ASHPs including changing ambient air properties at the inlet to an outdoor coil, modifying surface properties of an outdoor coil and its fins, optimizing the structure of an outdoor coil and employing additional external forces are reviewed and summarized. Thirdly, studies of applying VS technology to A/C units and ASHPs are reviewed. Fourthly, previous related studies on mathematical modeling of a VS ASHP unit are reviewed. Finally, the conclusions of the literature review are given.

2.2 Previous studies on frost formation process and its effects on the operating performances of ASHPs

Over the past many decades, a large number of studies have been carried out regarding a number of issues related to frosting for space heating ASHPs. These included the fundamental frosting mechanism, frosting process, the characteristics of frost, the factors affecting the frosting and how frosting effects the operation of an ASHP unit. These related studies have been reviewed and are summarized in this Section.

2.2.1 The mechanism of frost formation on an outdoor coil surface

For a space heating ASHP unit, when its outdoor coil surface temperature is lower than both the dew point and freezing point of the ambient air, frost will appear on the outdoor coil surface. Frost formation on an outdoor coil surface is a complex heat and mass transfer process in which the water vapor in the air flowing through the outdoor coil undergoes a phase transition. It was suggested that the mechanism of frost formation is the diffusion of water on a cold surface due to the driving forces of heat transfer and mass transfer [Sanders, 1974; Zhang et al., 2018b]. The former was the difference between the frost layer surface temperature and the ambient humid air temperature, and the latter the difference between the saturated water vapor partial pressure at the frost layer surface temperature and the water vapor partial pressure of the ambient humid air. Part of the condensed water vapor was deposited on frost layer surface to further facilitate its growth, and the other part diffused into the frost layer to increase its density. There were two key stages in the process of frost formation on the outdoor coil surface in an ASHP unit: the phase transition of water vapor and the formation of liquid nuclei on the outdoor coil surface, which mainly involved the phase transition driving force and nucleation barrier [Liang, 1993].

According to the phase transition kinetics, the phase transition of a substance was mainly due to the Gibbs free energy difference between its metastable phase and stable phase [Sun et al., 1995]. The phase transition process of a substance could be regarded as a transition from a metastable phase to a stable phase. Compared with the stable phase, the metastable phase of a substance possessed higher Gibbs free energy. Due to the difference in Gibbs free energy between the two phases, there was a phase

transition driving force, which drove the phase transition to take place [Min, 1982]. In the process of condensing and frosting, the phase transition of water vapor in moist air was that, after it flowed through a cold surface at a low temperature, water vapor would become supersaturated steam, which was at a metastable state. Due to its higher Gibbs free energy, it would spontaneously develop towards the trend of decreasing Gibbs free energy to reach a stable state. This was the reason for the existence of the phase transition driving force [Min, 1982]. For a space heating ASHP unit, when the outdoor ambient air condition is fixed, the driving force of phase transition during frosting on its outdoor coil surface is expressed as follows [Fletcher and Hasted, 1971; Kim et al., 2017]:

$$\Delta g = R(T_{a,\,i} - T_s)\ln\frac{P_{\sup}}{P_{sat}} \tag{2.1}$$

where Δg is the driving force of phase transition of during frosting, R the molar gas constant, $T_{a,\,i}$ the inlet air temperature to an outdoor coil, T_s the surface temperature of the outdoor coil, $P_{\sup}$ the supersaturated water vapor pressure, and P_{sat} the saturated water vapor pressure at T_s.

From Eq. (2.1) above, it can be seen that frosting is related to the supersaturation of water vapor in ambient air and the surface temperature of an outdoor coil.

Although the phase transition driving force is not affected by the properties of an outdoor coil surface, the process of liquid nuclei formation on the surface will

significantly be. According to the theory of phase transition nucleation [Huang, 2011], liquid nuclei formation needs to overcome a nucleation barrier, which is closely related to surface properties. It has been demonstrated that when the radius of the liquid core was fixed, the nucleation barrier was increased with an increase in the surface contact angle. A larger surface contact angle would lead to more difficult nucleation of water vapor on the surface [Na and Webb, 2003]. However, not all liquid nuclei could grow into condensing droplets. Only liquid nuclei with a radius greater than the critical liquid core radius could be retained and further grew into a droplet [Huang, 2011]. It has also been reported that a smaller critical liquid core radius would make it easier for a droplet to form, and the critical liquid core would be reduced with an increase in the saturation temperature of water vapor, or a reduction in the outdoor coil surface temperature. In addition, Min [1982] presented that for frosting on an outdoor coil surface, the formation of droplets would promote the subsequent growth of frost, because the droplets formed in the early frost formation stage were the basis of subsequent frost crystal growth.

2.2.2 The frost formation process and characteristics on an outdoor coil surface

In order to have a more in-depth understanding of the frost formation, a number of researchers have reported the results of analyzing frost formation process and characteristics over the past decades, as shown in Figs. 2.1-2.2 and Table 2.1 [Hayashi et al., 1977; Tao, 1993; Iragorry et al. 2004; Song and Dang, 2018], respectively. It was commonly accepted that there were three periods of frost growth process, as proposed by Hayashi et al. [1977], i.e., crystal growth period, frost layer growth period, and frost layer full growth period. During the crystal growth period, water vapor would

undergo a phase transition process on a cold surface, and continuously adhere to the cold surface in the form of crystals to provide the basis for further frost formation. Then, during the frost layer growth period, the thickness and density of frost layer were increased greatly, and the heat and mass transfer rate was the highest. Finally, the frost layer reached the quasi-steady state of heat transfer during the frost layer full growth period. When the surface temperature of frost layer was greater than 0 ^{o}C, the crystals on the top of the frost layer would begin to melt, which was also known as frost layer aging. In addition, Tao [1993] also proposed a three-period division definition for a frost growth process. Unlike that proposed Hayashi, it considered the process of droplet nucleation and coalescence, but not the alternate melting-freezing phenomenon on the frost layer surface. Combining the above two definitions, Song and Dang [2018] presented a more comprehensive and suitable division definition for the frost growth process on the outdoor coil surface of an ASHP unit. It included four periods, i.e., a droplet condensation period, solidified liquid tip-growth period, frost layer growth period and finally a frost layer full growth period, as shown in Fig. 2.3.

Table 2.1 Division definitions for the frost formation process [Hayashi et al., 1977; Tao, 1993]

Authors	Periods	Characteristics
Hayashi	Crystal growth	Separate rod type crystals generated and grew in one dimension
	Frost layer growth	Branch generated around rod type crystals and grew in three dimensions
	Frost layer full growth	Frost layer surface temperature reached 0 °C and melting-freezing phenomenon occurred alternately and periodically
Tao	Dropwise-condensation	Droplet nucleated and merged
	Solidified liquid tip-growth	Coalescent droplet solidified and crystals grew on its tip in one dimension
	Densification and bulk-growth	Branch generated around crystals and grew in three dimensions

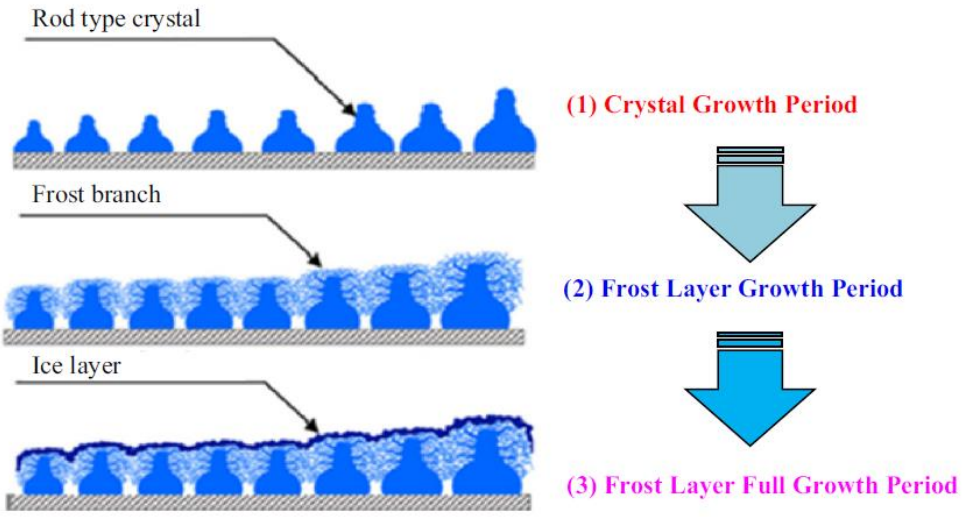

Fig. 2.1 The frost formation process having three periods defined by Hayashi [Hayashi, 1977; Song and Dang, 2018]

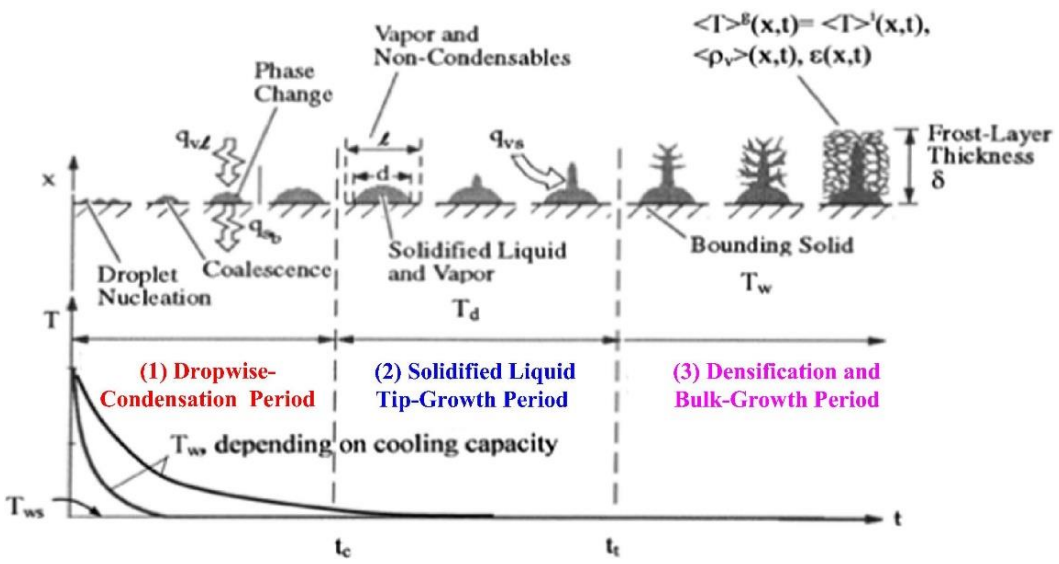

Fig. 2.2 The frost growth process having three periods defined by Tao et al. [Iragorry et al. 2004; Song and Dang, 2018]

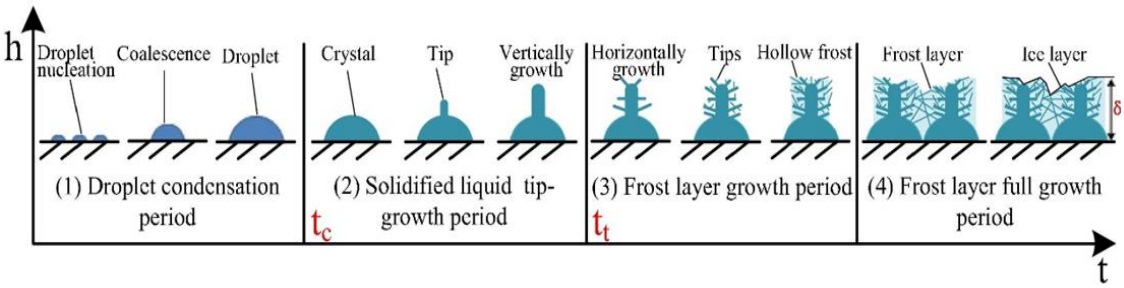

Fig. 2.3 The frost growth process having four periods defined by Song and Dang [2018]

It is well known that frost is a porous and loose substance composed of ice crystals. During a frost formation process, the morphological characteristics of its ice crystals would have great changes. In an earlier study, Kobayashi [1958] classified the ice crystal structure in a frost layer into seven categories, namely, plate, needle, sheath, dendrite, sectorated plate, hollow column and solid column. Kobayashi [1958] also

proposed that the supersaturation between the cold surface temperature and the water vapor in the ambient moist air was the main factor affecting the ice crystal structure in a frost layer. In the study of Sahin [2000], the classification of ice crystal structures was further simplified from the above seven categories to two categories, ice column and ice plate. The former included needle, sheath, hollow column and solid column, and the latter plate, dendrite and sectorated plate. In addition, Xu [2004] photographed the changes of ice crystal structures during an entire frost formation process with the help of microscopic camera technology, as shown in Fig. 2.4. The results demonstrated that an initial ice crystal structure on the cold surface was columnar, and after frost layer formation, the ice crystal structure was gradually changed to needle, plate and irregular as the frost layer thickened and its surface temperature increased. Furthermore, the results [Xu, 2004] also suggested that in the early stage of frost formation, the cold surface temperature and ambient air relative humidity were the main factors affecting the ice crystal structure, and as the thickness of the frost layer was increased, the ice crystal structure depended on the frost layer surface temperature. During the frost formation process, not only the surface temperature and thickness of the frost layer, but also its density and thermal conductivity would change.

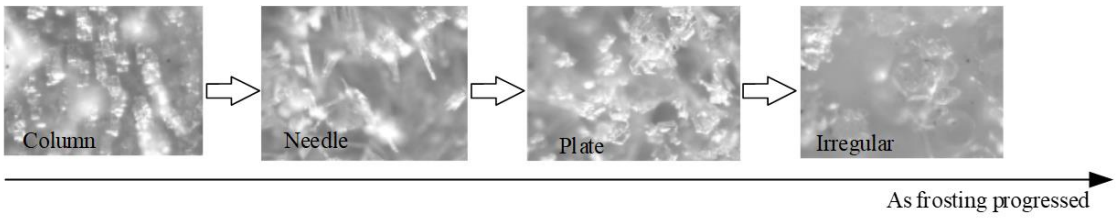

Fig. 2.4 The changes of ice crystal structures during an entire frost formation process [Xu, 2004]

2.2.3 Factors affecting the frost formation on an outdoor coil surface

The existing literature on the factors affecting the frost formation on the outdoor coil surface of an AHSP unit is extensive and mainly focuses on the investigation of the following factors, i.e., ambient air conditions, outdoor coil surface temperature, outdoor coil structure and its fin properties. The effects of these factors on the frost formation on an outdoor coil surface are respectively discussed as follows.

1) Ambient air conditions

Extensive research has shown that frost formation on the outdoor coil surface of an ASHP unit is closely related to the ambient air conditions, at which the unit is operated, including the ambient air temperature, air relative humidity and air flow rate.

It is generally accepted that ambient air temperature can greatly affect frost formation. Liu et al. [2007] established a mathematical model to study the effects of ambient air conditions on frost formation. The modeling results suggested that the thickness of the frost on the outdoor coil surface had a decreasing relationship with the ambient air temperature. When the ambient air temperature was at -5 ^{o}C and 0 ^{o}C, the growth rate of frost thickness was 0.17 mm/h and 0.06 mm/h, respectively. When the ambient air temperature was at 10 ^{o}C, there was almost no frost on outdoor coil surface. Guo et al. [2011] experimentally analyzed the frosting characteristics on the outdoor coil surface of an ASHP unit under different ambient air temperatures, and the results demonstrated that a lower ambient temperature would lead to the needle ice crystal structure in the frost layer and a lower frost density.

It has been well acknowledgement that ambient air relative humidity can have a significant effect on frost formation. Studies have suggested that the mass of frost would increase greatly with an increase in ambient air relative humidity [Cheng et al., 2001; Lee and Ro, 2011]. This was because a higher ambient air relative humidity would increase the water vapor pressure in moist air, which could increase the driving force of frosting, thereby accelerating mass transfer and frosting [Liu et al., 2007; Zhao et al., 2022]. The study results by Zhao et al. [2022] also pointed out that at a constant ambient air temperature, increasing air relative humidity would increase the dew point temperature of air, and the water vapor would more easily condense on the outdoor coil surface and further promote frost formation.

The literature on the effect of air flow rate on frost formation is however less consistent. Yan et al. [2003a] and Gong et al. [2010] respectively conducted experimental studies on the frosting characteristics in an outdoor coil surface under different air flow rates. Their experimental results indicated that a lower air flow rate could cause greater frost formation. Senshu [1990] also presented the same conclusion in an earlier literature. Liu and Yang [2004] established a mathematical model and conducted a numerical study on the factors affecting frost formation on outdoor coil surface. The results have shown that an appropriate increase in the air flow rate through the outdoor coil could help reduce the heat transfer temperature difference between the refrigerant and the ambient air, thereby effectively suppressing frosting. Based on a semi-experimental method and its modeling results, Shen et al. [2021] presented that increasing the air flow rate could reduce the driving force of frosting, which could be an effective method to suppress frosting for an ASHP unit. In addition, Kandula [2011] and Wang et al. [2018a] also pointed out that increasing the air flow rate could delay the frost

formation on the outdoor coil surface of an ASHP unit, and its total output heating capacity and COP could be both improved. However, the study results in some other literatures are not consistent with the above mentioned findings. For example, Kondepudi and O'Neal [1991] and Seker et al. [2004a] believed that a higher air flow rate would lead to more severe frosting on an outdoor coil surface. The experimental results of Guo et al. [2012] indicated that a reduction in air flow rate would increase the growth rate of the frost layer thickness on the outdoor coil surface of an ASHP unit, but the total mass and the average density of frost would be decreased. Although there appeared to be discrepancies between some of the reported results, it was certain that increasing air flow rate can delay and suppress frost formation. On the other hand, both the studies of Zhang et al. [2019] and Kondepudi [1991] proved that a higher air flow rate could lead to an evener frost layer on an outdoor coil surface, which was beneficial to improve the operating performance of an ASHP unit under frosting conditions.

2) Outdoor coil surface temperature

Extensive research has been conducted on the effects of cold surface temperature on frost formation. For a space heating ASHP unit, its outdoor coil surface is a frosted cold surface. Wang et al. [2010] carried out an experimental study on the frosting characteristics under different cold surface temperatures. The experimental results have shown that as cold surface temperature was decreased, frost formation rate was increased, and frost density was decreased. The numerical study of Yang et al. [2022] also demonstrated a similar conclusion that a lower cold surface temperature could lead to a thicker and fluffier frost layer. Lee et al. [2003] established a mathematical

model to predict frost formation on a cold surface, and their further modeling studies found that a lower cold surface temperature could result in a faster condensing rate of water droplets on the cold surface, thus increasing frost growth rate.

3) Outdoor coil structure and fin properties

A series of studies on the effects of outdoor coil structures and fin properties on the frost formation have been conducted. Wang et al. [2006] studied the frosting performances of an ASHP unit with different heat transfer surface areas of its outdoor coil. The results have shown that an increase in the outdoor coil area can increase the evaporating temperature, thereby reducing the frosting time during its heating operation. Kim et al. [2013] experimentally compared the frosting characteristics on an outdoor coil with different refrigerant flow directions, and found that the frost layer on the outdoor coil surface of the counter-flow type was evener than that of the parallel-flow type. The experimental results of Qin et al. [2014] suggested that fin spacing had a significant effect on the first occurrence time point of frost layer and its subsequent growth, and concluded that a smaller fin spacing could lead to an earlier frost layer formation and a greater frost growth rate. The experimental studies of Lee et al. [2010], Kim and Lee [2013] and Cheng et al. [2006] also presented similar conclusions that by increasing fin spacing, frosting on an outdoor coil surface could be delayed. In addition, a previous study [Na and Webb, 2003] pointed out that the contact angle of a fin surface could affect the condensation nucleation of water vapor, which could to a certain extent affect the frosting on the fin surface. The roughness of an outdoor coil surfaces also could affect frosting, and it is generally accepted that a

smoother surface could result in less frost mass [Hassan et al., 2010; Zou et al., 2011; Memon, 2020].

2.2.4 Effects of frost formation on the operating performances of ASHPs

Frost formation on an outdoor coil surface would bring a series of adverse effects on the operating performances of ASHPs, significantly affecting the further developments of ASHPs. There are two generally recognized negative effects of frost formation and accumulation on outdoor coil surface of ASHPs. Firstly, due to the low thermal conductivity of frost, a large amount of frost covering an outdoor coil surface would increase the heat transfer resistance between the ambient air and the outdoor coil, thereby deteriorating its heat transfer performance [Stoecker, 1957; Machielsen and Kerschbaumer, 1989]. As the heat transfer deteriorates, the output heating capacity from the ASHP unit would decrease. However, in order to meet the heating requirements, the ASHP unit must be operated at a lower evaporating temperature, which would further reduce its efficiency. Secondly, the accumulation of frost would reduce the air flow rate through an outdoor coil, and increase the flow resistance, which would affect the heat exchange between the air and the outdoor coil and increase the power consumption of an outdoor air fan [Stoecker, 1957; Barrow, 1985; Seker et al., 2004b; Yao et al., 2004].

In order to investigate more comprehensively the effects of frost formation on the operating performances of ASHPs, extensive experimental and simulation studies have been carried out. Senshu [1990] pointed out in an early research report that performance deterioration of ASHPs under frosting conditions was caused by a

vicious cycle, i.e., the accumulation of frost would cause a reduction evaporating temperature, and this then resulted in an increased growth rate of frost, thereby leading to a severer frost growth and accumulation. Guo et al. [2008] experimentally studied the effects of frosting on the performances of an ASHP unit at different frost growth periods. The experimental results indicated that at the initial period of frost formation on the outdoor coil surface, the heat transfer area was actually increased due to the rough surface of ice crystals that constituted an initial frost layer, so that the performance of the unit could be improved. This was similar to the results reported by Stoecker [1957], Hosoda and Uzuhashi [1967], Huang et al. [2008]. At the second period of frost growth, because the thickness of frost layer did not change significantly, the output heating capacity and COP of the ASHP unit were not greatly affected by frosting. However, at the third period of frost growth, frost layer thickness was increased rapidly, and the performance of the unit deteriorated rapidly. Chung et al. [2019] established a mathematical model for an ASHP unit to study the effect of frosting on its operating performances. The results also indicated that the performances were deteriorated at a later period of frost growth.

A series of studies have been conducted to investigate the extent of performance loss of ASHPs under frosting conditions. According to experimental studies by Wang et al. [2011; 2013], the heating performance of ASHPs could be reduced by 30 %-50 % under frosting condition. Vocale et al. [2014] presented that the COP of ASHPs operated under a frosting ambient condition with a high air relative humidity could be reduced by about 20 %. Votsis et al. [1989] found that the extent of reduction in COP of ASHPs due to frosting depended mainly on the ambient air conditions and the duration of frosting operation. In addition, defrosting was necessary to return the

normal operation of an ASHP unit, but the energy loss due to defrosting was equivalent to more than 12.9 % of its output heating capacity [Dong et al., 2012].

On the other hand, Huang et al. [2007] and Qiao et al. [2017] studied the transient characteristics of ASHPs under frosting conditions through experiments and simulations, respectively. Both indicated that uneven frosting on an outdoor coil surface would lead to uneven air flow rate, which could result in the unstable operation of the ASHP unit. Song [2010] found that frosting had a negative impact on the operation of a compressor, and the accumulation of frost would cause large fluctuations in the suction and discharge pressures of the compressor. Therefore, frosting would also affect the safety and stability of an ASHP unit.

2.3 Existing frosting suppression measures

Effective frosting suppression measures are very important for the further development of ASHPs, because they can help mitigate the negative impacts of frosting and thus improve the operating performances of ASHPs. Currently, there exist various frosting suppression measures, which are summarized and discussed in this section, as follows.

2.3.1 Changing ambient air properties at the inlet to an outdoor coil

As discussed earlier, frost formation on the outdoor coil surfaces of an ASHP unit is closely related to ambient air conditions. Therefore, various frosting suppression

measures of changing ambient air properties at the inlet to an outdoor coil have been proposed. These can be summarized as follows:

1) Preheating the inlet air

Since a high ambient air temperature is beneficial to frosting suppression, preheating the ambient air at the inlet to an outdoor coil has been regarded as a simple and effective measure to delay or reduce frosting on ASHPs [Kwak and Bai, 2010; Song et al., 2018]. To achieve more effective frosting suppression, the temperature of ambient air at the inlet should be higher than the freezing point temperature [Nasr et al., 2014]. However, this measure was less practical because increasing air temperature required a large amount of additional energy, which could increase the operating energy consumptions of ASHPs and was thus uneconomical [Kragh et al., 2005; Song, 2014].

2) Dehumidifying inlet air

Previous studies have been suggested that ambient air relative humidity was one of the most important factors affecting the frost formation on the outdoor coil surface of an ASHP unit. A higher moisture content of ambient air would lead to severer frosting. Therefore, various measures have been proposed to lower the relative humidity of ambient air at the inlet to an outdoor coil to suppress frosting. An earlier study by Kondepudi et al. [1995] proposed the use of solid desiccant to dehumidify inlet air. Their results suggested that the use of solid desiccant could effectively reduce the moisture content of inlet air and slow the growth rate of frost layer in a short period of

time. However, since there was not a desiccant regeneration device, the moisture adsorption performance of the desiccant would gradually weaken, resulting in a gradual deterioration of the frosting suppression effect, as the operation of the ASHP went on. In order to use desiccant continuously, Wang and Liu [2005] proposed an adsorbent bed which was installed at the air inlet to an outdoor coil, as shown in Fig. 2.5. The solid desiccant in the adsorbent bed was used to dehumidify the inlet air, and the surface of the adsorbent bed was coated with active carbon, which could be heated by solar energy to achieve solid desiccant regeneration. However, the structural design of the adsorbent bed needed to be further improved. In addition, Zhang et al. [2012a] also proposed a measure for dehumidification and regeneration using solid desiccant, which was to place an additional outdoor coil coated with a solid desiccant at the air inlet to the outdoor coil, as shown in Fig. 2.6, and to use the condensing heat to regenerate solid desiccant. Although this measure could achieve effective frosting suppression, it also increased the initial cost and required more installation space of an ASHP unit. Furthermore, liquid desiccants were easier to be regenerated than solid desiccants. Therefore, in both studies of Kinsara et al. [1996] and Zhang et al. [2010; 2012b], the use of liquid desiccants to dehumidify the ambient was suggested. However, because such dehumidification systems were too complex, their practical application were largely limited.

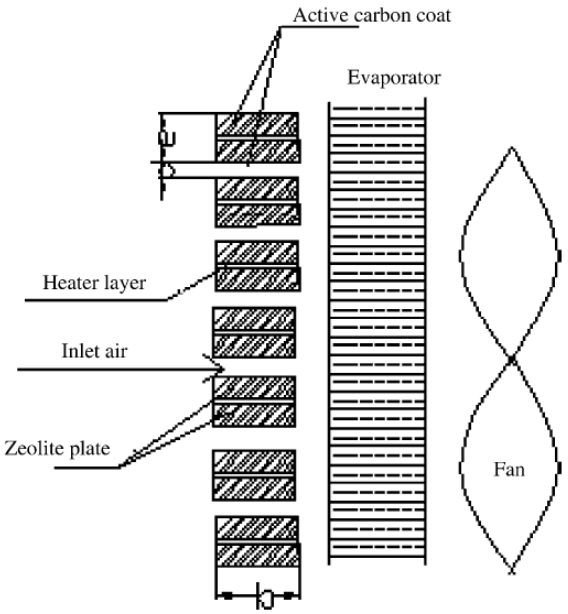

Fig. 2.5 Schematic diagram of an outdoor coil with adsorbent beds proposed by Wang and Liu [2005]

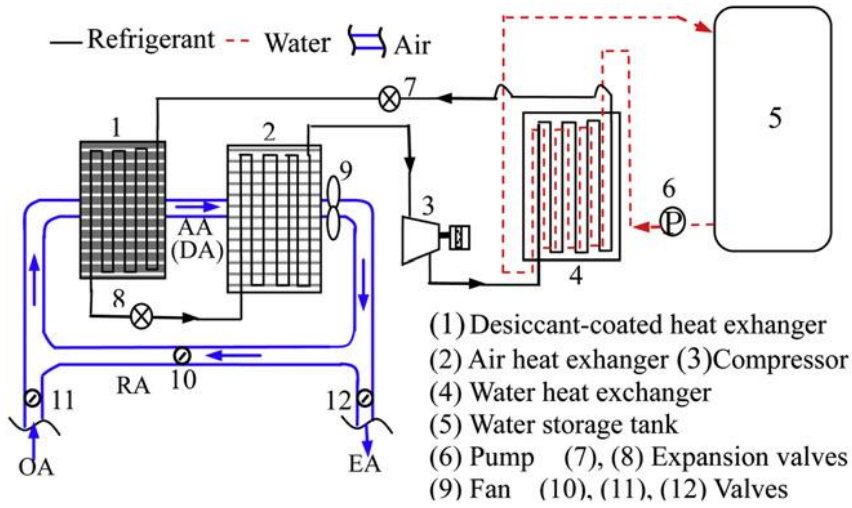

Fig. 2.6 A new ASHP unit with an additional desiccant-coated outdoor coil proposed by Zhang et al. [2012a]

3) Increasing air flow rate passing through an outdoor coil

As discussed earlier, researchers have carried out a large number of studies on the effects of air flow rate on frost formation, and it was shown that increasing air flow rate could delay frosting. Recently, Wang et al. [2018a] proposed to use high-velocity air flow to intermittently blow an outdoor coil surface of an ASHP unit to remove the condensing droplets in the early stage of frost formation. Although the experimental results have shown that this measure could significantly improve the frosting suppression performance of the ASHP unit, the required air flow velocity was very high, which was not suitable for ordinary household space heating ASHPs. In addition, the continuous accumulation of frost would gradually reduce the air flow rate through an outdoor coil, which could adversely affect the operation of ASHPs. Therefore, Zhang et al. [2019] proposed an outdoor air fan control mode of constant air flow rate for an ASHP unit, which was to increase outdoor air fan speed during frosting to keep the air flow rate through the outdoor coil unchanged. The experimental results suggested that such a control mode could reduce the growth rate of frost thickness and improve the evenness of frosting on the outdoor coil surface. However, this measure was still in the experimental research stage, and further detailed research was needed before it could be put into practical application.

2.3.2 Modifying surface properties of an outdoor coil and its fins

According to frosting mechanism, for a space heating ASHP unit, frosting is a process in which water vapor in ambient air undergoes a phase transition on its outdoor coil surface. The phase transition nucleation needs to overcome the Gibbs free energy

barrier, which is closely related to surface properties. Therefore, a frosting process is closely related to cold surface properties. In the current open literature [Kim et al., 2013; Wang et al., 2018b; Lee et al., 2004; Kim et al. 2016; Kim et al., 2017], frosting suppression measures of modifying surface properties of an outdoor coil have been extensively reported. These focused particularly on the investigation of the use of hydrophilic or hydrophobic surfaces for frosting suppression. The use of hydrophilic surfaces was proposed in earlier studies [Highgate et al., 1989]. Numerous studies have shown [Jhee et al., 2002; Kim et al.,2017; Wang et al., 2015; Ozbay et al. 2015; Van Dyke et al., 2015; Sommer et al., 2016] that an outdoor coil surface with hydrophilic coating could lead to a significantly lower growth rate of frost thickness, but a greater frost density. For the outdoor coil surface with hydrophobic coating, frost formation could be delayed due to the reduced adhesion of condensing water droplets on the outdoor coil surface, and frost density was lower, thus defrosting was easier [Wu and Webb, 2001; Jhee et al., 2002; Kim and Lee, 2011, 2012, 2013]. Although a certain extent of frosting suppression could be achieved by using hydrophilic or hydrophobic coated outdoor coil surface, there were some considerable drawbacks [Wang et al., 2018b]. For example, water droplets were retained on hydrophilic outdoor coil surfaces after defrosting [Li et al., 2014a], and the added coating could cause an additional heat transfer resistance for the outdoor coil. In addition, both hydrophilic and hydrophobic coatings have their own problems, such as short service life, weak surface strength, poor durability and high cost [Kim et al., 2017; Sheng et al., 2017; Song et al., 2018]. In addition, Rahman and Jacobi [2012; 2013; 2014] in an experimental study proposed the use of fins with microgroove surfaces, as shown in Fig. 2.7, to facilitate the discharge of the condensing droplets on the surface. The study results suggested that this measure could result in a reduction in the mass of frost per

unit area for an outdoor coil. However, the manufacturing process of such fin surfaces was very complicated.

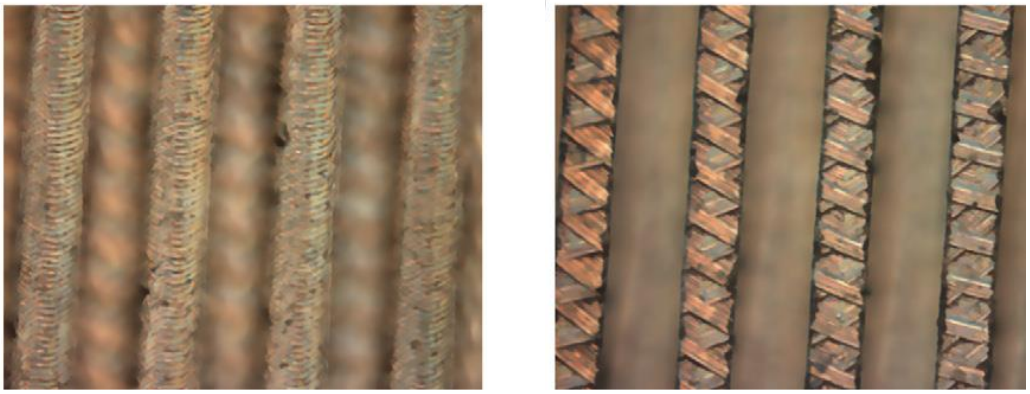

(a) Grooves (b) Pillars

Fig. 2.7 Images of a microgroove surface [Rahman and Jacobi, 2012]

2.3.3 Optimizing the structure of an outdoor coil

From the published literature, various measures have been proposed to optimize the structure of an outdoor coil to achieve frosting suppression [Sheng et al., 2017; Song et al., 2018]. The study by Park et al. [2016] indicated that an outdoor coil with louver fins could delay the frost accumulation and increase the frost evenness, and the heat transfer performance of the outdoor coil could be thus improved. Researchers [Niederer, 1976; Kondepudi and O'Neal, 1991; Watters et al., 2002; Lee et al., 2010; Yan et al., 2003a] have presented that increasing the fin spacing could slow down the growth rate of frost layer on an outdoor coil and delay the blockage of airflow passage. Yang et al. [2006] proposed a method to optimize the fin spacing on an outdoor coil, and the results showed that increasing the fin spacing at the air inlet to the outdoor coil could improve the heat transfer efficiency and delay frost formation. Gu et al. [2001]

in an experimental study pointed out that increasing the number of tube rows along the airflow direction would increase the resistance of airflow and lead to a greater growth rate of frost, and suggested that the number of tube rows along the airflow direction of the outdoor coil should not exceed three rows. Furthermore, reducing the pipe diameter [Cheng et al., 2006] and the counter refrigerant-air flow distribution of an outdoor coil [Kim et al., 2013] could also help enhance heat transfer efficiency, improve frost evenness and slow down the growth rate of frost. However, these measures mentioned above were generally considered as supplementary measures to suppress frost, because they mainly affect the heat transfer efficiency and frosting evenness on an outdoor coil. On the other hand, Wang et al. [2006] in an experimental study found that increasing the outdoor coil surface area could increase the evaporating temperature and frosting suppression could be thus achieved. However, since using a larger outdoor coil would increase the initial cost of an ASHP unit and require a larger installation space, this frosting suppression measure was not common in practical applications.

2.3.4 Employing additional external forces

The methods of employing additional external forces to suppress frost on an outdoor coil mainly included the applications of electric field, magnetic field, ultrasonic vibration technology or air jet technology [Sheng et al., 2017; Song et al., 2018]. Many researchers have carried out experimental studies on the effect of using electric field on frosting suppression [Maybank and BARTHAKUR, 1967; Babakin and Elykin, 1985; Ma and Peterson, 1995; Wang et al., 2004]. The study results demonstrated that the use of electric field could affect the diffusion mode of water vapor molecules

around a frost layer surface, and the frost would grow along the direction of the electric field, and its ice crystal structure was of slender and needle type, which could break easily under its own gravity or external force. Gou et al. [2009] experimentally investigated the effect of using magnetic field on frost formation, and found that the frost layer grown under the influence of an additional magnetic field was fluffy and easy to remove. However, the influence of magnetic field strength on frost thickness was complex and changeable [Zhao et al., 2015]. On the other hand, other researchers [Adachi et al., 1998; Yan et al., 2003b; Tan et al., 2014, 2015] have carried out experimental studies on the influence of ultrasonic vibration technology on frosting. The results of these studies all suggested that the use of ultrasonic vibration technology could reduce the frost accumulation on a cold surface, which was beneficial to frosting suppression. In the experimental study of Li et al. [2010; 2014a], it was found that using ultrasonic vibration technology, the size of water droplets in the early stage of frost formation was smaller, which could delay a frost formation process, and a schematic diagram of droplets falling off a cold surface under the action of ultrasonic vibration was also given, as shown here in Fig.2.8. In addition, a study by Sonobe [2015] found that the use of air jet technology could effectively remove the frost on a cold surface. In general, although these additional external forces could be effective in delaying frost formation or growth, their applications in practice were not actually common. This was because the use of ultrasonic vibration and air jet technologies would lead to high initial and operating costs and complex controls, while the mechanisms of electric and magnetic fields for frosting suppression were not yet sufficiently understood and thoroughly studied [Song et al., 2018; Tan et al., 2015; Wang et al., 2012; Liu et al., 2018].

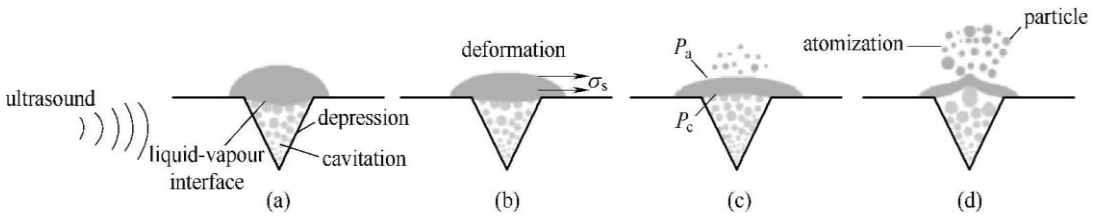

Fig. 2.8 Schematic diagram of droplets falling off a cold surface under the action of ultrasonic vibration [Li and Chen, 2014]

2.4 Studies of applying VS technology to A/C units and ASHPs

With the development of VS technology, more and more attention has been paid to its application to A/C units and ASHPs. The application of VS technology could enable VS operation control of compressors and air fans in A/C units or ASHPs.

During the past few decades, researchers have conducted much research on applying VS technology to A/C units, and simultaneous control of indoor air temperature and relative humidity can be achieved by using the VS control of compressor and indoor air fan in VS direct expansion (DX) A/C units. It has been shown in early open literature that the dehumidification performance of DX A/C units could be affected by supply air flow rate through an evaporator and DX evaporator surface temperature because these two could affect the condensation of water vapor on the evaporator surface, and evaporator surface temperature mainly depended on the evaporating temperature of the refrigerant being circulated in a DX A/C unit [Khattar et al., 1987; Chuah et al., 1998; Khattar and Handerson, 1999]. Varying the supply air fan speed of a VS DX A/C unit could cause the change in supply air flow rate, while changing both the compressor speed and supply air fan speed in a VS DX A/C unit could affect

the evaporating temperature. In a previous study by Krakow et al. [1995], a conventional proportional-integral-derivative (PID) control strategy was proposed to control indoor air relative humidity by adjusting supply air fan speed, and to control indoor air temperature by adjusting compressor speed. The speed changes would also affect the proportion of sensible and latent heat in the total output cooling capacity of an A/C unit.

In order to achieve the simultaneous control of the air temperature and relative humidity in a conditioned indoor space, it was necessary to study the cooling and dehumidification processes taking place in the evaporator of a VS DX A/C unit. Therefore, Li and Deng et al. [2007a; 2007b; 2007c] conducted a series of experimental studies on the inherent operating characteristics of an experimental VS DX A/C unit under different speed combinations of compressor and supply air fan. The results shown in Figs. 2.9-2.10, indicated that under a fixed inlet air condition, the experimental VS DX A/C unit could obtain different total output cool capacity and equipment sensible heat ratio (E SHR) at different speed combinations. The E SHR value could reflect the dehumidification performance of a VS DX A/C unit. A smaller E SHR value meant a better dehumidification performance. It was found from these studies that for a space cooling VS A/C unit, a higher compressor speed and lower supply air fan speed could lead to better dehumidification performance, while the higher compressor speed and higher supply air fan speed could lead to a higher total output cooling capacity. Xu et al. [2010] further conducted an experimental study on the inherent correlation between the total output cooling capacity and the E SHR values for an experimental VS DX A/C unit under different speed combinations of compressor and supply air fan. The experimental results are shown here in Fig. 2.11.

It can be seen that the total output cool capacity and E SHR of the experimental VS DX A/C unit were strongly coupled but constrained to each other within a quadrilateral. The study results of Li et al. [2014b], shown here in Fig. 2.12, revealed that different inlet air conditions, significantly affected the inherent correlation between the total output cooling capacity and the E SHR, resulting in the changes in the position or size of the inherent correlation quadrilaterals. These suggested that different inlet air conditions could have a significant impact on the cooling and dehumidification performances of a VS DX A/C unit.

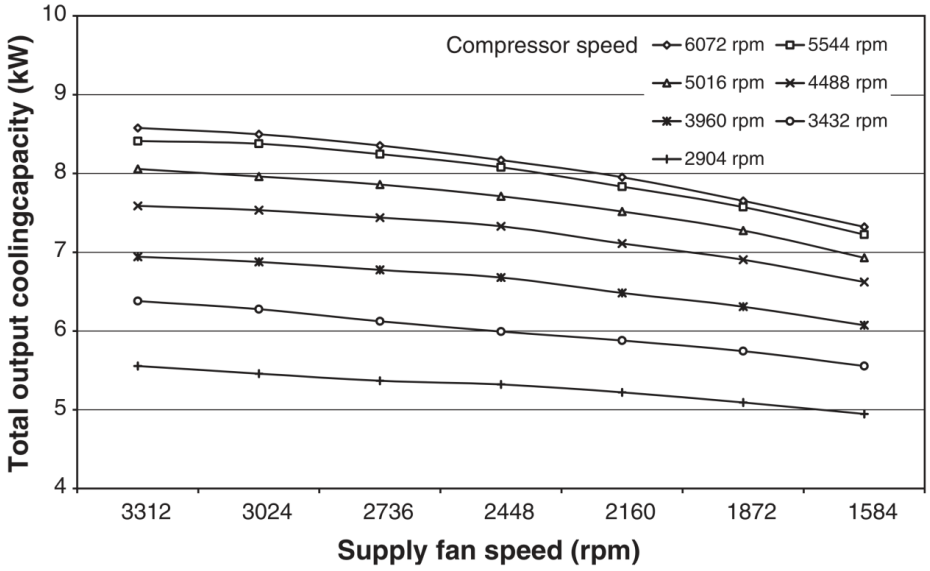

Fig. 2.9 The changes in the total output heating capacity from a VS DX A/C unit under different speed combinations of compressor and supply air fan at a fixed inlet air condition [Li and Deng, 2007a]

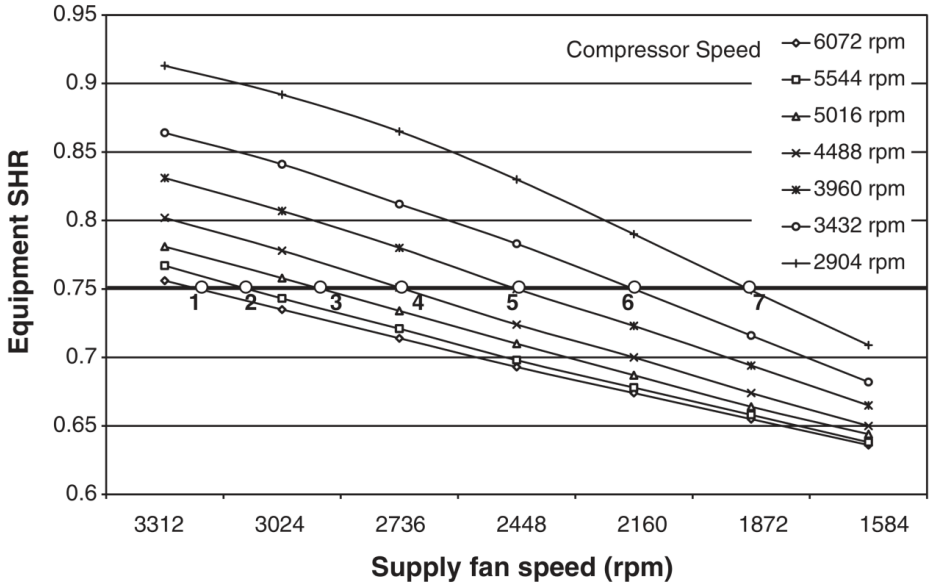

Fig. 2.10 The changes in the E SHR values of a VS DX A/C unit under different speed combinations of compressor and supply air fan at a fixed inlet air condition [Li and Deng, 2007a]

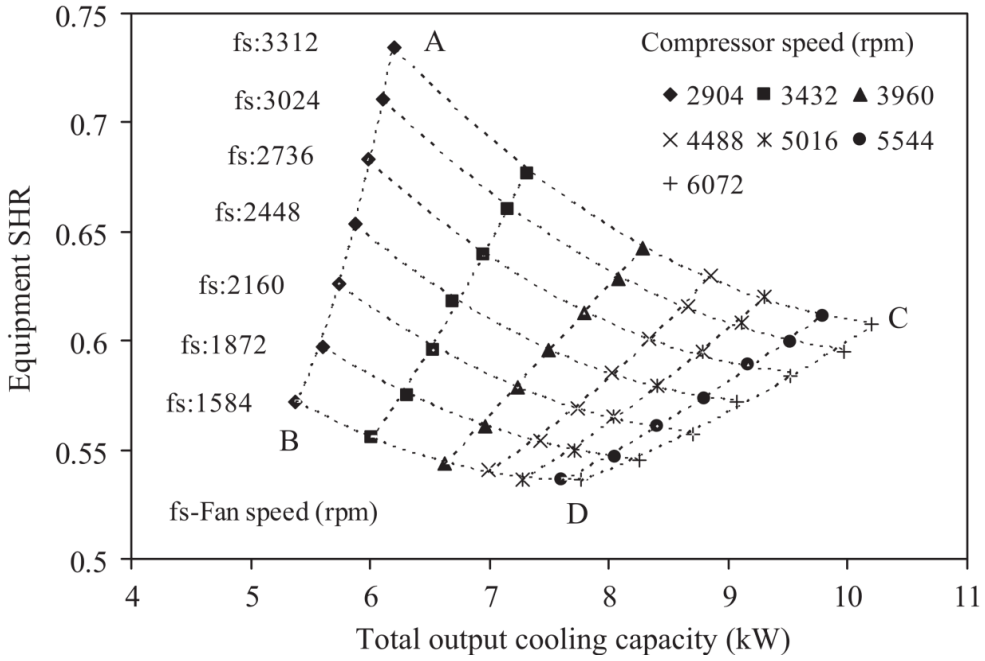

Fig. 2.11 The inherent correlation between the total output cooling capacity and E SHR of a VS DX A/C unit under different speed combinations of compressor and supply air fan at a fixed inlet air condition [Xu et al., 2010]

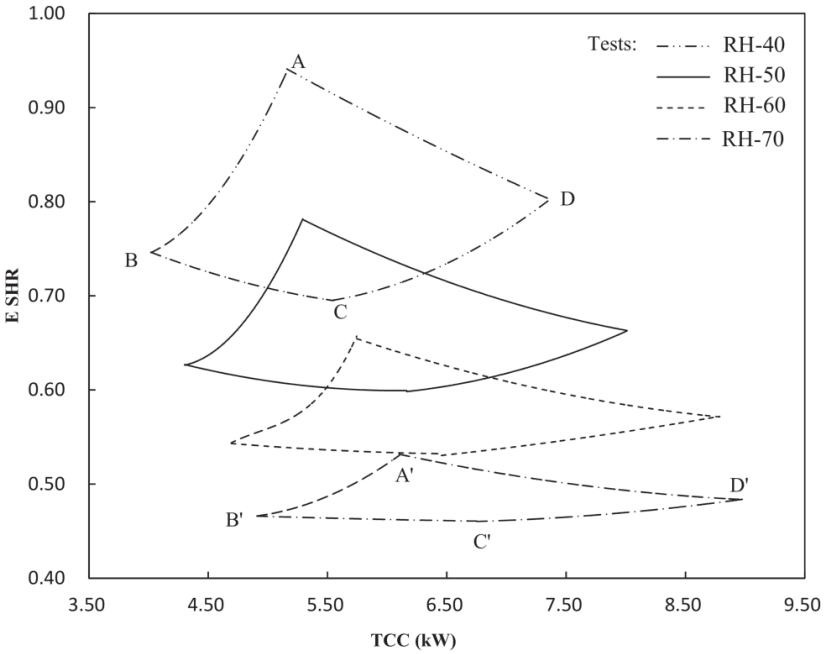

(a) under different inlet air relative humidity

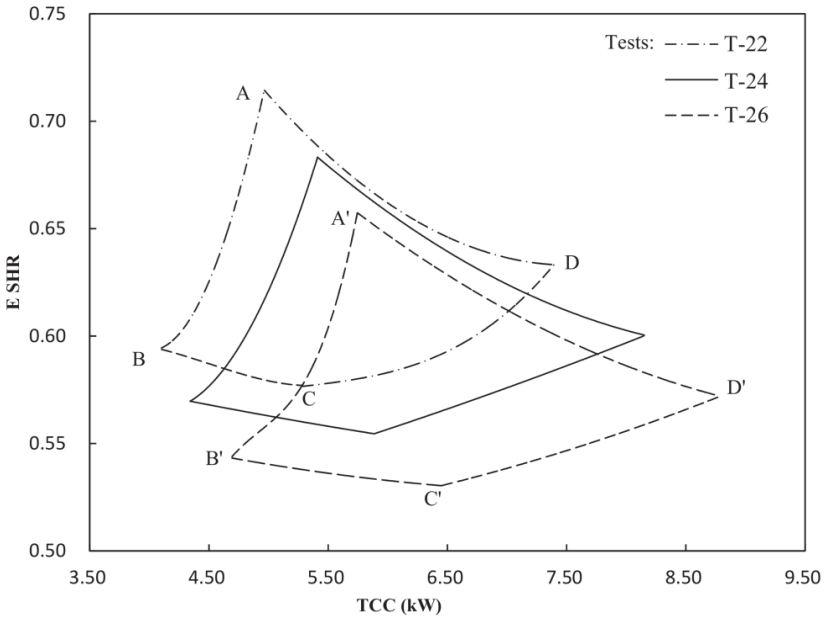

(a) under different inlet air temperature

Fig. 2.12 The quadrilaterals for inherent correlations between the total output cooling capacity and E SHR values of a VS DX A/C unit under different inlet air conditions [Li et al., 2014b]

In addition, the results of previous studies on the inherent operating characteristics of a VS A/C unit also suggested that the total cooling capacity and E SHR values could be used to control the air temperature and relative humidity in a conditioned indoor space. This provided a basis for developing novel strategies to control indoor air temperature and relative humidity simultaneously using DX A/C units. Li et al. [2017; 2018], Yan et al. [2018], Chen et al. [2018], and Yang et al. [2021], based on the above inherent correlations between the total cooling capacity and E SHR for VS DX A/C units, experimentally developed various control strategies to control the air temperature and relative humidity in a conditioned space, by varying the speed combinations of compressor and supply air fan, and their experimental results have shown that better control over indoor thermal comfort could be achieved.

From the above discussion on the inherent correlations, it may be naturally deduced that for a space heating VS DX ASHP unit, changing its compressor speed and outdoor air fan speed could also affect the air flow rate and the surface temperature of the outdoor coil (i.e., evaporator), which could in turn significantly affect the frosting on its outdoor coil surface. However, while the application of VS ASHPs became more and more popular because of its high efficiency and good operating stability, the research on the effects of VS operation on frosting suppression for a VS ASHP unit was rather limited. In an experimental study on the application of VS ASHPs in severe cold regions, Wei et al. [2020] have found that different compressor speeds of a VS ASHP unit had a significant impact on the frosting performance of the unit, and developed a new frosting map for VS ASHPs under different compressor speed, as shown here in Fig. 2.13. It was shown that with an increase in compressor speed, the operation status of a VS ASHP unit could change from frost-free to severe frosting.

However, only the effect of compressor speed change on frosting performance was considered.

In addition, Liang et al. [2020] proposed a characteristic index, named CICO, considering the configuration and operating parameters of an ASHP unit to evaluate its frosting suppression performance, as follows:

$$CICO = \frac{GF}{\left(nV_c\right)^2} \tag{2.2}$$

where G is outdoor air flow rate (m^3/s), F the outdoor coil surface area, n the compressor speed, and V_c the compressor displacement.

As seen from the above equation, CICO was related to a number of operational parameters of a space heating VS ASHP, such as outdoor air flow rate, compressor speed, outdoor coil surface area and compressor displacement. Frosting severity levels at different CICO values are shown in Fig. 2.14 [Liang et al., 2020]. It was suggested that a larger CICO value would lead to a better frosting suppression performance of an ASHP unit, and a higher air flow rate and lower compressor speed could result in a larger CICO value. Therefore, it can be seen that the different compressor speeds and outdoor air fan speeds could lead to different frosting suppression performances of a VS ASHP unit, but the influences of both speed changes on its total output heating capacity were not yet considered.

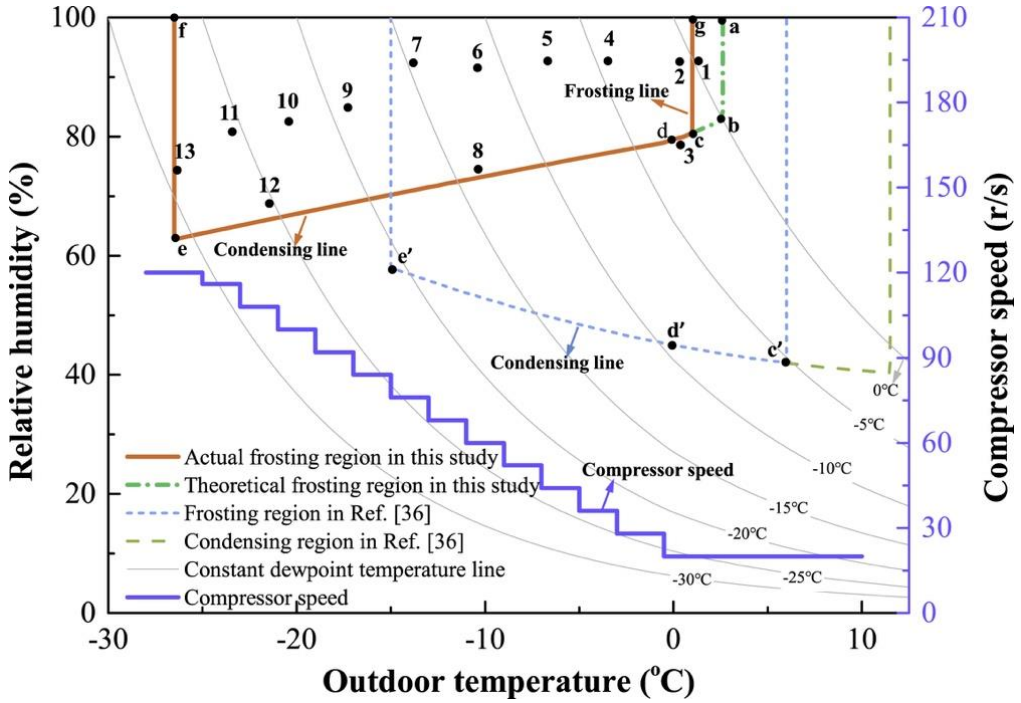

Fig. 2.13 A new frosting map for a VS ASHP unit under different compressor speeds developed by Wei et al. [2020]

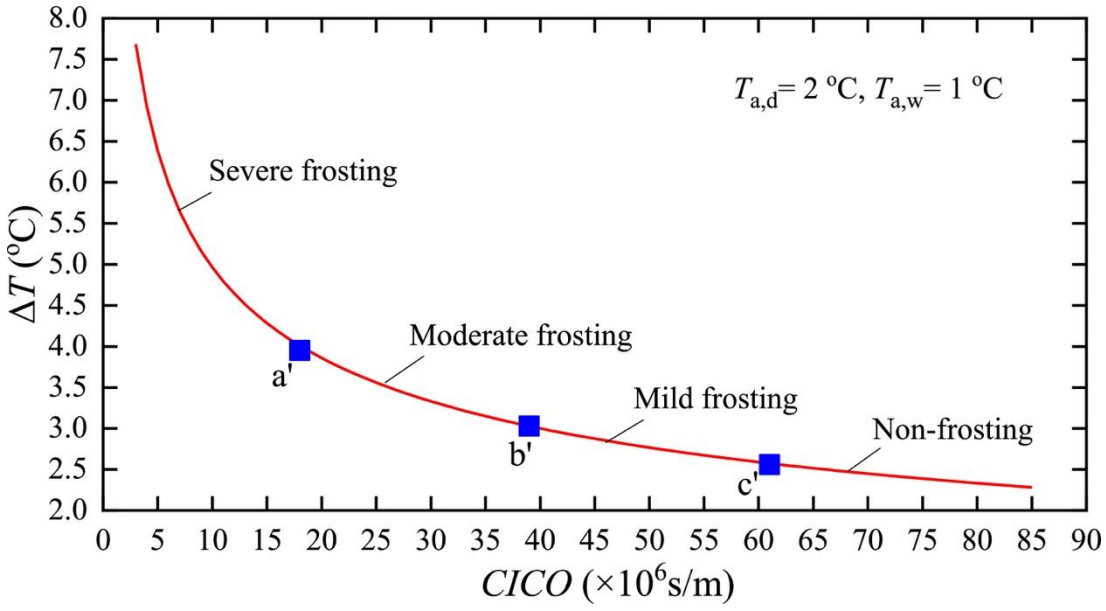

Fig. 2.14 The relationship between CICO values and frosting severity levels for ASHPs at outdoor ambient air condition of 2 °C (dry-bulb temperature) and 1 °C (wet-bulb temperature) [Liang et al., 2020]

2.5 Mathematical modeling of VS ASHP units

In addition to using experimental methods, mathematical modeling methods are also widely used in studying the operating performances and frosting related issues for ASHPs. This is because using mathematical modeling can not only save the research cost but also provide research flexibility of varying system configurations and operating parameters [Sami, 1993; Sami and Zhou, 1995; Choi and Kim, 2003]. In the field of heating, ventilation and air conditioning engineering, mathematical models of various units/systems have been widely developed and applied to predict operating performances, help optimize unit/system design, formulate control strategies, and detect/diagnose operating faults [Qi and Deng, 2009].

For existing mathematical models of ASHPs and frosting, they can be divided into two categories, namely, empirical models and physical models. An empirical model was developed based on the actual experimental data, which were first processed by statistical analysis, and then used to summarize into a mathematical relationship amongst various parameters. Empirical modeling methods mainly included regression analysis, polynomial curve fitting and artificial neural network (ANN). However, due to the imperfection and limitations of these methods, there have been still some unsolvable problems in the empirical modeling study [Diaz et al., 1999; Ding, 2007; Pacheco-Vega et al., 2001; Singh et al., 2006]. On the other hand, a physical model was developed based on the detailed physical relationships amongst all operating parameters, based on fundamental theories of energy and mass conservations.

On the other hand, three common methods have been used to develop physical models, including distributed, lumped and partial-lumped parameter methods, for ASHP units. Distributed parameter modeling method can better reflect the distribution characteristics of each parameter, with a high accuracy, but it took much computation time to solve a distributed model, with a potential poor calculation stability [Qi and Deng, 2009]. In contrast, lumped parameter modeling method was relatively simple, but it was difficult to reflect the detailed parameter distribution characteristics within a system component. Therefore, it was usually used in studying the overall performance of an ASHP unit. Finally, partial-lumped parameter modeling method referred to dividing a system component in an ASHP unit into several distinct regions, but for each region, a lumped parameter modeling approach would be applied. For example, a condenser was usually assumed to have three regions, i.e., a superheated region, a two-phase region and a subcooled region, but an evaporator was usually assumed to have two regions, i.e., a two-phase region and a superheated region. The partial-umped parameter modeling method was a compromise between distributed and lumped parameter modeling methods [Deng, 2000; Domanski, 1991], because its predicating accuracy and calculation speed were between those of the other two modeling methods.

In addition, the currently established ASHP models may also be divided into dynamic models and steady-state models. The calculation speed when solving steady-state models was fast, with a better calculation stability However, steady-state modelling was not suitable for studies where transient responses of an ASHP unit needed to be considered.

Therefore, although the accuracy of predicted results, calculation speed and stability must be considered in any modeling studies, it was generally difficult to achieve a high level modelling performances for all the three aspects simultaneously, so that an appropriate modeling mothed should be selected based on the actual need in a modelling study [Ding, 2007].

A complete VS ASHP unit was made of six key components, namely, a VS compressor, an indoor coil, an outdoor coil, an expansion device, a VS outdoor air fan and an indoor air fan. In a modeling study, it was often to establish the sub-models for each of these key components first, and then to connect these sub-models to form a complete model. The sub-models for the key component in a VS ASHP unit have been extensively reported in previous literature, as summarized in this Section.

2.5.1 Compressor sub-model

The thermal characteristic parameters for a compressor, including its refrigerant mass flow rate, suction and discharge pressures/temperatures, compressor speed and input power, etc., were crucial for a complete VS ASHP unit. In a reported modeling study by Deng [2000], VS operation has been considered when establishing a VS compressor sub-model. A previous study [Ndiaye and Bernier, 2010] demonstrated that different heat and mass transfer processes took place in different types of the compressor. As a result, it was highly recommended that the mathematical sub-model of a compressor should be developed based on its type in accordance with its characteristics.

In general, a compressor sub-model can be either dynamic or steady-state one. For the former, its calculation was very complex and time-consuming, therefore, the latter was more commonly used [Rasmussen and Alleyne, 2004]. In a compressor steady-state sub-model, the start-up process of the compressor was not considered by assuming that the compressor reached the specified running speed instantaneously.

On the other hand, for the mathematical modeling of a VS ASHP unit, two methods for developing its compressor sub-model were used [Lu, 2003]. One was to use four indicators, namely, indicated efficiency, mechanical efficiency, motor efficiency and gas transmission coefficient, to illustrate the actual operating performance of the compressor, and then, based on these indicators, operating parameters such as electrical power to, and refrigerant mass flow rate through, the compressor can be derived. This method was more intuitive and can clearly show the relationship between compressor operating performances and its structural parameters. However, this method involved more parameters, and some of these parameters needed to be determined empirically, such as volume coefficient, pressure coefficient, temperature coefficient and leakage coefficient, etc., resulting a reduced calculation accuracy. In addition, some other parameters such as compressor structure, were difficult to obtain. For these reasons, an empirical method to develop the sub-model of a compressor was proposed [Li, 2013a]. It was based on the actual experimental data of a compressor, so that the correlations of its operating parameters can be fitted. For a specific compressor, this method may lead to a good modelling accuracy, with however limited applicability to other compressors.

2.5.2 Indoor coil sub-model

At present, a large number of indoor coil dynamic and steady-state sub-models have been proposed and successfully applied to various modeling studies for space heating ASHPs. For the modeling studies that needed to describe the dynamic responses to the changes in operating conditions, a dynamic sub-model should be used. Otherwise, a steady-state sub-model was sufficient. Both dynamic and steady-state sub-models of an indoor coil can be established by using three methods, i.e., the lumped parameter method, the distributed parameter method and the partial-lumped parameter method.

It has been shown that the lumped parameter method could be used to establish an indoor coil sub-model to estimate its steady-state performances without a phase transition in the indoor coil [Elmahdy et al., 1977; Jacobi and Goldschmidt, 1990; Vargas and Parise, 1995; Rasmussen and Alleyne, 2004]. However, the accuracy of predicted results by using a lumped parameter indoor coil sub-model can be unacceptable. Therefore, in order to imprvoe the modeling accuracy and applicability to an indoor coil with a phase transition, a distributed parameter method for indoor coil modeling was proposed [MacArthur, 1984; Jia et al., 1995; Bensafi et al., 1997]. The distributed parameter modelling method would divide an indoor coil into several control volumes, and then used the lumped parameter modeling method for each control volume. This method may both complicate the calculation process and require more calculation time. Therefore, a partial-lumped parameter method for indoor coil modeling was proposed, with its modeling accuracy and required calculation time between those of the lumped parameter and distributed parameter modeling methods [Domanski, 1991; Deng, 2000; Rasmussen and Alleyne, 2004]. The partial-lumped

parameter modeling method may divide an indoor coil into three regions, i.e., a superheated region, a two-phase region and a subcooled region, and then used the lumped parameter modeling method for each region.

2.5.3 Outdoor coil sub-model

Both outdoor coils and indoor coils were heat exchangers. Therefore, for an outdoor coil in a space heating ASHP unit under frost-free operation, its modeling method was similar to that of an indoor coil as mentioned in Section 2.5.2, but an outdoor coil would be divided into two regions (a two-phase region and a superheated region). For an outdoor coil of a space heating ASHP unit under frosting operation, the effects of frosting on the heat exchange of the outdoor coil must be considered. Therefore, when establishing an outdoor coil sub-model under frosting conditions, a frosting module should be integrated into the sub-model. In this section, frosting models and outdoor coil sub-models integrated with a frosting module are reviewed.

Based on different simplified geometries, such as a flat plate or cylindrical surface, researchers have developed various frosting models and conducted modeling studies under different frosting conditions. O'Neal and Tree [1985] firstly investigated numerically the frost formation on parallel plates. In the later studies conducted by Hermes et al. [2014] and Nascimento et al. [2015], semi-empirical correlations for the frost density on flat plates and parallel plate channels were established. Lee et al. [1997] developed a mathematical model for the frost formation on a cold flat surface by considering the molecular diffusion of water vapor, and heat generated by the sublimation of water vapor in the frost layer. A one-dimensional transient formulation

was presented by Ismail et al. [1999] to numerically evaluate the parameters involved in the process of frost formation on a flat cold surface with air flow, such as the frost layer surface temperature, frost density and thickness distribution along the air flow direction and the void fraction. Na and Webb [2004] proposed an improved supersaturated frosting model, in which supersaturated water vapor on the frost layer surface was considered, the correlation of frost thermal conductivity was improved, a rationally tortuosity factor was used, and local frost density variation could be calculated. In a numerical study conducted by Lee et al. [2003], empirical correlations of the heat transfer coefficients and the diffusion equation for a frost layer were used to establish a mathematical model to predict the frost formation on a cold flat surface.

On the other hand, in the past decades, a large number of models based on actual outdoor coil geometries have been developed to describe the frost growth on an outdoor coil surface and predict its effects on the operating performances of the outdoor coil. Oskarsson [1990] and Oskarsson et. al [1990] developed different models to examine the performances of outdoor coils with dry, wet and frosting surfaces. Kondepudi and O'Neal [1993] developed a mathematical model to predict the performances of an outdoor coil with the changes in the thickness of a frost layer. Chen et al. [2000] developed a physical model of frost growth on a plate-fin outdoor coil, in which the frost layer was modeled as a transient one-dimensional porous medium coupled to a two-dimensional transient heat transfer model of the fins. Yao et al. [2004] developed a mathematical model of frosting for the air-side of an outdoor coil in an ASHP unit, and it was shown that this model could accurately predict the operating performances of the ASHP unit under frosting conditions. Cui et al. [2011] used a computational fluid dynamics (CFD) model to predict the frosting behavior on

a tube-and-fin outdoor coil. Recently, Zhang [2021] and Zhang et al. [2022] established a new mathematical model to predict the frost distribution and growth on a tube-and-fin outdoor coil of an ASHP unit. This new model consisted of two sub-models, one for frosting on the edges of the windward fins and the other for frosting on the tube and fin surfaces. Model validation and a follow-up modeling study suggested that this model could accurately predict the heat transfer performance on the air side of the outdoor coil and the frost growth characteristics on the surfaces of the fins and tube.

2.5.4 Expansion device sub-model

The expansion device in a VS ASHP unit was used to regulate the refrigerant pressure and mass flow rate. There were three types of expansion devices commonly used in ASHP units. The first was a capillary tube, which was low cost but had a limited regulation range, making it unsuitable for ASHPs or A/C units that required precise refrigerant flow control [Xia et al., 2019]. The second type was a thermostatic expansion valve, which had a longer regulation response time and lower accuracy. The last type was an electronic expansion valve (EEV), which had high sensitivity and flexibility, making it more suitable for VS ASHPs with a large adjustment range of the refrigerant mass flow. Therefore, EEVs have been increasingly used in VS ASHP units

An EEV may typically be modeled by using a steady-state model due to its low thermal inertia. An isenthalpic orifice equation can be used to model an EEV since the refrigerant expansion in an expansion valve was generally considered as an isenthalpic

process [MacArthur and Grald, 1987]. Empirical models based on experimental data for EEVs were also established to predict the refrigerant flow through EEVs [Damasceno et al.,1990; Park et al., 2007; Ye et al., 2007]. With the help of multivariate analysis, a regression expression for the flow factor of an EEV was established by Xue et al. [2008], and it has been demonstrated that the flow factor was influenced by the geometry parameters of an EEV, the refrigerant temperature and pressure at the inlet, and the refrigerant thermo-physical characteristics. Furthermore, Li [2013b] added an expansion factor to the Bernoulli Equation for a short orifice in order to build a correlation for the refrigerant mass flow coefficient of an EEV. The degree of subcooling and the EEV opening were the only two crucial variables employed to establish the coefficient correlation. A further experimental examination has revealed that the refrigerant mass flow coefficient correlation could describe the refrigerant flow behavior in an EEV with minimal error.

2.5.5 Air fan sub-model

Both indoor and outdoor air fans were used to circulate the required air flow rates through indoor or outdoor. In an ASHP unit, an indoor air fan was used to supply heated air to a heated indoor space, for thermal comfort. The relationships between the key operating parameters of an air fan, such as air volume, pressure, power input and efficiency, etc., can be generally described based on air fan performance curves. For a VS air fan, its operating performance curves under different speed can be determined by the test data from manufacturers or using the fan performance law, which stated that an increase in air fan pressure was proportional to the square of the change in air fan speed. Mei and Levermore [2002] employed a ten-neuron sigmoid

ANN model to describe the operating performance of a VS air fan, and it has been suggested that using this method could have a closer approximation with the actual experimental data.

2.5.6 Complete models for ASHP units

With the availability of the sub-models for all the key components, as reviewed in Sections 2.5.1 to 2.5.5 in a VS ASHP unit, a complete model for a VS ASHP may be obtained by connecting all sub-models along the flow direction of both refrigerant and air, with the outputs from one component being the inputs to the component downstream.

2.6 Conclusions

ASHPs are one of the key devices to help realize carbon emission reduction and mitigate global energy crisis. It can be expected that ASHPs will have a broader market prospect worldwide. However, frosting on the outdoor coil surface of a space heating ASHP unit remained a key problem restricting its further development. From the literature review presented in this Chapter, it can be seen that although a large number of theoretical, experimental and modeling studies have been carried out on frosting fundamentals and frosting suppression for space heating ASHPs, there are still issues that need to be addressed. The conclusions of this literature review presented in this Chapter are as follows:

Firstly, according to the frosting mechanism, for a space heating ASHP unit, frost will appear and accumulate on its outdoor coil surface when the temperature of its outdoor coil surface is lower than both the dew point temperature of ambient air and freezing point temperature of water. Frosting can not only reduce the output heating capacity and COP of an ASHP unit, but also deteriorate its operational stability and safety. In order to ensure the normal operation of the ASHP unit, periodic defrosting has to be carried out. This would increase the energy consumption of the unit and negatively impact indoor thermal comfort. Therefore, effectively suppressing or delaying frosting is of great significance to improving the operating performances of ASHPs, in terms of operating energy efficiency and stability.

Secondly, various measures for frosting suppression or frost-free operation of ASHPs have been developed in previous studies. However, most of these measures have not been successfully applied in practice due to their own inadequacies, such as high initial or operating cost, poor lifespan, complicated manufacturing process, and unclear frosting suppression mechanism. Therefore, further developments on effective frosting suppression measures are highly needed.

Thirdly, currently, the reported frosting suppression measures included changing air temperature and relative humidity at the outdoor coil inlet, modifying the structure or surface property of the outdoor coil or fins, and using external forces. However, studies on frosting suppression by changing or controlling outdoor air flow rate or outdoor coil surface temperature, which can significantly affect frosting on an outdoor coil surface are very limited.

Fourthly, previous related studies on controlling VS DX A/C units suggested that using different compressor and outdoor air fan speed combinations can lead to different evaporating temperatures, resulting in different outdoor coil surface temperatures, and effecting simultaneous indoor air temperature and humidity control. Performance maps relating E SHR and the total output cooling capacity from a VS DX A/C unit were also developed. It was therefore possible that the same method of using different compressor and outdoor air fan speed combinations can be applied to an VS ASHP unit, to effectively change its evaporating temperature in its outdoor coil, thereby affecting the condensing of water vapor and frosting on the outdoor coil surface. However, changing these two speeds will also cause different total output heating capacities from a VS ASHP unit. There have been currently no systematic studies on the combined effects of varying compressor and outdoor air fan speeds of a VS ASHP unit on frosting suppression performances and heating performances. No performance maps for a VS ASHP unit that can be used to comprehensively evaluate its outdoor coil surface state and the total output heating capacity under different speed combinations to guide its frosting suppression operation without compromising the required output heating capacity, are currently available.

Fifthly, there have been extensive modeling studies of ASHPs. The sub-models of the key components of a VS ASHP unit are extensively available. These sub-models can be linked to establish a complete mathematical model for a VS ASHP unit. The model of a VS ASHP unit so established can be used to numerically study the operating performances of the VS ASHP unit, in terms of frosting suppression and output heating capacity, performances at different ambient conditions, under different compressor and outdoor air fan speed combinations.

The literature review presented in this Chapter has demonstrated that changing compressor and outdoor air fan speed combinations of a VS ASHP unit to change its outdoor coil surface temperature can be very effective for frosting suppression. As a result, performance maps that can illustrate the comprehensive relationship between frosting suppression and space heating performances of a VS ASHP unit under different speed combinations should be developed. These maps can be applied to guide frosting suppression operation of a VS ASHP unit and used as a basis for developing a suitable control strategy for VS ASHP units to achieve frosting suppression as much as possible while outputting the required heating capacity. These will be addressed in this Thesis.

Chapter 3

Proposition

3.1 Background

As mentioned in Chapters 1 and 2, ASHPs have been promoted and used in many parts of the world to achieve energy-saving and emission-reduction. It is expected that ASHPs will have an even wider application in the future. However, for space heating ASHPs, frosting is still an urgent issue that needs to be addressed. Frosting brings a series of negative effects to the safe and efficient operations of ASHPs, and defrosting also requires additional energy consumption. Therefore, in order to mitigate these negative effects, a large number of frosting suppression measures for space heating ASHPs have been proposed, but most of them have not been successfully put into practical application due to their various drawbacks.

On the other hand, using different compressor and outdoor air fan speeds in a VS ASHP unit may result in different outdoor coil surface temperatures, thus leading to different frosting suppression performances. This may also result in different output heating capacity from the unit. However, only scattered studies on applying VS technology to frosting suppression for ASHPs may be identified, and there have been a lack of systematic and comprehensive studies on the effects of varying compressor and outdoor air fan speeds on the frosting suppression and heating performances of a VS ASHP unit, which is very important for guiding the frosting suppression operation of ASHPs.

3.2 Project title

In order to enable to study systematically and comprehensively frosting suppression by varying simultaneously compressor and outdoor air fan speeds, condensing-frosting performance maps for a space heating VS ASHP unit, have been proposed and studied experimentally and by modeling in this Thesis. These maps could show the relationship between the output heating capacity and outdoor coil surface status (dry, wet or frosting) of the unit and may therefore be used as the basis to guide the efficient and safe operation of the ASHP unit for frosting suppression while at the same time providing the required output heating capacity. Therefore, the research project reported in this Thesis is entitled "Experimental and modeling studies on developing a condensing-frosting performance map for a variable speed air source heat pump unit for frosting suppression".

3.3 Aims and objectives

The research project presented in this Thesis has the following aims and objectives:

1) To build an experimental VS ASHP unit to experimentally investigate the frost suppression and heating performances of the unit under different speed combinations of its compressor and outdoor air fan, and install a visualization system to observe and record its outdoor coil surface status (i.e., dry, wet and frosting);

2) To experimentally study the comprehensive effects of varying the compressor and outdoor air fan speeds of the experimental VS ASHP unit on its outdoor coil surface temperature and output heating capacity from the unit, and to experimentally develop condensing-frosting performance maps for the experimental unit under different speed combinations at different ambient air conditions;

3) To establish and experimentally validate a physical-based mathematical model for the experimental VS ASHP unit. The validated model will be used to obtain condensing-frosting performance maps for the experimental unit at other non-experimental unit configurations and non-experimental ambient conditions;

4) To develop a novel control strategy for the experimental VS ASHP unit based on its condensing-frosting performance maps to achieve frosting suppression operation while providing the required output heating capacity.

3.4 Research methodologies

Both experimental and modeling methods will be adopted in the research project reported in this Thesis.

Firstly, to facilitate the all the intended experimental work, an experimental VS ASHP unit will be established in an existing environmental chamber in the Department of Building Environment and Energy Engineering, The Hong Kong Polytechnic University. A visualization system to observe and record the outdoor coil surface

status will be included in the experimental unit. IN addition, there are two simulated spaces in the environmental chamber, one for a simulated indoor heated space, the other simulated outdoor space. All operating parameters of both the experimental VS ASHP unit and the environmental chamber can be real-time monitored and recorded.

Secondly, by using the established experimental VS ASHP unit, extensive experimental work will be carried out to study the frost suppression and heating performances of the experimental unit under different speed combinations of its compressor and outdoor air fan, and to develop its condensing-frosting performance maps.

Thirdly, a physical-based mathematical model for the experimental VS ASHP unit will be established by referring to some of previously reported related mathematical models. The established model will be validated using experimental data collected from the experimental unit, and the validated model will be used in further modeling study to obtain condensing-frosting performance maps for the experimental VS ASHP unit at other non-experimental unit configurations and ambient air conditions.

Finally, based on the developed condensing-frosting performance maps for the experimental VS ASHP unit, a novel control strategy for its frosting suppression operation will be experimentally developed. Controllability tests will be carried out to examine the controllability and effectiveness of the developed novel control strategy.

Chapter 4

An experimental setup for the experimental VS ASHP unit

4.1 Introduction

As stated in Chapter 3, to achieve effective frosting suppression operation of ASHPs, in the research project reported in this Thesis, it was intended to develop condensing-frosting performance maps for the experimental VS ASHP unit and to further develop a novel control strategy for its frosting suppression operation by experimental and modeling methods. Therefore, a special experimental setup was established in the Multi-Function Chamber Laboratory in the Department of Building Environment and Energy Engineering, The Hong Kong Polytechnic University, to facilitate the required experimental work. The established experimental setup mainly consisted of the experimental VS ASHP unit, the environmental chamber and a built-in computerized data monitoring and acquisition system for the setup.

In this Chapter, the experimental setup established for this research project is reported in detail. A detailed description of the experimental ASHP unit is firstly given, followed by detailing the environmental chamber. Finally, the built-in computerized data monitoring and acquisition system is detailed.

4.2 The experimental VS ASHP unit

The experimental VS ASHP unit, in accordance with its schematics shown in Fig. 4.1, was specially established in the environmental chamber. R410A was employed as the

refrigerant in the experimental VS ASHP unit. The nominal output heating capacity of the unit was at 8.5 kW at a nominal operating ambient condition of 7 ^{o}C (air dry-bulb temperature, $T_{a,\,d}$) and 6 ^{o}C (air wet-bulb temperature, $T_{w,\,d}$).

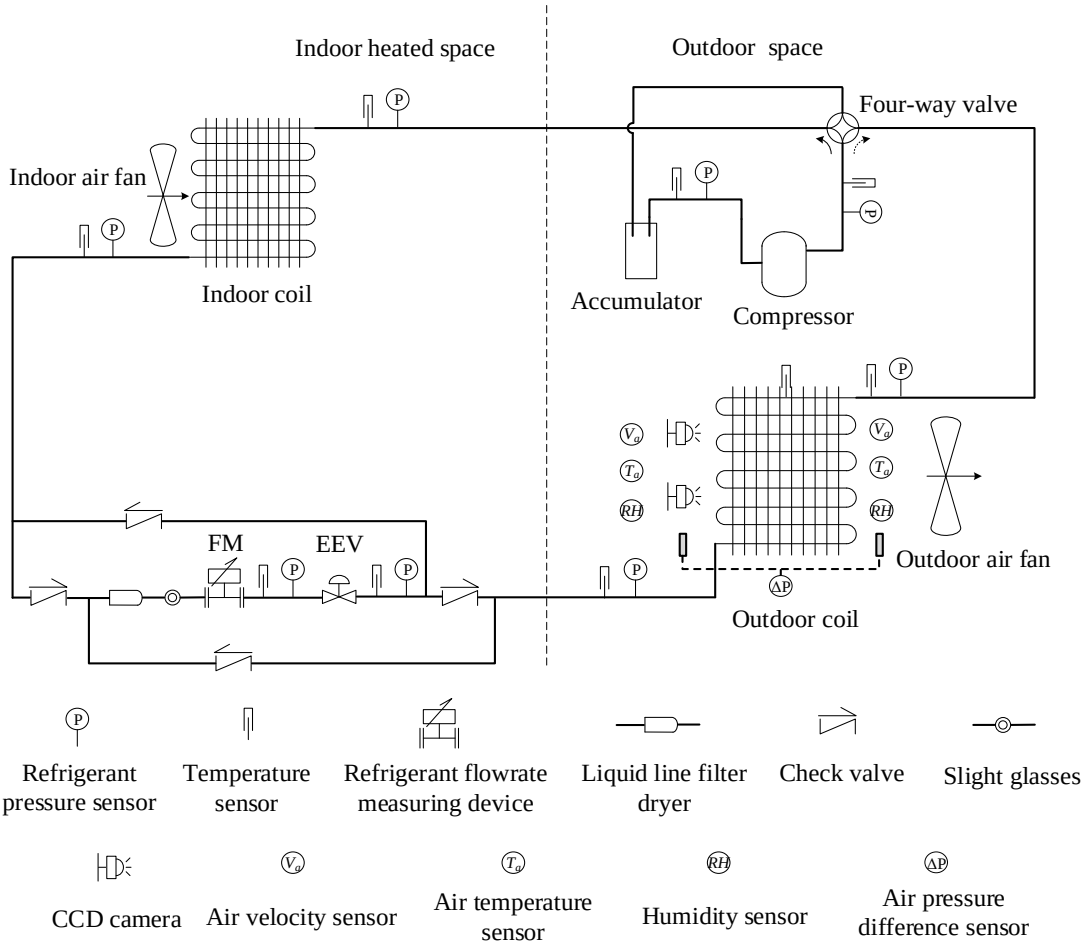

Fig. 4.1 The schematics of the experimental VS ASHP unit established in the existing environmental chamber

The experimental VS ASHP unit consisted of a VS compressor, a multi-circuit outdoor coil, a VS outdoor air fan, an EEV, a four-way reverse valve, a multi-circuit indoor coil and an indoor air fan. As shown in Fig. 4.1, the VS compressor, outdoor coil and VS outdoor air fan were placed in the outdoor space of the environmental chamber,

while the indoor coil and indoor air fan in the indoor heated space. In order to facilitate the operation of the experimental VS ASHP unit under different compressor speeds and outdoor air fan speeds, both the compressor and the outdoor air fan had built-in variable speed drives (VSDs), so that their speeds could be varied manually or by program. The outdoor coil had seven circuits arranged in three rows, and each circuit had the same heat transfer surface area. Furthermore, the operation of the EEV was regulated by a built-in PID controller, which was used to control the degree of refrigerant superheat. The detailed technical specifications of the key components in the experimental VS ASHP unit are listed in Table 4.1.

Table 4.1 Details of the key components in the experimental ASHP unit

Components	Specifications	Values / Details
Compressor	Number	1
	Compressor type	Rolling rotor; variable speed
	Adjustable frequency (Hz)	20-100
	Rated heating capacity (kW)	8.5
	Refrigerant	R410A
Outdoor Coil	Dimensions (mm)	650 (L) × 700 (H) × 60 (W)
	Fin type	Wavy
	Fin thickness (mm)	0.1
	Fin pitch (mm)	2.5
	Tube External diameter (mm)	9.52
	Tube pitch (mm)	25
	Number of tube rows	3
	Number of tube circuits	7
	Surface areas (m^2)	26.77
Outdoor Air Fan	Number	1
	Fan type	Variable speed
	Air flow rate (m^3/s)	0-1.57

4.3 The environmental chamber

The existing environmental chamber had two rooms, as shown in Fig. 4.2, one as the simulated indoor heated space and the other as the simulated outdoor space. The dimension of each room was 3.7 m (L) × 3.7 m (W) × 3.3 m (H). In the simulated indoor heated space, the required experimental winter space heating load was created and maintained by a separate DX A/C unit and a sensible and latent load generation unit (LGU). On the other hand, the required experimental ambient air conditions in the simulated outdoor space were created and maintained by the experimental VS ASHP unit, a booster air cooling unit and an LGU, where the air temperature and air relative humidity could be controlled from -3 ^{o}C to 30 ^{o}C and 30 % to 90 %, respectively.

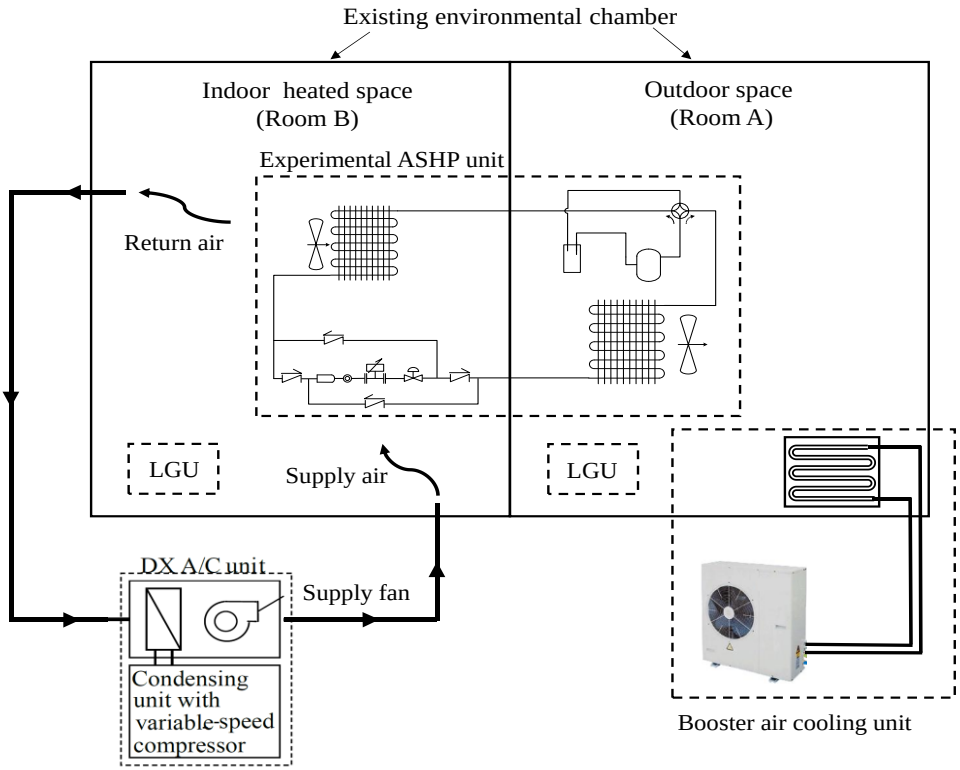

Fig. 4.2 The schematics of the experimental setup

4.4 The computerized data monitoring and acquisition system

Various high-precision sensors and transducers to measure the key operating parameters of the experimental setup, such as temperatures, pressures and flow rates of air and refrigerant, etc., and all measured data were computerized for real-time monitoring and recording.

On the refrigerant side of the experimental VS ASHP unit, a refrigerant mass flow meter was installed between the indoor coil and the EEV to measure the refrigerant mass flow rate. Both of temperature sensors and refrigerant pressure sensors were installed at the inlet to, and the outlet from the compressor, the EEV, the indoor coil and the outdoor coil to measure the refrigerant temperatures and pressures at these locations.

On the air side of the experimental VS ASHP unit, air temperature, air velocity and air relative humidity sensors were installed on both the windward and leeward sides of both the indoor coil and the outdoor coil. An air pressure difference sensor was also installed on the air side of the outdoor coil to measure the air pressure difference across it. In addition, in order to measure the outdoor coil surface temperature, a total of sixteen temperature sensors were installed at different positions of each of the seven outdoor coil circuit, as illustrated in Fig. 4.3. The average value of the reading of the sixteen temperature sensors was taken as the averaged outdoor coil surface temperature.

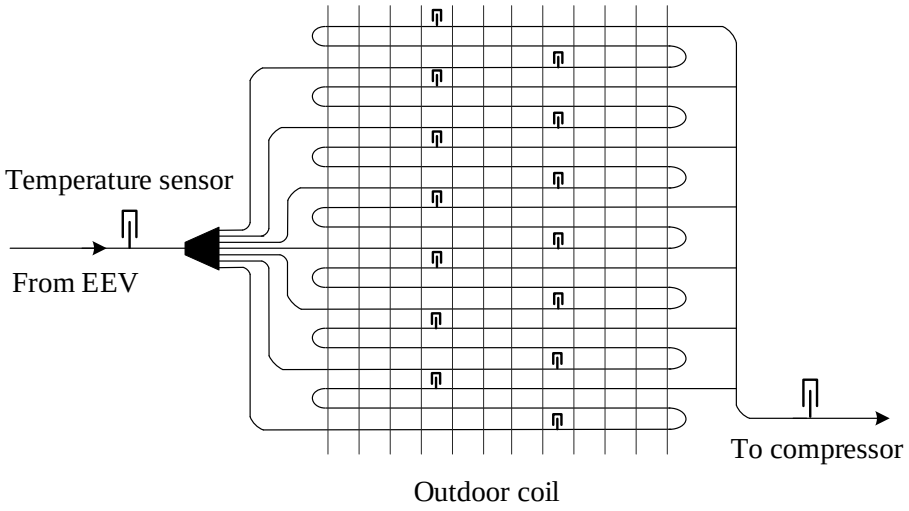

Fig. 4.3 The schematics of the installation positions for the outdoor coil surface temperature sensors

On the other hand, a visualization system was built into the experimental VS ASHP unit to real time observe and record its outdoor coil surface status (dry, wet or frosting). It included two charge-coupled device (CCD) cameras installed on the windward side of the outdoor coil, as shown in Fig. 4.1. One was a panoramic CCD camera used to observe the surface status of the entire outdoor coil on the windward side, the other a 100× microscopic zoom CCD camera used to observe the fin surface status of the outdoor coil.

Furthermore, power meters were also installed in the experimental setup to monitor and record the energy consumptions of the compressor and the outdoor air fan. The data sampling interval for all operating parameters in the experimental setup was 1 s. The details of all the sensors and transducers used in the experimental setup and the uncertainties of the experimental parameters are given in Tables 4.2 and 4.3, respectively.

Table 4.2 Details of the sensors / transducers used in the experimental setup

Sensors / transducers	Accuracy	Range
Temperature sensor (PT1000)	± 0.15 ℃	-50-200 ℃
Humidity sensor	± 3.0 %	0-100 %
Refrigerant pressure sensor	± 0.4 %	0-40 bar
Air velocity sensor	± 0.1 m/s	0-5 m/s
Air pressure difference sensor	± 0.1 Pa	-125-125 Pa
Refrigerant mass flowmeter	± 0.5 %	0-0.07 kg/s
Electronic scale	± 0.001 kg	0-30 kg
Power meter	± 1.0 %	/
CCD camera 1	/	100× micro magnification
CCD camera 2	/	panoramic

Table 4.3 Uncertainties of indirectly measured parameters

Experimental parameters	Uncertainty	Unit
Total output heating capacity	± 1.83 %	kW
COP	± 1.96 %	/

4.5 Conclusions

An experimental setup was specially established for carrying out the required experimental work of the research project reported in this Thesis. It consisted of the experimental VS ASHP unit, the environmental chamber and the built-in computerized data monitoring and acquisition system.

The compressor and the outdoor air fan speeds of the experimental VS ASHP unit could be varied manually or by program according to experimental requirements. All necessary operating parameters of the experimental setup could be measured, monitored and recorded real time by the installed high-precision sensors and transducers. The installation of the visualization system on the experimental VS ASHP unit enabled the real-time observation of the outdoor coil surface status.

The availability of the established experimental setup was expected to provide an essential basis in carrying out the experimental work in the research project reported in this Thesis, such as experimentally investigating the frosting suppression and heating performances of the experimental VS ASHP unit under different speed combinations of its compressor and outdoor air fan, developing condensing-frosting performance maps, validating a mathematical model for the experimental VS ASHP unit and examining a novel control strategy for frosting suppression operation of the experimental VS ASHP unit.

The photo images showing the experimental setup are given in Appendix.

Chapter 5

An experimental study of developing condensing-frosting performance maps for the experimental VS ASHP unit for frosting suppression

5.1 Introduction

As mentioned in previous Chapters, developing an effectiveness frosting suppression measure is critical for a space heating ASHP unit, as this can ensure efficient operation of the ASHP unit and help reduce the extra energy consumption caused by frosting and defrosting. However, most of current reported frosting suppression measures have not been successfully implemented in practice due to their own shortcomings, such as high initial and running costs, poor stability and durability.

On the other hand, with the advancement of VS technology, VS ASHPs are increasingly used due to their improved energy efficiency level and operational reliability. For a VS ASHP unit, varying its compressor and outdoor air fan speeds may result in different outdoor coil surface temperatures, thus leading to different frosting suppression performances. This may however also result in different output heating capacity from the unit. Currently, there are only scattered studies on applying VS technology to frosting suppression for ASHPs, and the simultaneous impact of heating performances was often neglected.

In order to study the effects of varying compressor and outdoor air fan speeds on the frosting suppression and heating performances of a VS ASHP unit systematically and comprehensively, a condensing-frosting performance map for a VS ASHP unit was

proposed and developed in the research project reported in this Thesis, which could clearly show the three different statuses of the outdoor coil surface, i.e., dry, wet or condensing and frosting, at different levels of the total output heating capacities, when the ASHP was operated at different speed combinations of the compressor and outdoor air fan and under different ambient conditions.

Therefore, an experimental study on developing condensing-frosting performance maps for the space heating experimental VS ASHP unit reported in Chapter 4 has been carried out, and the study results are reported in this Chapter. Firstly, experimental procedures and operating conditions corresponding to different ambient conditions are described in detail. Secondly, experimental results and related discussions are reported. Finally, a conclusion is given

5.2 Experimental procedures and operating conditions

As known, water vapor in humid air would only condense on an outdoor coil surface when its surface temperature was below the dew point of humid air but above the freezing point of water. However, frost would appear on the outdoor coil surface when its surface temperature was below both the dew point of humid air and the freezing point of water. Therefore, surface temperature of the outdoor coil in the experimental ASHP unit can be used to judge the occurrence of either condensing or frosting on outdoor coil surface. Furthermore, since the total output heating capacity was also a key parameter that directly described the space heating performance of an ASHP, in this experimental study, therefore, the operating characteristics and condensing-frosting performance maps to be developed for the outdoor coil in the experimental

ASHP unit were expressed in terms of the relationships between its surface temperatures and total output heating capacities of the experimental unit under different combinations of the compressor and outdoor air fan speeds, and at different operating outdoor ambient conditions.

With reference to the Specifications in the Chinese National Standards of GB/T 18430. 2-2016 [2016] and JB/T 13573-2018 [MIIT China, 2018], which were similar to those in Air-Conditioning, Heating, and Refrigeration Institute (AHRI) Standard 210/240-2008 [2008] and the weather data in typical meteorological years in China, three typical operating winter outdoor ambient conditions for ASHPs were used in this experimental study, as shown in Table 5.1. In Operating Condition 1, the ambient condition in the simulated outdoor space in the environmental chamber as described in Chapter 4 was maintained at $T_{a,\,d}$ of 7.0 ± 0.2 °C and $T_{a,\,w}$ of 6.0 ± 0.2 °C, which was the nominal design condition for space heating ASHPs specified by the above-mentioned Chinese National Standard [2016]. In Operating Condition 2, the average outdoor ambient conditions in the typical meteorological year in Shanghai City, China, in winter, i.e., $T_{a,\,d}$ of 4.5 °C, and $T_{a,\,w}$ of 3.0 °C, were used, to reflect the severeness of frosting in locations having a not-too-low ambient air temperature but at a higher air humidity. Furthermore, in Operating Condition 3, the ambient condition in the outdoor space was maintained at $T_{a,\,d}$ of 2.0 ± 0.2 °C and $T_{a,\,w}$ of 1.0 ± 0.2 °C, which was the standard frosting condition specified by the above-mentioned Chinese National Standard [2016]. In all the experiments, air temperature inside the simulated indoor heated space was maintained at 20.0 ± 0.5 °C, in accordance with the Chinese National Standard of GB 50736-2012 [2012] for space heating in winter. The speed of indoor air fan was maintained constant at 30 Hz, and its air flow rate was 0.7 m^3/s.

Table 5.1 Operating Conditions for the experimental ASHP unit

Operating Condition	Ambient conditions in the outdoor space		
	$T_{a,\,d}$	$T_{a,\,w}$	RH
1	7.0 ± 0.2 ℃	6.0 ± 0.2 ℃	86.8 ± 3.0 %
2	4.5 ± 0.2 ℃	3.0 ± 0.2 ℃	78.4 ± 3.0 %
3	2.0 ± 0.2 ℃	1.0 ± 0.2 ℃	83.9 ± 3.0 %

For all Operating Conditions, the experimental ASHP unit was operated under different combinations of compressor and outdoor air fan speeds. As using all possible speed combinations was neither practical nor necessary, representative discrete experimental compressor and outdoor air fan speeds were selected, as shown respectively in Tables 5.2 and 5.3. In addition, considering the stability and safety of the compressor operation, the variation range of the compressor speed was selected from 20 % to 80 % of the maximum speed, i.e., from 20 Hz to 80 Hz. Therefore, a total of 42 speed combinations were used at each Operating Conditions. At each speed combination, when the fluctuation in refrigerant mass flow rate was not greater than 6.0 %, a steady-state operating condition of the experimental ASHP unit was assumed to arrive. Then, the experimental ASHP was operated for 30 minutes and its key operating parameters, such as outdoor coil surface temperature, and the total output heating capacity, were then measured / evaluated at the fixed sampling interval of 1s. During the 30 minute-period, no significant changes in outdoor air flow rate may be observed, even when the outdoor coil was frosted.

The instantaneous total output heating capacity of the experimental ASHP unit was evaluated by

$$Q = m_r \left(h_{cr,\,i} - h_{cr,\,o} \right) \tag{5.1}$$

where m_r is the measured refrigerant mass flow rate, $h_{cr,\,i}$ and $h_{cr,\,o}$ refrigerant enthalpy at the inlet to, and the outlet from the indoor coil, evaluated based on the measured indoor coil temperatures and refrigerant pressures.

When reporting the experimental results in Sections 5.3.1 and 5.3.2, the average data over the 30 minute-period for the total output heating capacity and outdoor coil surface temperature were used. Hence, in Sections 5.3.1 and 5.3.2, all these parameters are referred to their 30 minute-average values. The primary consideration of using 30 minutes duration was due to the operational stability during frosting operation. During a frosting operation, in the first 30 minutes after reaching a stable operation, the experimental ASHP can be operated steadily without significant changes in the air flow rate and output heating capacity. However, thereafter, more and more frost would deposit on outdoor coil surface, leading to an increased air flow resistance, and thus a gradually reduced outdoor air flow rate and output heating capacity. Hence, meaningful experimental results may not be obtained.

In addition, at Operating Condition 1, i.e., $T_{a,\,d}$ of 7.0 ℃ and $T_{a,\,w}$ of 6.0 ℃, a further comparative experiment was carried out to examine the operational characteristics of the outdoor coil in the experimental ASHP unit operated at three different states of condensing, condensing/frosting and frosting, but at almost the same total output heating capacity. The results of the comparative experiment are detailed in Section 5.3.3.

Table 5.2 Selected experimental compressor speeds in all Operating Conditions

	1	2	3	4	5	6	7
VSD Frequency (Hz)	20	30	40	50	60	70	80
% of the maximum speed	20 %	30 %	40 %	50 %	60 %	70 %	80 %

Table 5.3 Selected experimental outdoor air fan speeds in all Operating Conditions

	1	2	3	4	5	6
Rotational speed (rps)	205	328	451	574	697	820
Air flow rate (m^3/s)	0.53	0.74	0.94	1.15	1.36	1.57
% of the maximum speed	25 %	40 %	55 %	70 %	85 %	100 %

5.3 Experimental results and discussions

Extensive experimental work on the operational characteristics to obtain the condensing-frosting performance maps of the experimental ASHP unit under different speed combinations of the compressor and outdoor air fan at the three Operating Conditions has been carried out. Variable surface temperatures of the outdoor coil and the total output heating capacities of the experimental ASHP unit were obtained, and are reported in this Section.

5.3.1 The outdoor coil surface temperature and the total output heating capacity at different compressor and outdoor air fan speed combinations

Experimental work at the three Operating Conditions was carried out to study the changes in both outdoor coil surface temperature and the total output heating capacity of the experimental ASHP unit when its compressor and outdoor air fan speeds were varied. Since the trends of the changes for the obtained experimental results at the three Operating Conditions were similar, in this Section therefore, only those at Operating Condition 1 are detailed.

The experimental data of outdoor coil surface temperature and the total output heating capacity of the experimental ASHP unit obtained in Operating Condition 1 at different compressor speeds and outdoor air fan speeds are shown in Fig. 5.1 and Fig. 5.2, respectively. In Fig. 5.1, the dew point line of ambient air at Operating Condition 1 of 4.96 ℃ and the frosting point line of water of 0 ℃ are also shown.

As seen in Fig. 5.1, surface temperature of the outdoor coil was increased as outdoor air fan speed was increased, or as compressor speed was decreased. When the compressor was operated at a higher speed, the rate of increase in surface temperature of the outdoor coil would be greater than that at a lower speed, as outdoor air fan speed was increased. In addition, it was observed that three different states of the outdoor coil surface, i.e., dry, wet or condensing and frosting, could occur, as the speeds of compressor and outdoor air fan were varied. When outdoor coil surface temperature was higher than the dew point of ambient air, in the simulated outdoor space, outdoor coil surface was dry. When the surface temperature was lower than both the dew point

of ambient air and the freezing point of water, frosting took place. Furthermore, when the surface temperature was at between the dew point and the freezing point, condensing occurred. It was also observed that the same outdoor coil surface temperature could be resulted in when the experimental ASHP unit was actually operated under different speed combinations of the compressor and outdoor air fan.

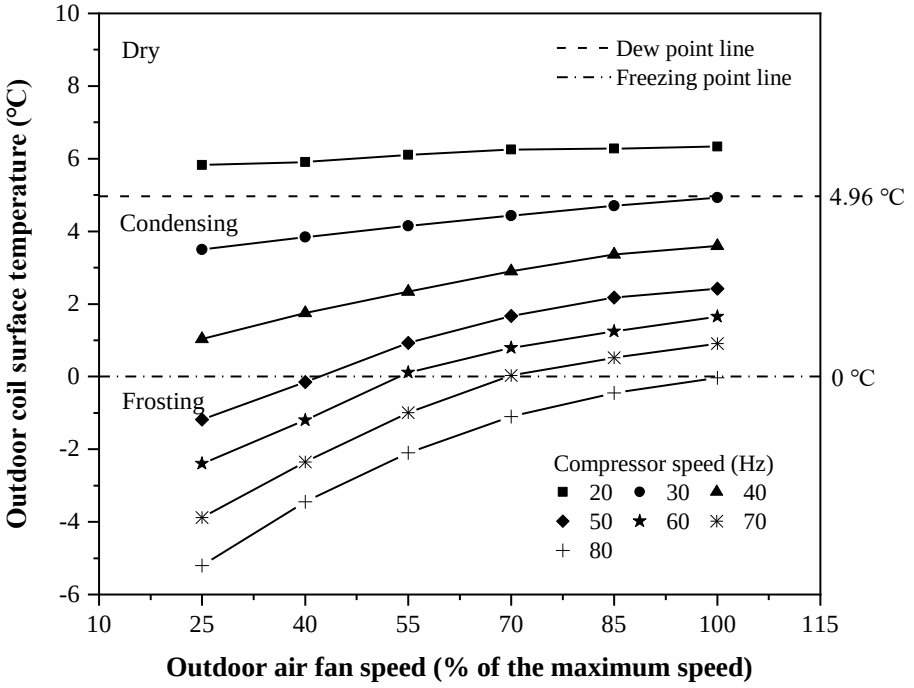

Fig. 5.1 The changes in outdoor coil surface temperature of the experimental ASHP unit under different compressor and outdoor air fan speed combinations at Operating Condition 1

On the other hand, Fig. 5.2 shows that increasing both compressor speed and outdoor air fan speed would increase the total output heating capacity of the experimental ASHP unit. However, the changes in outdoor air fan speed at a lower compressor speed would influence less on the changes in the total output heating capacity than that at a higher compressor speed. Moreover, when the experimental ASHP unit was

operated at different speed combinations of the compressor and outdoor air fan, a wide range of the total output heating capacity, from the minimum of 2.1 kW to the maximum of 12.2 kW, could be resulted in.

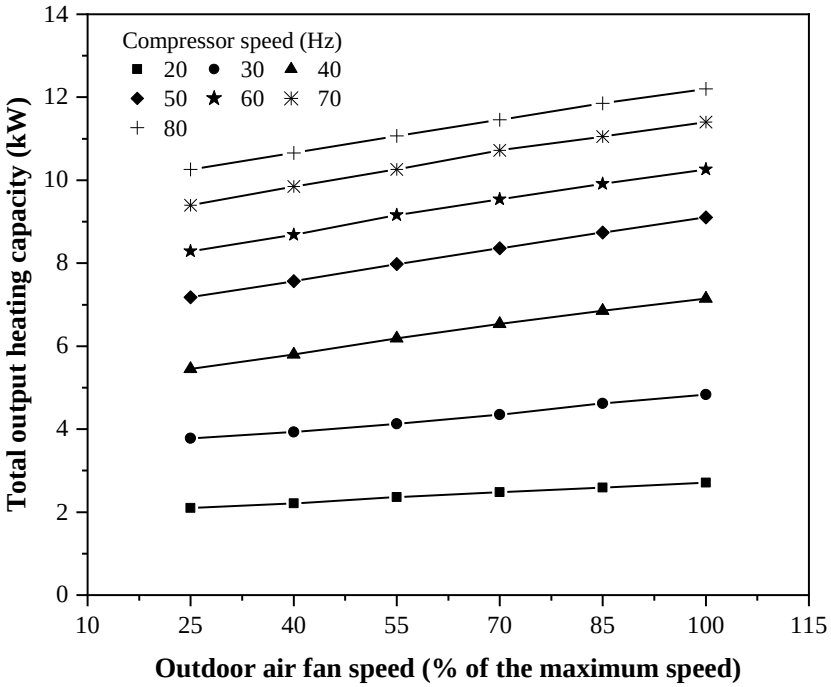

Fig. 5.2 The changes in total output heating capacity from the experimental ASHP unit under different compressor and outdoor air fan speed combinations at Operating Condition 1

As seen from Fig. 5.1 and Fig. 5.2, the rates of changes in both outdoor coil surface temperature and the total output heating capacity were different, when the speeds of compressor and outdoor air fan were varied. An increase in compressor speed would increase refrigerant mass flow rate, and hence the total output heating capacity. If outdoor air flow rate however remained unchanged, the increase of refrigerant mass flow rate would result in a decrease in refrigerant evaporating temperature, and thus outdoor coil surface temperature, which was not conducive to frosting suppression.

On the other hand, at a fixed compressor speed, an increase in the outdoor air fan speed would increase air flow rate passing through the outdoor coil. A higher Reynolds Number of air flow would result in greater heat transfer between air and outdoor coil surface, leading to both a higher total output heating capacity and a higher evaporating temperature, which was beneficial to frosting suppression.

5.3.2 The condensing-frosting performance maps for the experimental ASHP unit at the three Operating Conditions

Using the experimental data obtained, which are discussed in Section 5.3.1, condensing-frosting performance maps for the outdoor coil in the experimental ASHP unit at the three Operating Conditions were developed, as shown in Figs. 5.3, 5.5 and 5.6, respectively.

Fig. 5.3 shows the developed condensing-frosting performance map at Operating Condition 1, which was obtained by X-Y plotting the total output heating capacities from the experimental ASHP unit and the outdoor coil surface temperatures, at different speed combinations. As seen from Fig. 5.3, at different compressor and outdoor air fan speed combinations, the total output heating capacity of the experimental ASHP unit and its outdoor coil surface temperature were mutually constrained but correlated within a trapezoid A-B-C-D. At point A, the experimental ASHP unit was operated at the minimum experimental compressor and outdoor air fan speeds of 20 % and 25 % of their respective maximum speeds, and at point C, maximum experimental compressor and outdoor air fan speeds of 80 % and 100 % of their respective maximum speeds. At point B, the experimental ASHP unit was

operated at its maximum experimental compressor speed but minimum experimental outdoor air fan speed, and at point D, minimum experimental compressor speed but maximum experimental outdoor air fan speed. Also as seen, varying compressor speed from 20 Hz to 80 Hz and the outdoor air fan speed from 25 % to 100 % result in significant variations in outdoor coil surface temperature and the total output heating capacity of the experimental ASHP unit, at between -5.2 ℃ and 6.33 ℃, and between 2.1 kW and 12.2 kW, respectively. However, it was not possible to produce those outdoor coil surface temperature / total output heating capacity combinations outside the trapezoid A-B-C-D.

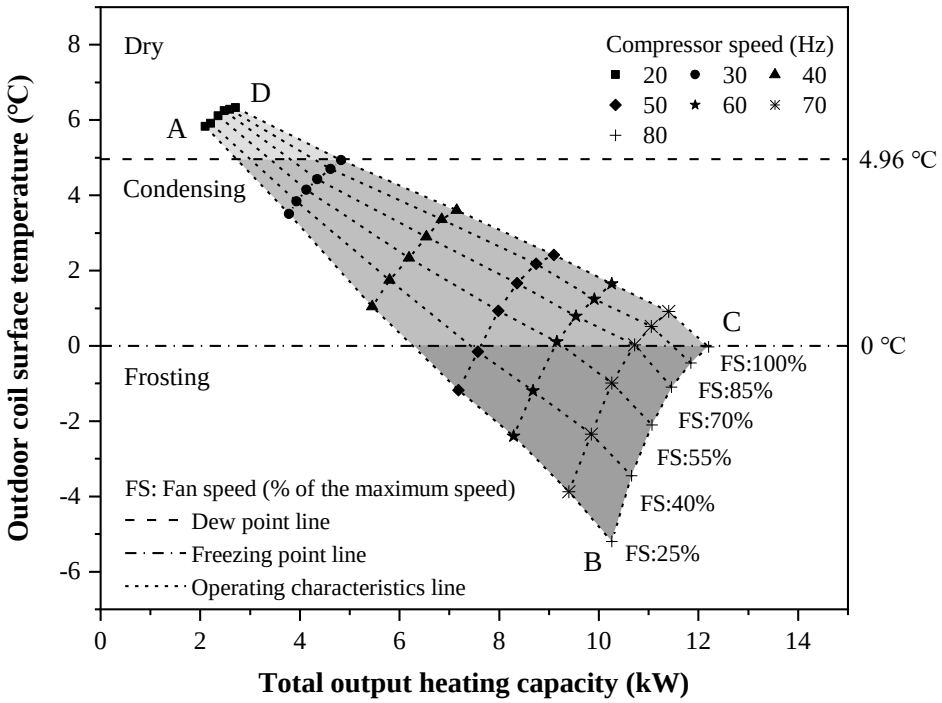

Fig. 5.3 The developed condensing-frosting performance map of the experimental ASHP unit at Operating Condition 1

On the other hand, the trapezoid A-B-C-D may be divided into dry, condensing or wet and frosting regions, using the ambient air dew point (4.96 ℃) line and water freezing point (0 ℃) line. As seen, a small area above the ambient air dew point (4.96 ℃) line was the dry region, and an area below the water freezing point (0 ℃) line the frosting region. In between, there lay the condensing region. Thus, with such a performance map, the condensing / frosting characteristics on the outdoor coil surface, corresponding to different total output heating capacities could be clearly expressed. Additionally, the states of the outdoor coil surface, i.e., dry, condensing or wet and frosting, as reflected by the three regions in Fig. 5.3, were also confirmed by the imagines captured by the CCD cameras installed in the experimental setup, as shown in Fig. 5.4. The Figure illustrates the states of the outdoor coil surface when the experimental ASHP unit was operated for 30 minutes under different speed combinations of compressor and outdoor air fan (20 Hz & 100 %, 50 Hz & 100 % and 80 Hz & 25 %), respectively, at Operating Condition 1.

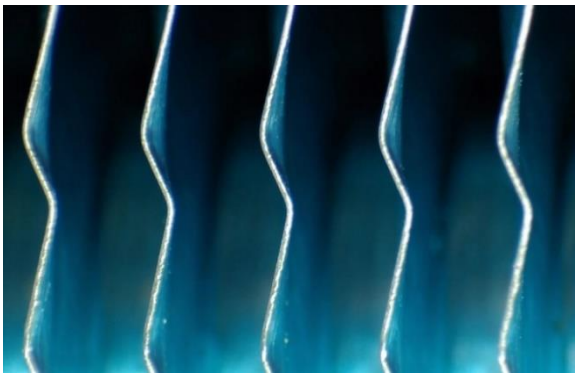

(a)

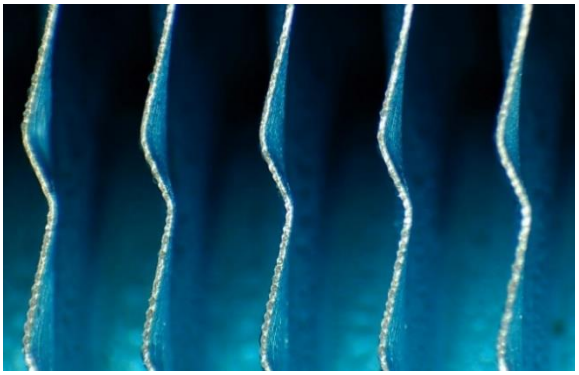

(b)

(c)

Fig. 5.4 The images of the surface states of the outdoor coil (a) Dry; (b) Condensing; (c) Frosting

Furthermore, Fig. 5.5 and Fig. 5.6 show the developed condensing-frosting performance maps in Operating Conditions 2 and 3, respectively. As seen, at different speed combinations, outdoor coil surface temperatures and total output heating capacities were also mutually constrained but correlated within a trapezoid A'-B'-C'-D' in Fig. 5.5, and a trapezoid A"-B"-C"-D" in Fig. 5.6, respectively. In Fig. 5.5, at Operating Condition 2, since the dew point of ambient air at 4.5 ℃ ($T_{a,d}$) / 3.0 ℃ ($T_{a,w}$), i.e., 1.07 ℃ was quite close to the freezing point of water, condensing region area was relatively small, as compared to the other two regions. However, at Operating

Condition 3, ambient air dew point was already lower than the freezing point of water, so that there was no condensing region, but with a very large frosting region, as shown in Fig. 5.6. This suggests that at Operating Condition 3, or the standard frosting condition of 2.0 ℃ ($T_{a,d}$) / 1.0 ℃ ($T_{a,w}$), the experimental ASHP unit would be operated at frosting condition for most of its operating points. Hence, the condensing-frosting performance map at Operating Condition 3 could reflect an unfortunate fact that when the ambient air temperature was close to, or below the freezing point of water, an ASHP was very likely to be operated at frosting condition.

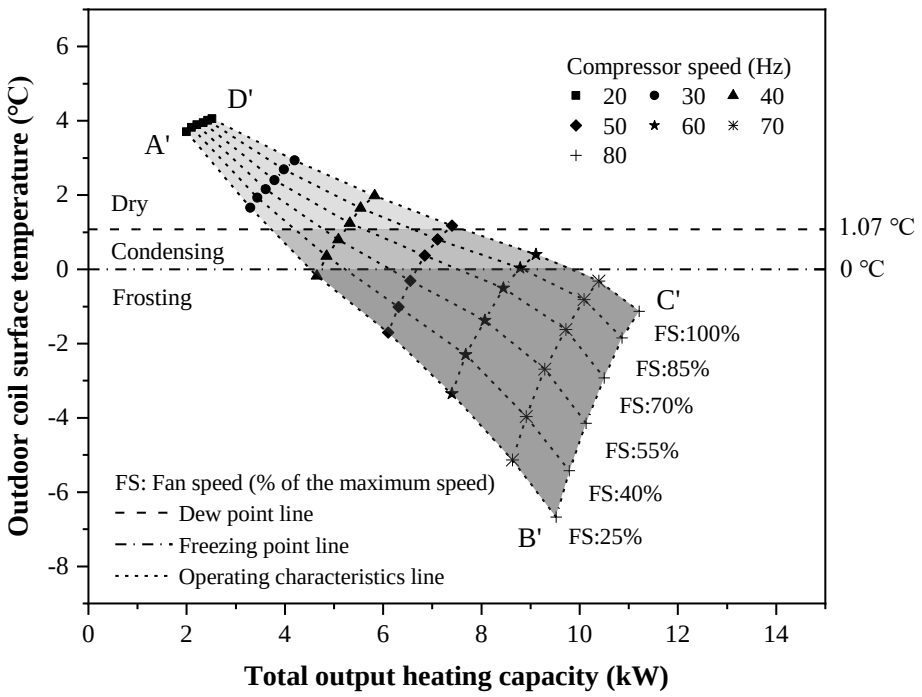

Fig. 5.5 The developed condensing-frosting performance map of the experimental ASHP unit at Operating Condition 2

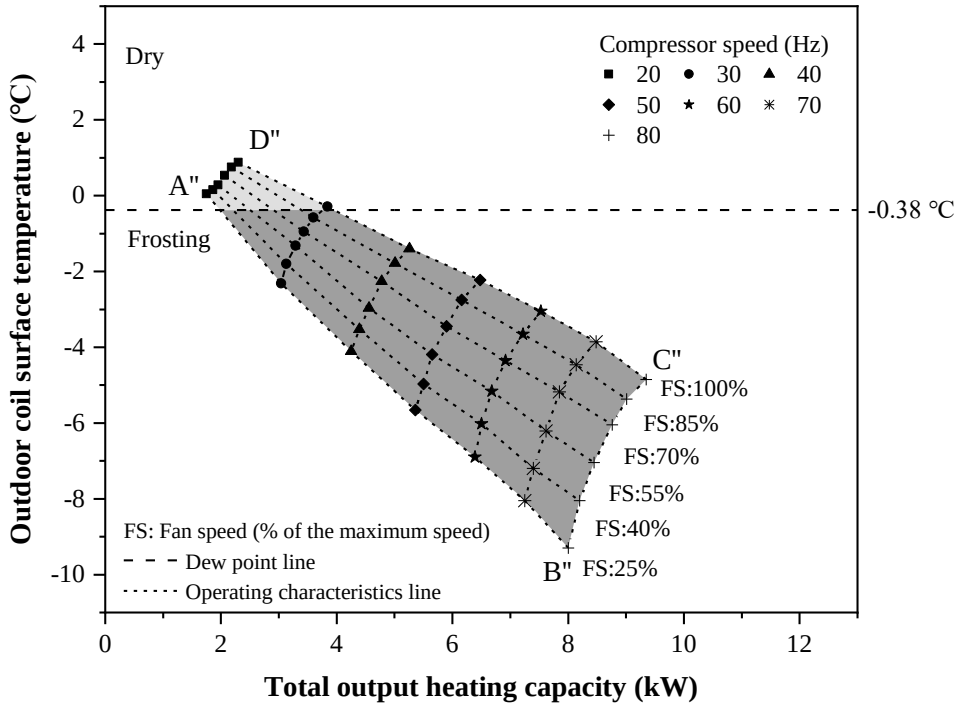

Fig. 5.6 The developed condensing-frosting performance map of the experimental ASHP unit at Operating Condition 3

In Fig. 5.7, the three performance maps at the three Operating Conditions, shown in Figs. 5.3, 5.5 and 5.6, respectively, are illustrated together. It can be seen that although the shapes and variation trends of the three maps were similar, their exact positions and areas in Fig. 5.7 were different. At different operating outdoor ambient conditions, the horizontal length for each of the maps, which represented the output heating performance of the experimental ASHP unit, varied greatly. When the outdoor ambient temperature was increased from 2 ℃ to 4.5 ℃, and from 2 ℃ to 7 ℃, the percentage changes in corresponding output heating capacity were at 21 % and 33 %, respectively. This demonstrated that at a higher outdoor ambient temperature, the adjustable heating capacity range of the ASHP unit between its maximum and minimum would also be increased accordingly. Furthermore, it can also be seen that since the total output heat capacity of the ASHP unit was significantly affected by its

operating environmental conditions, the trapezoid would move along the horizontal axis under different operating environmental conditions. In addition, the condensing-frosting performance maps shown in Fig. 5.7 also shows that as the operating ambient temperature decreases, the experimental ASHP unit is likely to operate at a frosted state. However, at a relatively higher ambient air temperature, it was actually possible to achieve frost-free operation through varying compressor and outdoor air fan speeds.

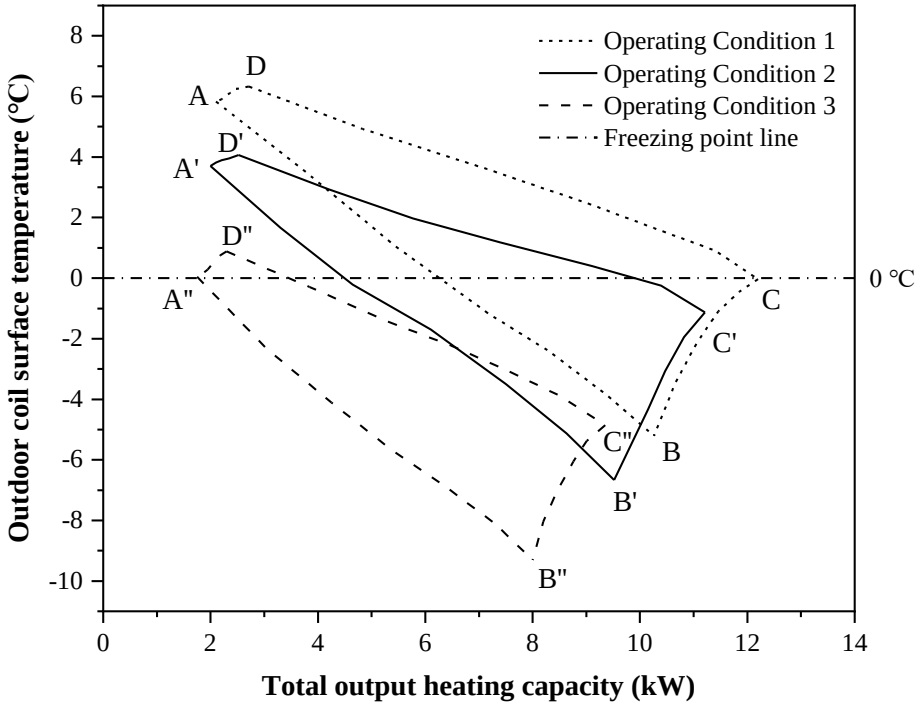

Fig. 5.7 The developed condensing-frosting performance maps of the experimental ASHP unit at the three Operating Conditions

5.3.3 The comparative experiment at Operating Condition 1

It can be seen from the developed condensing-frosting performance maps shown in Section 5.3.2 that the experimental ASHP unit can operate at different speed combinations to output the same total heating capacity, but at different outdoor coil surface states. In order to achieve frosting suppression by means of using different speed combinations of compressor and outdoor air fan while maintaining the required output heating capacity, the operational characteristics of the outdoor coil in the experimental ASHP unit when operated at three different statuses of condensing, condensing / frosting and frosting, but at almost the same total output heating capacity (with relative error of less than 1 %) should be further looked into in details. Therefore, a further comparative experiment at Operating Condition 1 was carried out to critically exam i) the duration when the experimental ASHP unit can be continuously operated without the need for defrosting, ii) the operating efficiency during their continuous operating period in terms of coefficient of performance (COP) as evaluated by Eq. (5.2) below, and iii) the surface temperature of outdoor coil. As shown in Fig. 5.8, three operating points, E, F and G were selected from the condensing-frosting performance map shown in Fig. 5.3. In Fig. 5.8, point E locates in the condensing region and point G the frosting region, but point F very close to the freezing point line, and may therefore be regarded as at the state of condensing/frosting. The experimental data obtained in Operating Condition 1 were then re-visited, and the speed combinations and the average total output heating capacities during the 30 minute-period at the above three operating points were at 9.10 kW, 9.16 kW and 9.10 kW, respectively, as shown in Table 5.4. It can be seen that all the relative errors were less than 1 % (based on the output heating capacity at point E).

The instantaneous COP of the experimental ASHP unit was evaluated by

$$COP = \frac{Q}{W} \tag{5.2}$$

where W is the measured total power input to both the compressor and outdoor air fan, of the experimental ASHP unit.

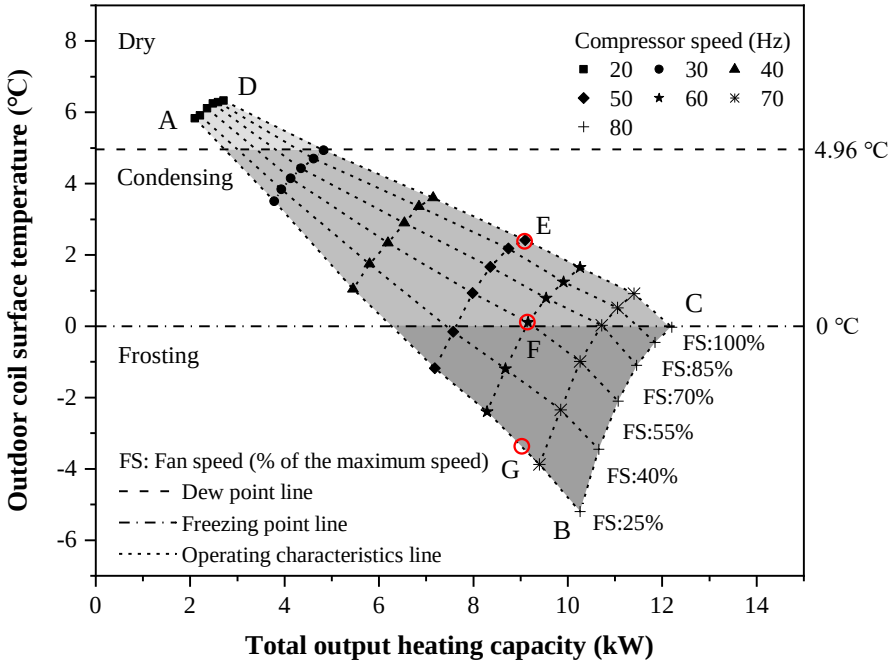

Fig. 5.8 Three selected operating points in the developed condensing-frosting performance map at Operating Condition 1

Table 5.4 Operating speed combinations and average total output heating capacities at the three selected points

Point	Compressor speed	Outdoor air fan speed	Average total output heating capacity during the 30 minute-period	Relative error in output heating capacity
E	50 Hz	100 %	9.10 kW	-
F	60 Hz	55 %	9.16 kW	0.66 %
G	65 Hz	25 %	9.10 kw	0

In this comparative experiment, a test at each of the three points was carried out and totally there were hence three tests. As explained earlier, as the outdoor coil surface was at different states of condensing, condensing / frosting and frosting, the duration when the experimental ASHP unit can be continuously operated without needing defrosting in each test can therefore be different. For the tests at Point F and G, the operation of the experimental ASHP unit was not ended until the air flow passage of the finned outdoor coil was fully blocked by frost and the measured air flow rate on the windward side of outdoor coil dropped to 0 m^3/s. For the test at point E, since outdoor coil surface was not frosted, the experimental ASHP unit can be continuously operated without needing defrosting. However, in this test, it was manually shut down after 4 hours. Therefore, the resulted operating durations for the three tests (points E, F and G) were at 14400, 9700 and 3500 seconds, respectively.

The results for the three tests at points E, F and G are shown in Figs. 5.9 and 5.10, respectively. As seen from Fig. 5.9, when the experimental ASHP unit was operated at point E, a fairly constant outdoor coil surface temperature at an average of 2.42 ℃ may be maintained, and no frost was formed on outdoor coil surface. At point F, the

resulted outdoor coil surface temperature was slightly higher than the freezing point of water (0 ℃) during approximately the first hour the operation of the experimental ASHP unit, so that only condensing occurred on its outdoor coil surface. However, after the first hour, surface temperature gradually dropped to below 0 ℃, and frost became visible on the outdoor coil surface. At 9700 seconds into the test, as surface temperature continued to drop, more and more frost was deposited on coil surface so that air flow passage was fully blocked and the operation of the experimental ASHP unit terminated. However, at point G, as the outdoor coil was operated at frosting condition, outdoor coil surface temperature quickly dropped to below 0 ℃ shortly after the start-up of the test, and frost started to deposit on coil surface. A fairly stable outdoor coil surface temperature between -2 ℃ and -3 ℃ was only maintained at the first half an hour of the test, but thereafter, outdoor coil surface temperature dropped sharply, and air flow passage was fully blocked, and the experimental unit was shut down at 3500 seconds into the test.

On the other hand, the test results also showed that although the experimental ASHP unit could produce the same or similar total output heating capacity operating at the three points, their operating efficiencies in terms of COP can be quite different. Fig. 5.10 shows the COP values for the three tests, evaluated using Eq. (5.2) and average over the three different test durations of 14400, 9700 and 3500 seconds. At point E, its average COP was the highest at 4.36, and at point G, the lowest at 3.58. At point F, the average COP was in between at 4.09.

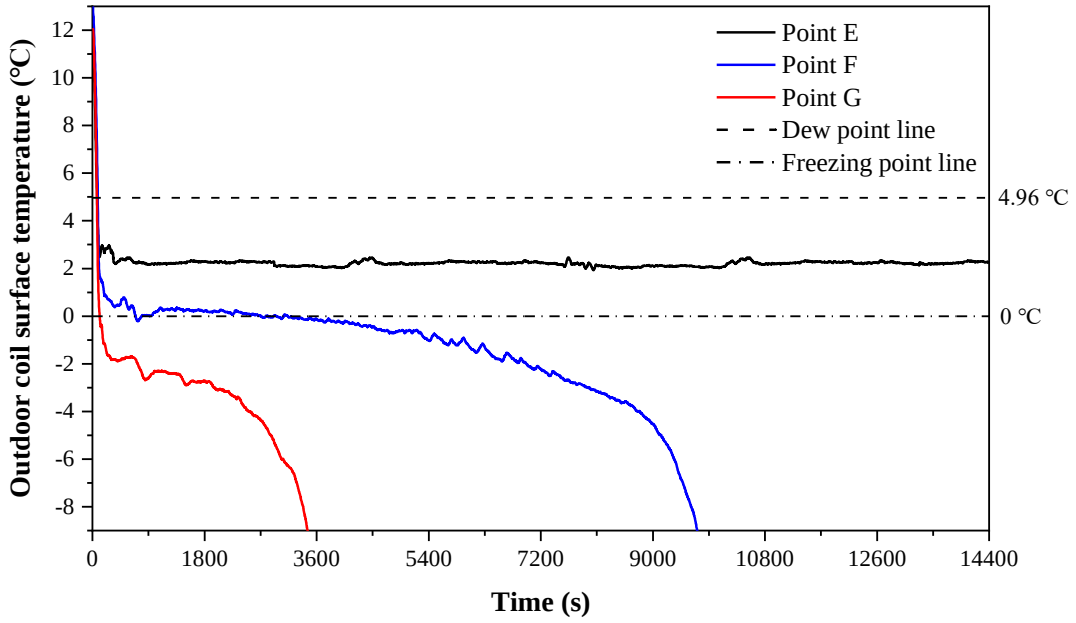

Fig. 5.9 Time variations of outdoor coil surface temperature and operating durations in the three tests of the comparative experiment

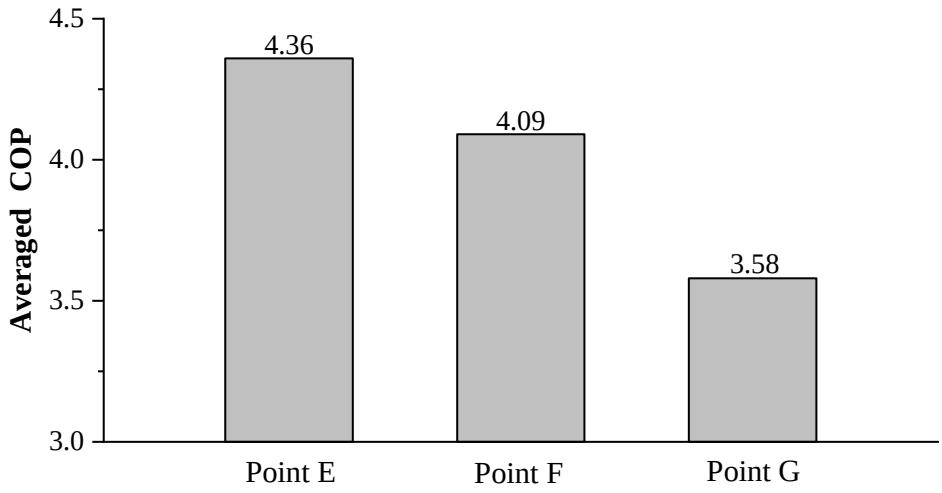

Fig. 5.10 The average COP of the experimental ASHP unit in the three tests of the comparative experiment

5.4 Discussions

From the experimental results reported in the Sections 5.3.1, 5.3.2 and 5.3.3, it is obvious that the different speeds of the compressor and outdoor air fan have a significant impact on outdoor coil surface temperatures and total output heating capacities from an ASHP unit. And due to the change of the outdoor coil surface temperature, the frosting suppression performance of the ASHP unit is also different. The following will further discuss and analyze the specific influence of the compressor speed and outdoor air fan speed on the outdoor coil surface temperature and total output heating capacity.

It is well known that the compressor drives the refrigerant flow in the experimental ASHP unit. Changing its speed would affect the refrigerant mass flow rate of the system and therefore affect the convective heat transfer in the refrigerant side. The specific calculation formula is as follows:

$$Q = m_r (h_{er,\,o} - h_{er,\,i}) \tag{5.3}$$

where $h_{er,\,i}$ and $h_{er,\,o}$ is refrigerant enthalpy at the inlet to, and the outlet from the outdoor coil.

For the rolling rotor compressor used in the ASHP unit, its refrigerant mass flow rate could also be evaluated by

$$m_r = n\rho_r \lambda V \tag{5.4}$$

where n is the compressor speed, ρ_r the refrigerant density at the suction port of the compressor, λ the gas transmission coefficient and V the compressor stroke volume.

Therefore, the refrigerant mass flow rate would be increased with an increase in compressor speed. Fig. 5.11 illustrates the changes in refrigerant mass flow rate under different compressor and outdoor air fan speed combinations at Operating Condition 1. As seen, the change in compressor speed significantly impacted the refrigerant mass flow rate of the experimental ASHP unit. Increasing compressor speed would increase refrigerant mass flow rate, and thus the total output heating capacity from the ASHP unit.

Furthermore, energy conservation yielded:

$$m_r(h_{er,\,o} - h_{er,\,i}) = \alpha F(T_m - T_e) \tag{5.5}$$

where α is the convective heat transfer coefficient of outdoor coil, F the heat exchange area of outdoor coil, T_m the mean temperature of the air through the outdoor coil and T_e the outdoor coil surface temperature.

According to Eq. (5.5), at a constant outdoor ambient condition and a fixed outdoor air fan speed, increasing refrigerant mass flow rate led to a decrease in outdoor coil surface temperature. Therefore, increasing compressor speed would not only increase

the total output heating capacity, but also reduce the outdoor coil surface temperature, which may deteriorate the frosting suppression performance of an ASHP unit. This was consistent with the experimental results reported in Section 5.3.1.

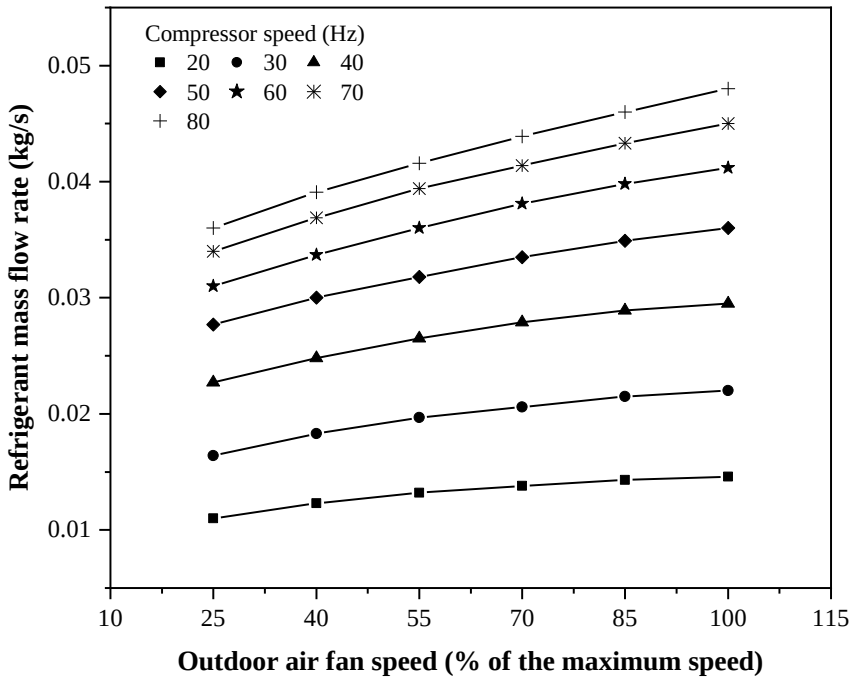

Fig. 5.11 The changes in refrigerant mass flow rate under different compressor and outdoor air fan speed combinations at Operating Conditon 1

On the other hand, an increase in outdoor air fan speed would directly lead to an increase in air flow rate on the air side of the outdoor coil. The heat transfer coefficient, K, was proportional to air flow rate. Hence an increase in air flow rate led to an increase in heat transfer coefficient, K. According to Eq. (5.5), if the total output heating capacity from the ASHP unit remained unchanged, an increase in heat transfer coefficient, K, resulted in an increased outdoor coil surface temperature.

Moreover, it can be seen from Fig. 5.11 that the increase in outdoor air fan speed can also increase the refrigerant mass flow rate. Although the increase is not as large as that caused by the change of the compressor speed, it could also increase the total output heating capacity from the ASHP unit. Consequently, increasing outdoor air fan speed can increase the total output heating capacity from the ASHP unit and the outdoor coil surface temperature, which is conducive to frosting suppression. However, it should be noted that in general, if outdoor air flow rate is too large to be over an up limit, the heat transfer enhancement due to increased air flow rate may be diminished, and hence over increasing fan speed is unnecessary. Therefore, care must be taken in determining the maximum outdoor air fan speed.

In general, varying the compressor and outdoor air fan speeds all can change the outdoor coil surface temperature and the total output heating capacity, but the changing rules are different. And there is a mutually restrictive relationship between the outdoor coil surface temperature and the total output heating capacity. Therefore, developing the condensing-frosting performance maps is necessary, which can clearly show the heating performance and frosting suppression performance of the ASHP unit operating at different speed combinations of compressor and outdoor air fan.

From the results reported in Section 5.3.2, at different outdoor coil surface temperatures, different levels of frosting suppression for the experimental ASHP unit can be resulted in, but at different levels of the total output heating capacity. The developed condensing-frosting performance maps reported in this Section clearly demonstrated that for the experimental ASHP unit, operating at different speed combinations under a fixed ambient condition, a higher outdoor coil surface

temperature and thus a better frosting suppression performance may be achieved, but usually at the expenses of losing some of its total output heating capacity.

The comparative experiment results reported in Section 5.3.3 demonstrated that when the experimental ASHP unit was operated at different speed combinations that can lead to the same or similar total output heating capacities, its operating characteristics in terms of outdoor coil surface states and the total output heating capacity can be remarkably different. When operated at condensing condition, the experimental ASHP can be continuously operated without the need of defrosting and at a higher operating efficiency. However, when operated at frosting condition, the experimental ASHP unit can only be operated with relatively short period of about an hour, requiring frequent defrosting and at a lower operating efficiency. Accordingly, in the case of meeting the requirement of the total output heating capacity, the ASHP unit should be operated at the speed combination in the frost-free region. If the outdoor ambient conditions are harsh and it is impossible to avoid operating in the frosting region, the speed combinations with higher outdoor coil surface temperatures should be selected, which can reduce the frosting severity of ASHPs. By using the developed condensing-frosting performance maps, it can help designers or users find the expected speed combinations quickly and clearly.

In addition, as seen from the experimental results reported in Section 5.3.2, outdoor ambient conditions would impact significantly on the resulted performance maps. On the other hand, different configurations for ASHPs can also lead to different performance maps. Clearly, it is costly and time-consuming to obtain condensing-frosting performance maps only using an experimental approach. Therefore, a follow

up numerical study to the experimental study reported in this Chapter should be carried out. A comprehensive mathematical model, as a key part of the numerical study, should be developed and validated using the experimental data reported in this Chapter. The validated model will then be used to obtain, numerically, the condensing – frosting performance maps for ASHP units of different configurations at different ambient conditions. This numerical study will be reported in Chapter 6.

5.5 Conclusions

In this Chapter, an experimental study on developing the condensing-frosting performance maps for the experimental VS ASHP unit is presented. Experiments were carried out at different speed combinations of compressor and outdoor air fan at three Operating Conditions corresponding to different outdoor ambient conditions.

The experimental results at the three Operating Conditions showed that for the experimental ASHP unit varying the speeds of both compressor and outdoor air fan would significantly impact its outdoor coil surface temperature and its total output heating capacity. At different compressor and outdoor air fan speed combinations, outdoor coil surface temperatures and the total output heating capacities were mutually constrained but correlated within a trapezoid in a condensing-frosting performance map. According to outdoor coil surface temperature, a trapezoid in a performance map may be divided into a dry region, a condensing region and a frosting region. It can be seen for these obtained condensing-frosting performance maps at three Operating Conditions that a frosting region usually corresponded to a higher output heating capacity but a dry or condensing region a lower output heating capacity. This implied

that for the experimental ASHP unit, a better frosting suppression performance may be achieved, at however the expense of losing some output heating capacity.

Furthermore, it can also be seen from the results of the comparative experiment at Operating Condition 1 that there existed multiple different speed combinations which can lead to the same total output heating capacity from the experimental ASHP unit, but they were located at different regions of dry, condensing and frosting. The comparative experimental results suggested that at a required output heating capacity, an ASHP should be operated at a speed combination located at the dry or condensing region for frost-free operation and thus higher operating efficiency. When it was impossible to avoid operating in the frosting region, the speed combinations that led to a higher outdoor coil surface temperature should be selected to reduce the frosting severity of ASHPs.

The condensing-frosting performance maps experimentally developed and reported in this Chapter could clearly reveal the relationships between the frosting suppression performance and the total output heating capacity for an ASHP operating at different speed combinations of its compressor and outdoor air fan, at different operating ambient conditions. These maps would enable the designers / operators of ASHPs to easily determine suitable speed combinations from frost-free operation. However, in the experimental study presented in this Chapter, given its nature, the configurations of the experimental VS ASHP unit, such as the outdoor coil surface area, were fixed, and the experimental ambient conditions were limited. Therefore, as pointed out in Section 5.4, for further obtaining condensing-frosting performance maps at other non-experimental unit configurations and non-experimental ambient conditions by

modeling, it was highly necessary to develop a comprehensive physics-based mathematical model for the experimental VS ASHP unit. Furthermore, it was expected that the obtained condensing-frosting performance maps can be used as the basis for developing a novel control strategy to achieve frosting suppression for the experimental VS ASHP unit. These will be reported in detail in Chapters 6 and 7, respectively.

Chapter 6

A modeling study on developing condensing-frosting performance maps for the experimental VS ASHP unit

6.1 Introduction

To comprehensively study both frosting suppression and heating performances for an ASHP unit under VS operation, an experimental study to obtain condensing-frosting performance maps for the experimental VS ASHP unit is reported in Chapter 5. However, the experimental VS ASHP unit had a fixed configuration, and the experiments were carried out at a limited number of experimental ambient conditions. Moreover, obtaining the performance maps experimentally was time-consuming and costly. Therefore, it was necessary to develop a physics-based mathematical model that can be used to numerically obtain condensing-frosting performance maps at non-experimental unit configurations and non-experimental ambient conditions. With the performance maps that covered all possible operating ambient conditions and different unit configurations, obtained experimentally and numerically, appropriate speed combinations may be selected to provide guidance to the design and efficient operation of the VS ASHP unit, so as to both provide the required output heating capacity and achieve frosting suppression.

Therefore, in this Chapter, the development and experimental validation of a mathematical model for the experimental VS ASHP unit are firstly detailed. Then, a follow-up modeling study using the validated model is presented, where condensing-frosting performance maps for the experimental VS ASHP unit at non-experimental configurations and operating conditions were obtained. Finally, conclusions are given.

6.2 Development of a mathematical model for the experimental VS ASHP unit

6.2.1 Modeling of the experimental VS ASHP unit

A physics-based mathematical model for obtaining condensing-frosting performance maps for the experimental VS AHSP unit reported in this Chapter is conceptually illustrated in Fig. 6.1, and was made of sub-models for key components including compressor, outdoor coil, EEV and indoor coil. As seen in Fig. 6.1 (a) and Fig. 6.1 (b), two different sub-models for the outdoor coil, corresponding to frost-free operation and frosting operation of the experimental ASHP unit, respectively, were used. The reason was as follows: when the state of the outdoor coil surface was frost-free, i.e., either dry or condensing, the experimental ASHP unit was at a steady state, and a steady-state sub-model for the outdoor coil, or evaporator, was sufficient. However, when the state of the outdoor coil surface was frosting, a quasi-steady-state sub-model for the outdoor coil should be used, as frosting was a transient but yet gradual process. Other than the sub-model for the outdoor coil, all the sub-models for other components, including the compressor, indoor coil, and EEV in the complete model for the experimental ASHP were the same at either frost-free operation or frosting operation. At frost-free operation, it was sufficient to use a simple steady-state distributed-parameter sub-model for the outdoor coil, with a superheated region and a two-phase region on its refrigerant side, as shown in Fig. 6.1 (a), so that the computational complexity could be much reduced, and the computational stability also improved. In addition, the condensation heat in condensing state have been considered in the steady-state model. However, at frosting operation, the outdoor coil sub-model included a calculating module for frost layers shown in Fig. 6.1 (b), and was further divided into

a number of segments along the refrigerant flow direction, as shown in Fig. 6.2, using the segment by segment method when solving the outdoor coil sub-model.

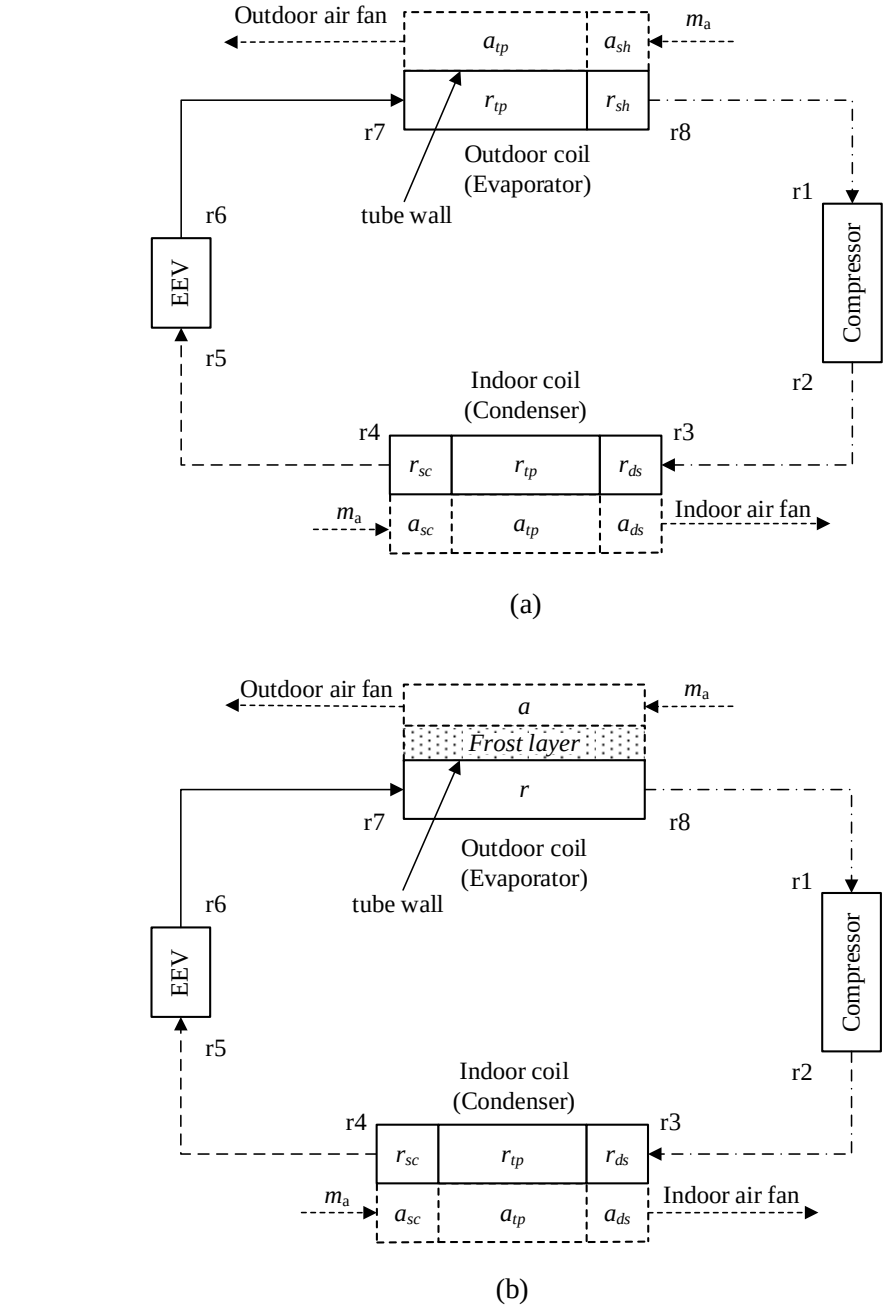

Fig. 6.1 Conceptual model for the experimental VS ASHP unit (a) at frost-free operation; (b) at frosting operation

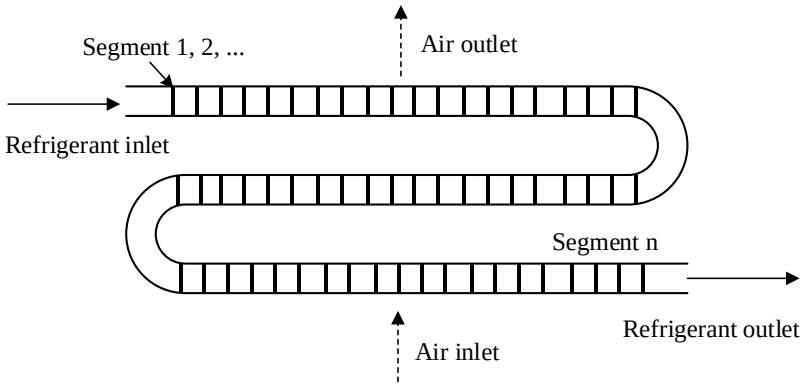

Fig. 6.2 Schematic diagram of the segments in the outdoor coil sub-model at frosting operation

All the equations for the sub-model of outdoor coil at frost-free operation and those for the sub-models of compressor, indoor coil and EEV at both the frost-free and frosting operations were actually from the previously published the steady-state mathematical models for DX A/C units developed by Yang et al. [2020] and Pan et al. [2012]. The equations for the outdoor coil sub-model at frosting operations were actually from the mathematical model for the airside of an outdoor coil under frosting operation developed by Yao et al. [2004]. As shown in Fig. 6.1, the sub-models in the complete model for the experimental ASHP unit were systematically linked through the refrigerant flow on the refrigerant side, and the outputs from one sub-model were the inputs to the next sub-model connected downstream. Furthermore, the equations for the thermal properties of the refrigerant used in the experimental ASHP unit, R410A, were obtained from Refprop [Lemmon et al., 2013] and the State Equations for humid air from ASHRAE Handbook [2009]. In addition, the following assumptions were made when developing the model:

On the refrigerant-side of the experimental VS ASHP unit:

- A fixed setting of degree of refrigerant sub-cooling, T_{sc}, at 5 °C;
- A fixed setting of degree of refrigerant superheat, T_{sh}, at 5 °C;
- Isenthalpic expansion at the EEV;

On the air-side of the outdoor coil at frost-free operation:

- Counter-flow heat exchange between the air and refrigerant;

On the air-side of the outdoor coil at frosting operation:

- A quasi-steady-state process of frosting;
- One dimensional heat and mass transfer between air flow and refrigerant;
- No radiation heat exchange between the humid air and frost layer.

Based on the above assumptions, the main equations used in the mathematical model were given as follows.

The energy equations used in the developed model were:

$$Q_a = m_a(h_{a,i} - h_{a,o}) \tag{6.1}$$

$$Q_r = m_r(h_{r,o} - h_{r,i}) \tag{6.2}$$

$$Q_r = \xi Q_a \tag{6.3}$$

where m_a and m_r are the air and refrigerant mass flow rates, respectively, $h_{a,i}$ and $h_{r,i}$ the air and refrigerant enthalpy at the inlet to outdoor / indoor coil, respectively, $h_{a,o}$ and $h_{r,o}$ the air and refrigerant enthalpy at the outlet from outdoor / indoor coil, respectively, and ξ the heat leakage coefficient.

The pressure drops of the refrigerant in the heat exchangers, i.e., indoor coil and outdoor coil, could not be neglected as it would significantly affect the operating performances of an ASHP unit. Moreover, how to evaluate the pressure drop was also crucial to the calculation procedures and accuracy of the model. Hence, the equations for refrigerant pressure drop used in this model are also specifically listed as follows:

For two-phase refrigerant flow [Brown, 2003]:

$$\Delta p_{r,tp} = \left[f_{r,tp} \frac{L}{D_i} + n\zeta + \frac{(x_o - x_i)}{\bar{x}} \right] \frac{v_{r,m}^2}{2\bar{\rho}_r} \tag{6.4}$$

For single-phase refrigerant flow [Wang and Touber, 1991]:

$$\Delta p_{r,s} = f_{r,s} \frac{L}{D_i} \cdot \frac{\rho \bar{u}_{r,s}^2}{2} \tag{6.5}$$

where f_r is the friction factor of the refrigerant, ζ the local loss coefficient of the coil bend, $v_{r,m}$ the refrigerant mass flux, and $\bar{u}_{r,s}$ the average flow rate of the refrigerant.

Furthermore, in the sub-model for outdoor coil at frosting operations, frost accumulation rate was expressed by:

$$m_f = m_a(d_{a,i} - d_{a,o}) = m_\delta + m_\rho \tag{6.6}$$

where m_δ and m_ρ are the frost accumulation rates at increased frost thickness and at increased frost density, respectively.

For each time step, the changes in frost thickness and frost density were evaluated by:

$$\Delta\delta_f = \frac{m_\delta}{A_t \rho_f} \Delta t \tag{6.7}$$

$$\Delta\rho_f = \frac{m_\rho}{A_t \delta_f} \Delta t \tag{6.8}$$

where A_t is the total outdoor coil surface area, and Δt the specified time step.

The thermal conductivity of frost layer, λ_f, was as follows [Sanders, 1974]:

$$\lambda_f = 0.001202\rho_f^{0.963} \tag{6.9}$$

In addition, frost accumulation on outdoor coil surface would also seriously affect air flow rate on its air side, which could lead to the changes in air-side pressure drop and

evaporating temperature on the refrigerant side. The air side pressure drop under frosting conditions was evaluated as follows [Turaga et al., 1988]:

$$\Delta p_a = f_a \frac{\left(m_a / A_{\min}\right)^2}{2\rho_a} \frac{A_t}{A_{\min}} \tag{6.10}$$

where f_a is the friction factor of the air, and $A_{\min}$ the cross-sectional area of the air flow passed though.

Except for the equations listed above, all the other equations in the complete model of the experimental VS ASHP unit were available from Yang et al. [2020], Pan et al. [2012] and Yao et al. [2004].

6.2.2 Calculation procedure of the complete experimental VS ASHP unit model

The flow charts for solving the complete model of the experimental VS ASHP unit are illustrated in Fig. 6.3, with Fig. 6.3 (a) for solving the steady-state model at frost-free operation, and Fig. 6.3 (b) for solving the quasi-steady-state model at frosting operation. As shown in Fig. 6.3 (a), there were four iterative loops when solving the model at frost-free operation, and the dichotomous method was used in these iterative loops. The first one (Loop I) was used to evaluate the compressor discharge pressure, p_{r2}, by solving the compressor sub-model, and the second one (Loop II) to evaluate the refrigerant mass flow rate passing through the ASHP unit. The third and fourth loops (Loop III and Loop IV) were used to determine the refrigerant pressure and

enthalpy at the compressor suction, p_{r1} and h_{r1}, respectively. The detailed computation procedures are described as follows:

Before running the model, outdoor ambient air conditions and the configuration details for the experimental VS ASHP unit were input to the model. Then, initial values of the refrigerant enthalpy at compressor suction, h_{r1}, the refrigerant pressures at compressor suction and discharge, p_{r1} and p_{r2}, were assumed. The calculation procedures could then be started from solving the compressor sub-model by using these assumed initial values, and then the refrigerant mass flow rate, m_{r1}, could be obtained. Afterwards, the indoor coil sub-model was solved to evaluate the degree of refrigerant sub-cooling at indoor coil outlet, $T_{sc}^{'}$, which was then compared to the specified setting of T_{sc} at 5°C. If the difference between the two was greater than an acceptable range, i.e., the convergence criterion of this loop was not met, the initial value of p_{r2} was updated, and the calculation procedure of this iterative loop repeated, until the convergence criterion was met.

After completing the calculation of Loop I, the outputs from the indoor coil sub-model (m_{r4}, p_{r4}, h_{r4} and T_{r4}) were used as the inputs to Loop II, and the sub-models for EEV and outdoor coil were solved to obtain the refrigerant pressure at the outdoor coil outlet, p_{r8}. Since the outdoor coil outlet was directly connected to compressor suction, the values of p_{r8} and p_{r1} should be the same. Otherwise, the input value of m_{r4} in this loop needed to be updated until p_{r8} was equal to p_{r1}. In addition, the final output refrigerant mass flow rate, m_{r8}, from this loop should be equal to m_{r1} value obtained

from the compressor sub-model. If not, the initial input value of p_{r1} needed to be updated to ensure that the refrigerant mass flow rate was equal to one another at each loop node. During this procedure, the outdoor coil surface temperature was obtained by solving the air-side module in the outdoor coil sub-model.

After completion Loop III, the refrigerant enthalpy at compressor suction, h_{r1}, was used as the convergence criterion for Loop IV. If the refrigerant enthalpy at the outdoor coil outlet, h_{r8}, was not equal to h_{r1}, h_{r1} was updated and the calculation procedures repeated starting from the compressor sub-model until the convergence was reached. When all the convergence criteria in these four iteration loops were satisfied, the complete calculation procedures for solving the model of the experimental VS ASHP unit at frost-free operation were ended.

On the other hand, when the experimental VS ASHP unit was at frosting operation, the flow chart for solving the model is shown in Fig. 6.3 (b). When solving the quasi-steady-state model at frosting operation, a specified time step and a total calculation time were required. Within each time step, however, the VS ASHP unit was considered as at a steady state, and the procedures of having four iteration loops for solving the steady-state model as shown in Fig. 6.3 (a) were followed. Then, the outputs from the previous time step were input to the next time step, and the calculations were not ended until the total calculation time reached the specified value.

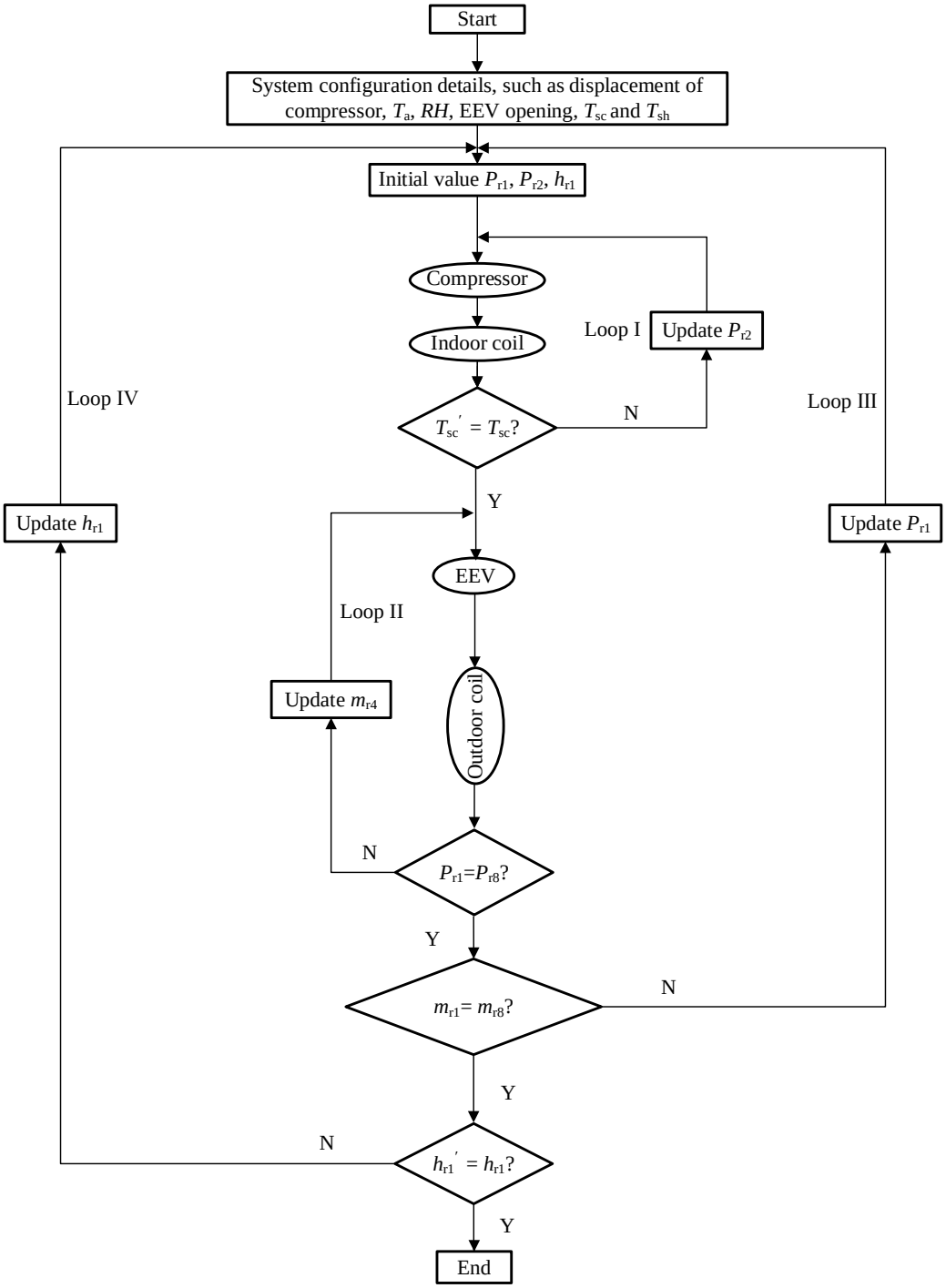

(a) at frost-free operation

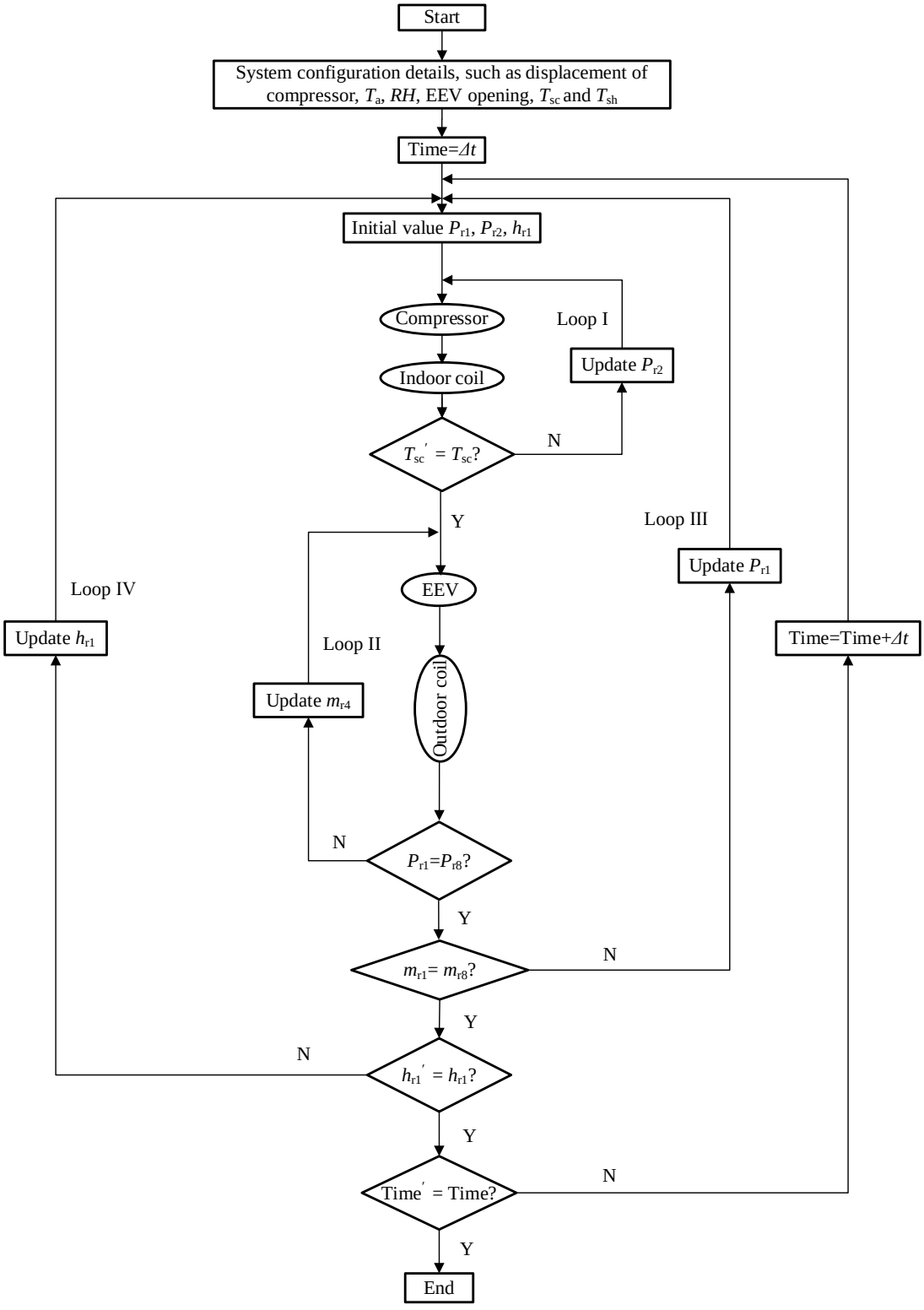

(b) at frosting operation

Fig. 6.3 Flow charts of the calculation procedure for the complete VS ASHP unit model

6.3 Experimental validation of the developed mathematical model

In the experimental study on developing the condensing-frosting performance maps reported in Chapter 5, a condensing-frosting map was expressed in terms of the relationship between the outdoor coil surface temperature and the total output heating capacity from the experimental VS ASHP unit at different compressor and outdoor air fan speed combinations. In addition, COP was a common parameter representing the operating energy efficiency of an ASHP unit. Therefore, the following three operating parameters of the experimental VS ASHP unit were used when validating the complete model at both frost-free and frosting operations: i) Outdoor coil surface temperature; ii) Total output heating capacity, expressed as Eq. (5.1); iii) COP, expressed as Eq. (5.2).

When validating the model, the above three operating parameters experimentally obtained and reported in Chapter 5 were compared with those predicted by the developed model, at the three Operating Conditions as shown in Table 5.1, and the compressor and outdoor air fan speeds as shown in Tables 5.2 and 5.3, respectively.

Figs. 6.4, 6.5 and 6.6 show the comparisons between the experimentally measured and the model predicted values of the total output heating capacities, outdoor coil surface temperatures and COP of the experimental VS ASHP unit, under the three Operating Conditions shown in Table 5.1, respectively. As shown in Fig. 6.4, the relative errors between the experimental and model predicted values of the total output heating capacity were within ±7 %, with an average relative error of 3.7 %. For the outdoor coil surface temperature, the errors between the experimental and predicted values

were within ±0.5 °C, with an average error of 0.2 °C, as shown in Fig. 6.5. Moreover, the relative errors between the experimental and predicted values for COP were within ±6 %, with an average relative error of 3.6 %, as shown in Fig 6.6. Therefore, the predicted total output heating capacities, outdoor coil surface temperatures and COP values using the validated model agreed well with the experimentally measured values.

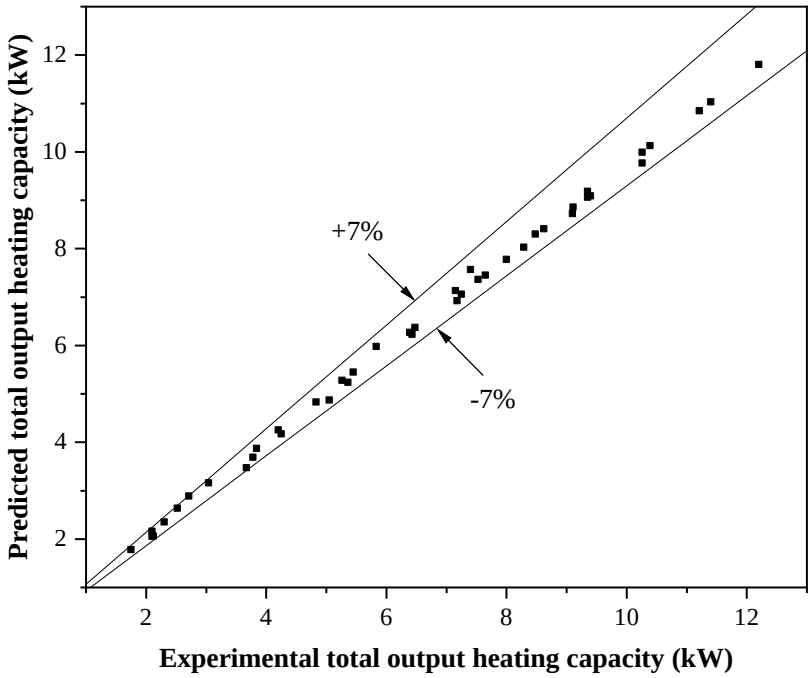

Fig. 6.4 Relative errors between experimental and predicted values of the total output heating capacity of the experimental VS ASHP unit

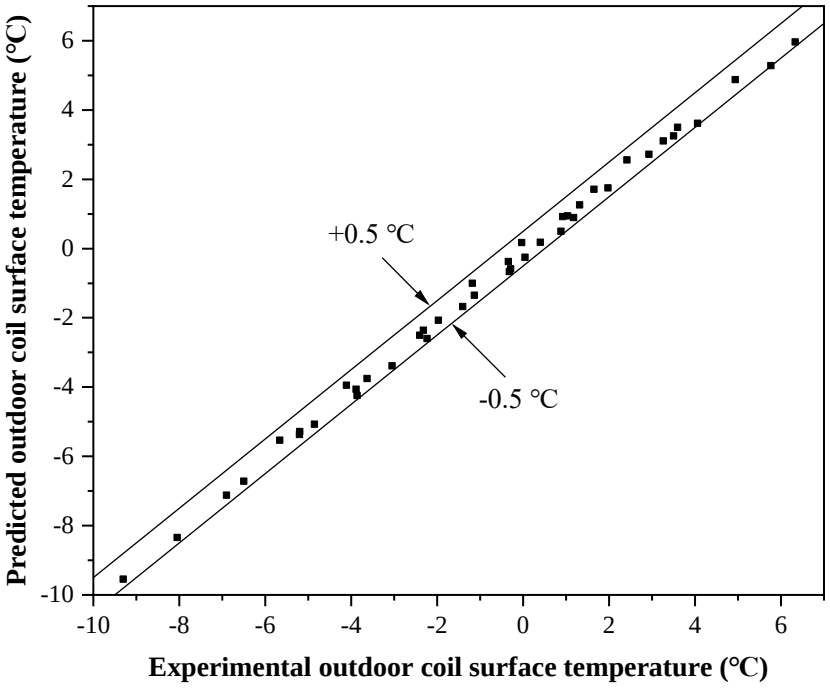

Fig. 6.5 Errors between experimental and predicted values of the outdoor coil surface temperature of the experimental VS ASHP unit

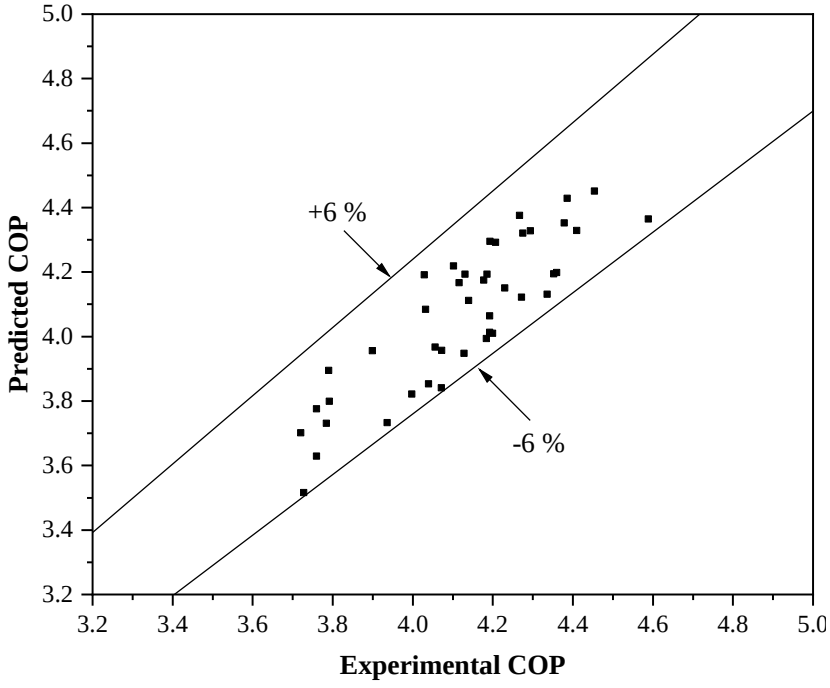

Fig. 6.6 Relative errors between experimental and predicted values of COP of the experimental VS ASHP unit

Figs. 6.7, 6.8 and 6.9 show the comparison between the experimental and predicted condensing-frosting performance maps for the experimental VS ASHP unit under the three Operating Conditions shown in Table 5.1, respectively. As seen, similar to the experimental condensing-frosting performance maps reported in Chapter 5, for the predicted performance maps, the predicted total output heating capacities and the predicted outdoor coil surface temperatures of the experimental VS ASHP unit were also mutually constrained within a quadrilateral region of ABCD, which is plotted together with the experimental quadrilateral region of A'B'C'D' in these figures. Comparing the performance maps obtained experimentally with those predicted by the model, both maps had similar quadrilateral shapes, with similar variation trends. At the three Operating Conditions, comparing the performance maps obtained experimentally and predicted by the validated model, the maximum and minimum relative errors for the variation range of the total output heating capacity were at 4.5 % and 3.3 %, and those for the variation range of outdoor coil surface temperature at 0.23 °C and 0.13 °C, respectively.

Therefore, the above comparison results suggested that the mathematical model for the experimental ASHP unit has been experimentally validated and can be further used in a follow-up modeling study to obtain condensing-frosting performance maps of the experimental VS ASHP unit at other non-experimental configurations and operating conditions to provide a more comprehensive guidance for frosting suppression operation of ASHPs. However, it must be acknowledged that there were some inherent limitations for this model. For example, a number of assumptions were used when developing the model, which can lead to predication errors. Also, the model was

developed based on a specific VS ASHP unit, which implied that further modifications may be necessary when applying the model to other types of ASHPs.

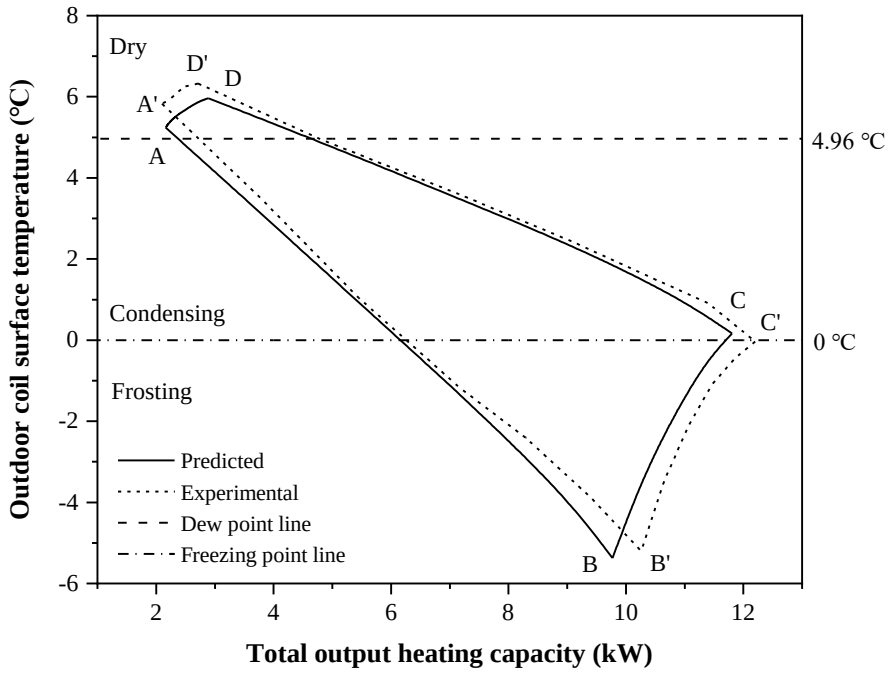

Fig. 6.7 Comparison of the predicted and experimental condensing-frosting performance maps of the experimental VS ASHP unit at Operating Condition 1

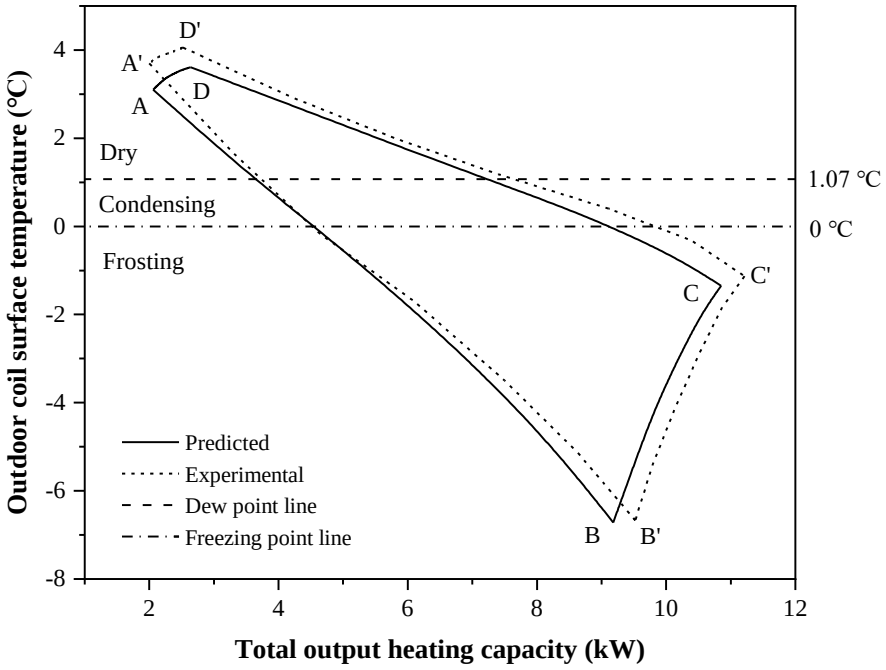

Fig. 6.8 Comparison of the predicted and experimental condensing-frosting performance maps of the experimental VS ASHP unit at Operating Condition 2

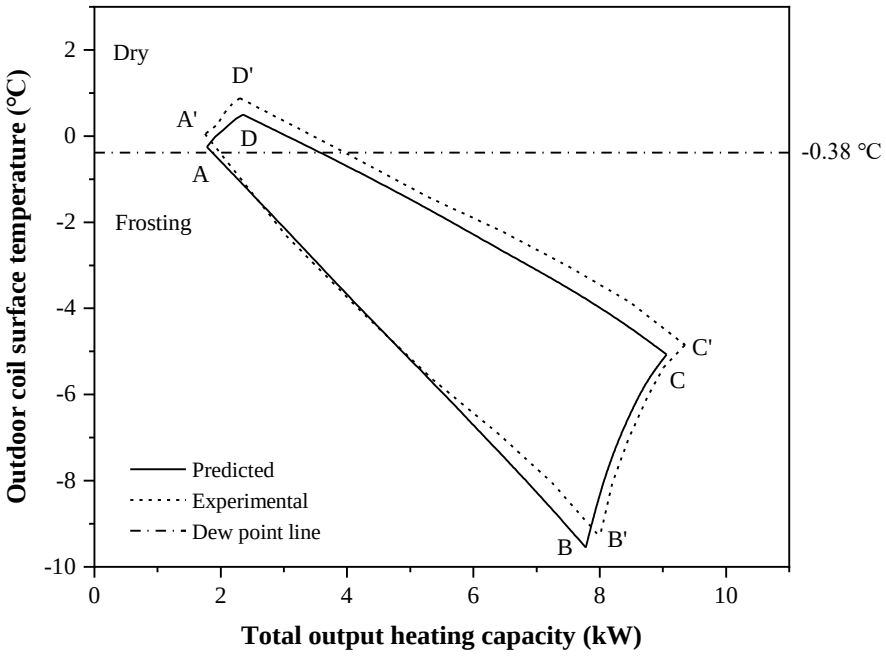

Fig. 6.9 Comparison of the predicted and experimental condensing-frosting performance maps of the experimental VS ASHP unit at Operating Condition 3

6.4 A follow-up modeling study using the validated model

With the availability of the experimentally validated model for the experimental ASHP unit at both frost-free and frosting operation, it was then possible to carry out a follow-up modeling study to obtain condensing-frosting performance maps for the experimental VS ASHP unit at other non-experimental configurations and outdoor operating ambient conditions. In this modeling study, there were two Study Groups, Group I for varying outdoor coil surface areas, and Group II varying outdoor operating ambient conditions. In both groups, indoor air parameters, compressor speeds and outdoor air fan speeds were the same as those used in model validation, i.e., Tables 5.2 and 5.3.

6.4.1 Study Group I: Predicted condensing-frosting performance maps for the experimental VS ASHP unit at varying outdoor coil surface areas

In this Study Group, condensing-frosting performance maps at three different outdoor coil surface areas, i.e., 50 % *F*, 100 % *F* and 150 % *F*, where *F* was the surface area of the outdoor coil in the experimental VS ASHP unit shown in Table 4.1, were obtained by using the validated model. Three Study Cases were organized at three different sets of operating ambient parameters, as detailed in Table 6.1.

Table 6.1 Details of Study Cases in Study Group I

Study Case	Fixed operating ambient parameters		Varying configurational parameters
I–1	$T_{a,d}$ – 7 °C	RH – 90 %	50 % F *
			100 % F
			150 % F
I–2	$T_{a,d}$ – 4.5 °C	RH – 90 %	50 % F
			100 % F
			150 % F
I–3	$T_{a,d}$ – 2 °C	RH – 90 %	50 % F
			100 % F
			150 % F

* F = 26.77 m^2

The modeling results in three Study Cases are presented in Fig. 6.10, where the condensing-frosting performance maps for the experimental VS ASHP unit at three different outdoor coil surface areas under three different sets of operating conditions are shown. As seen from Fig. 6.10, as the outdoor coil surface area was increased, the surface temperatures of, and the total output heating capacities from, the experimental VS ASHP unit would in general be increased when operated at different speed combinations. When the outdoor coil surface area was increased from 50 % to 100 % and from 100 % to 150 %, firstly in Study Case I–1, the outdoor coil surface temperatures on average were increased by 1.22 °C and 0.59 °C, the output heating capacities on average increased by 0.32 kW (5.17 %) and 0.33 kW (5.57 %), the maximum output heating capacities increased by 0.36 kW (3.12 %) and 0.24 kW (2.06 %), and their corresponding COP increased by 0.11 (3.09 %) and 0.03 (0.79 %), respectively; secondly, in Study Case I–2, the outdoor coil surface temperatures on average were increased by 1.16 °C and 0.45 °C, the output heating capacity on average

increased by 0.50 kW (8.21 %) and 0.17 kW (2.99 %), the maximum output heating capacities increased by 0.71 kW (6.91 %) and 0.27 kW (2.46 %), and their corresponding COP increased by 0.23 (6.82 %) and 0.09 (2.45 %), respectively; and thirdly, in Study Case I–3, the outdoor coil surface temperatures on average were increased by 0.60 °C and 0.77 °C, the output heating capacity on average increased by 0.37 kW (6.70 %) and 0.30 kW (6.43 %), the maximum output heating capacities increased by 0.68 kW (8.11 %) and 0.35 kW (3.86 %), and their corresponding COP increased by 0.24 (8.11 %) and 0.10 (3.18 %), respectively.

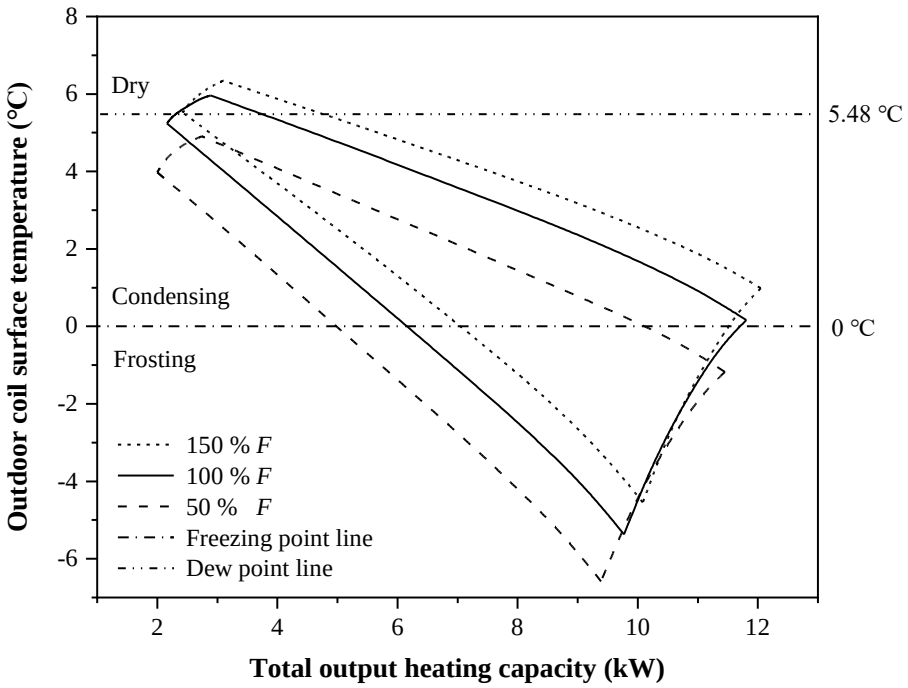

(a) Study Case I–1

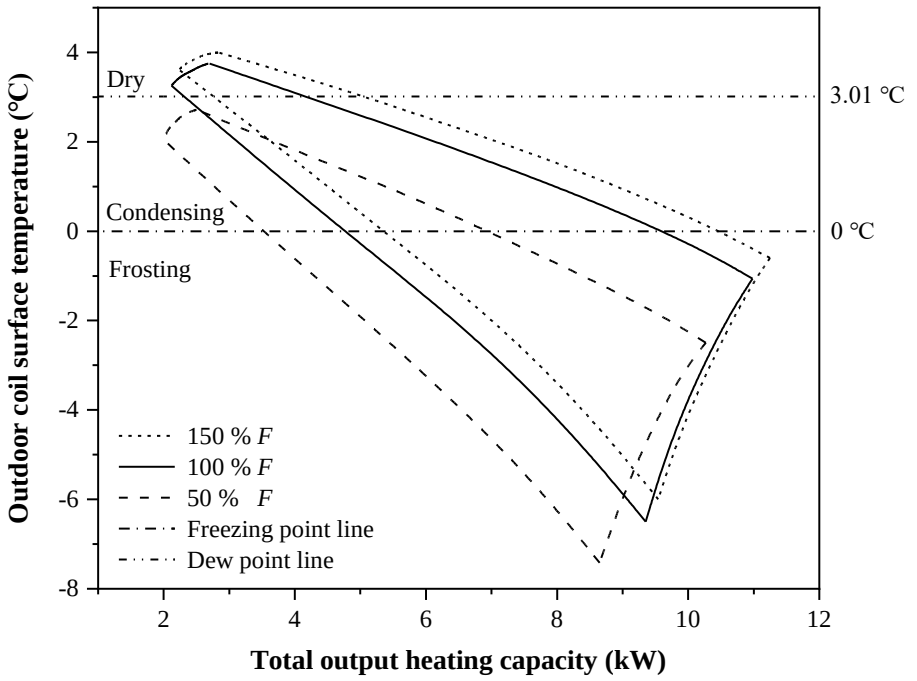

(b) Study Case I–2

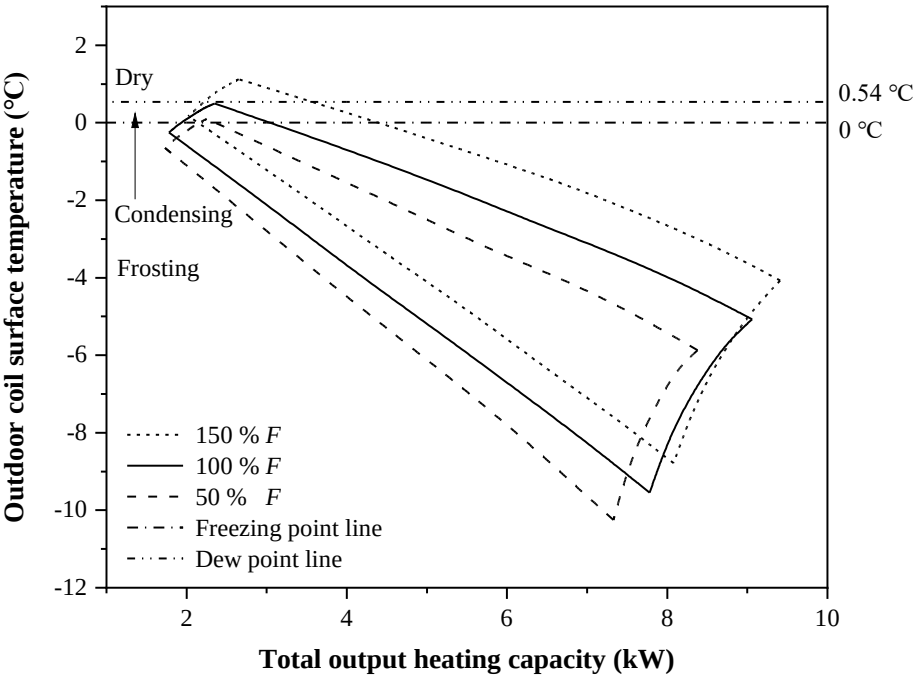

(c) Study Case I–3

Fig. 6.10 Predicted condensing-frosting performance maps for the experimental VS ASHP unit with different outdoor coil surface areas

Table 6.2 lists the predicted evaporating and condensing pressures of the experimental VS ASHP unit in Study Case I–1 operated at four special boundary speed combinations (i.e., maximum compressor and outdoor air fan speed, maximum compressor speed and minimum outdoor air fan speed, minimum compressor speed and maximum outdoor air fan speed, and minimum compressor and outdoor air fan speed). These four operating speed combination points in a performance map also corresponded to the maximum total output heating capacity, the minimum outdoor coil surface temperature, the maximum outdoor coil surface temperature and the minimum total output heating capacity, respectively. From Table 6.2, it can be seen that a higher compressor speed would lead to a lower evaporating pressure but a higher condensing pressure. However, a higher outdoor air fan speed would result in a slight increase in both evaporating and condensing pressures. Likewise, the evaporating and condensing pressures of the experimental VS ASHP unit were increased with the increase in outdoor coil surface area at a fixed operating ambient condition. By referring to the obtained condensing-frosting performance maps, the effect of increasing the outdoor coil surface area on the evaporating pressure and condensing pressure of the experimental VS ASHP unit operated at different speed combinations was consistent with that on the outdoor coil surface temperature and total output heating capacity. This was because a higher evaporating pressure would lead to a higher evaporating temperature of the refrigerant, which in turn would affect the outdoor coil surface temperature. Similarly, the changes in condensing pressure would affect the indoor coil surface temperature, which would eventually lead to the changes in the output heating capacity. On the other hand, the variation trends in evaporating and condensing pressures in Study Cases I–2 and I–3 were similar to those in Study Cases I–1, and are therefore not repeated here.

Table 6.2 Evaporating and condensing pressures in Study Case I–1 (7 ℃ & 90% *RH*)

CS & FS *	Varying configurational parameters	Evaporating pressure (kPa)	Condensing pressure (kPa)
80 Hz & 100 %	50 % *F*	762.58	2220.75
	100 % *F*	799.24	2326.50
	150 % *F*	820.31	2441.45
80 Hz & 25 %	50 % *F*	634.35	2067.45
	100 % *F*	659.74	2175.80
	150 % *F*	680.31	2274.71
20 Hz & 100 %	50 % *F*	905.82	1750.25
	100 % *F*	955.69	1791.72
	150 % *F*	964.23	1815.94
20 Hz & 25 %	50 % *F*	901.65	1695.38
	100 % *F*	937.49	1720.07
	150 % *F*	942.61	1744.94

* CS: Compressor speed; FS: Outdoor air fan speed (% of the maximum speed)

In general, increasing the outdoor coil surface area could lead to improved heating and frosting suppression performances, and may be employed to compensate for the loss of the total output heating capacities when the ASHP unit was operated at a higher surface temperature for better frosting suppression performances. When the outdoor coil surface area of the experimental VS ASHP unit operated at three typical conditions was increased from 50 % to 150 %, its outdoor coil surface temperature, output heating capacity, maximum output heating capacity and the corresponding COP on average were increased by 1.37 - 1.82 °C, 11.07 % - 13.53 %, 5.24 % - 12.29 %, and 3.90 % - 11.55 %, respectively, and the area of frost-free region, i.e., condensing and dry regions, in the performance map was enlarged. However, it was also clear from the results shown in Fig. 6.10 that although increasing the outdoor coil

surface area could help improve both heating and frosting suppression performances of an ASHP unit, its effectiveness was not proportionally significant. For example, as seen in Fig. 6.10 (a) in Study Case I–1, as the surface area was increased from 50 % *F* to 150 % *F*, a 300 % increase in surface area would only lead to an increase in frost-free area by 69.4 %. Besides, the significance of improving heating and frost suppression performances of the experimental VS ASHP unit by increasing its outdoor coil surface area was enhanced as the operating condition deteriorated. Furthermore, increasing surface area would also lead to an increase in the initial cost of manufacturing an ASHP unit. Therefore, an appropriate balance between improving the frosting suppression performance of a VS ASHP unit by using a larger surface area in its outdoor coil and the associated initial cost should be established.

6.4.2 Study Group II: Predicted condensing-frosting performance maps for the experimental VS ASHP unit at different outdoor operating conditions

There were four Study Cases in Study Group II, and the details of these Cases are shown in Table 6.3. In all Study Cases in Study Group II, a fixed outdoor coil surface area, i.e., 100 % *F*, was used.

Table 6.3 Details of Study Cases in Study Group II

Study Case	Fixed operating and configurational parameters		Varying operating parameters
II–1	RH – 90 %,	100 % F	$T_{a,\,d}$ – 7 ℃ $T_{a,\,d}$ – 4.5 ℃ $T_{a,\,d}$ – 2 ℃
II–2	$T_{a,\,d}$ – 7 ℃,	100 % F	RH – 90 % RH – 60 % RH – 30 %
II–3	$T_{a,\,d}$ – 4.5 ℃,	100 % F	RH – 90 % RH – 60 % RH – 30 %
II–4	$T_{a,\,d}$ – 2 ℃,	100 % F	RH – 90 % RH – 60 % RH – 30 %

The modeling study results in Study Case II–1 are presented in Fig. 6.11, where the predicted condensing-frosting performance maps for the experimental VS ASHP unit at different outdoor air temperatures, but a fixed *RH* and outdoor coil surface area are illustrated. It can be seen that when the outdoor ambient air temperature was changed, the shapes of the three performance maps remained similar, but with different size and locations in a surface temperature-output heating capacity diagram. As the outdoor air temperature was increased, the performance maps moved up right, suggesting a larger frost-free area of a map, or a better frosting suppression performance. Quantitatively, when outdoor air temperature was increased from 2 °C to 4.5 °C and from 4.5 °C to 7 °C, the outdoor coil surface temperatures on average were increased by 2.40 °C and 1.47 °C, the output heating capacities on average increased by 1.15 kW (19.91 %) and 0.52 kW (7.31%), the maximum output heating capacities increased by 1.92 kW

(21.19 %) and 0.83 kW (7.53 %), and their corresponding COP increased by 0.44 (13.95 %) and 0.10 (2.64 %), respectively. In general, the variation range of the total output heating capacity from the unit was increased by 32.55 %, and that of the outdoor coil surface temperature by 1.29 °C, respectively, when outdoor air temperature was increased from 2 °C to 7 °C. These increases virtually changed the size of a performance map, and a larger map was resulted in at a higher outdoor air temperature.

Furthermore, the point in the condensing-frosting performance map where the VS ASHP unit can provide the maximum output heating capacity under frost-free operation should also be noted. At the outdoor air temperature of 2 °C and relative humidity of 90 %, the maximum output heating capacity of the VS ASHP unit under frost-free operation was 3.10 kW with COP of 2.71. At the fixed outdoor air relative humidity, the maximum output heating capacity under frost-free operation was significantly increased as the outdoor air temperature was increased. The maximum output heating capacity of the VS ASHP unit under frost-free operation was increased to 9.50 kW with COP of 3.76 and 11.81 kW with COP of 3.70 when the outdoor air temperature was increased to 4.5 °C, and to 7 °C, respectively. Therefore, the modeling study results from Study Case II–1 demonstrated that at a fixed outdoor air relative humidity, a higher outdoor air temperature could provide more favorable external operating environment for a higher total output heating capacity and better frosting suppression performance for an ASHP unit.

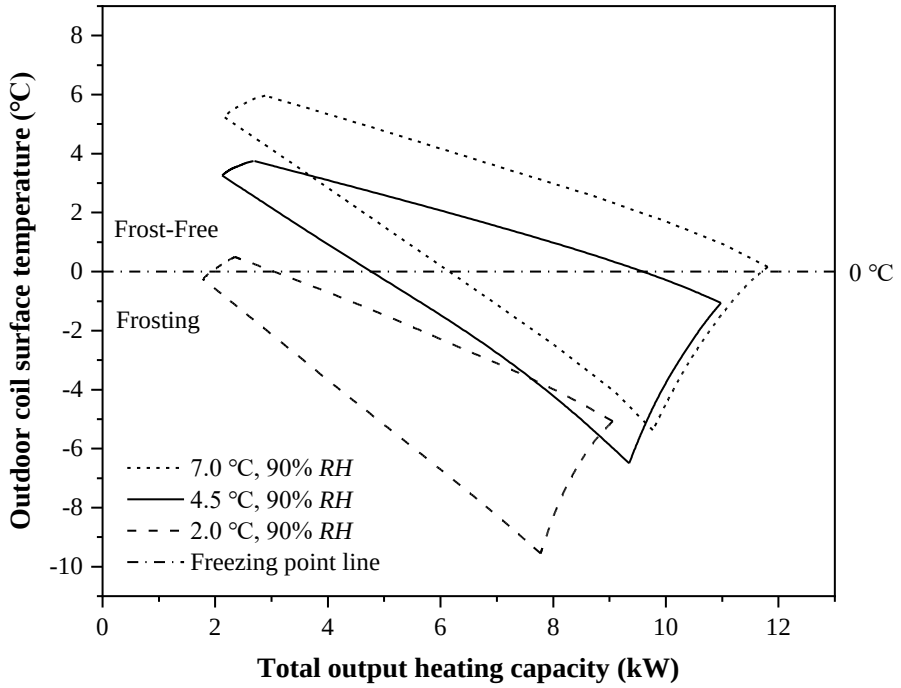

Fig. 6.11 Predicted condensing-frosting performance maps for the experimental VS ASHP unit at different outdoor ambient air temperatures in Study Case II–1

Fig. 6.12 shows the modeling study results of Study Cases II–2, II–3 and II–4, where the condensing-frosting performance maps for the experimental VS ASHP unit at a fixed outdoor air temperature but different outdoor air relative humidity are depictured in Fig. 6.12 (a), (b) and (c), respectively. As seen, the performance maps, at the three fixed outdoor air temperatures, all shifted to the lower left as outdoor air relative humidity was reduced, but the changes in the size of these maps were not significant. As shown in Fig. 6.12, when outdoor air relative humidity was reduced from 90 % to 60 % and then from 60 % to 30 %, firstly at outdoor air temperature of 7 °C, the outdoor coil surface temperatures on average were decreased by 0.71 °C and 0.57 °C, and the output heating capacities on average decreased by 0.22 kW (3.16 %) and 0.14 kW (1.96 %), respectively; secondly, at outdoor air temperature of 4.5 °C, the outdoor coil surface temperatures on average were decreased by 0.93 °C and 0.60 °C, and the

output heating capacities on average decreased by 0.32 kW (4.73 %) and 0.21 kW (3.44 %), respectively; and thirdly, at outdoor air temperature of 2 °C, the outdoor coil surface temperatures on average were decreased by 0.35 °C and 0.34 °C, and the output heating capacities on average decreased by 0.15 kW (2.72 %) and 0.14 kW (2.67 %), respectively. In general, at a fixed outdoor air temperature, a 30 % reduction in outdoor air relative humidity resulted in an average reduction of 0.14 - 0.32 kW and 0.34 - 0.93 °C in total output heating capacity and outdoor coil surface temperature, respectively. As a result, as relative humidity was reduced, the outdoor coil surface temperatures and output heating capacities were also reduced, although not significant.

On the other hand, it should be noted that at a fixed outdoor air temperature, a lower outdoor air relative humidity would lead to a lower dew point of outdoor air. This consequently caused an increase in the frost-free area of the map. As seen in Fig. 6.12 (a) - (c), at an outdoor air relative humidity of 30 %, the dew points were at -8.36 °C, -10.32 °C and -12.29 °C, respectively, so that no frosting region was present in the performance maps obtained. Besides, the impacts of air relative humidity on the maximum output heating capacity of the VS ASHP unit under frost-free operation were different when the outdoor air temperature was reduced. The maximum output heating capacity of the VS ASHP unit under frost-free operation peaked at 90 % *RH* when outdoor air temperature was 7 °C, at 60 % *RH* when outdoor air temperature was 4.5 °C, and at 30 % *RH* when outdoor air temperature was 2 °C.

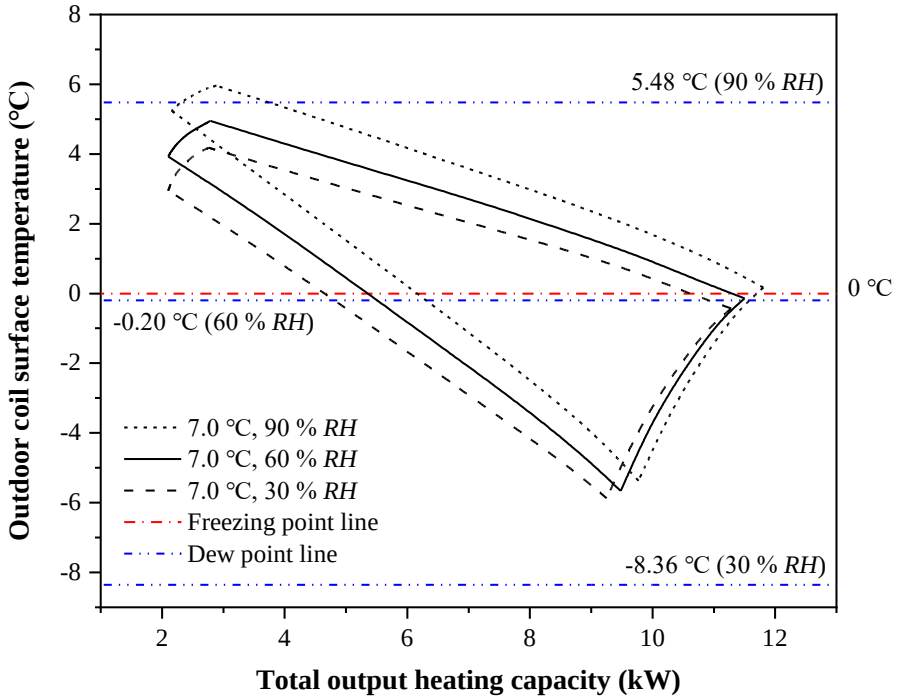

(a) Study Case II–2

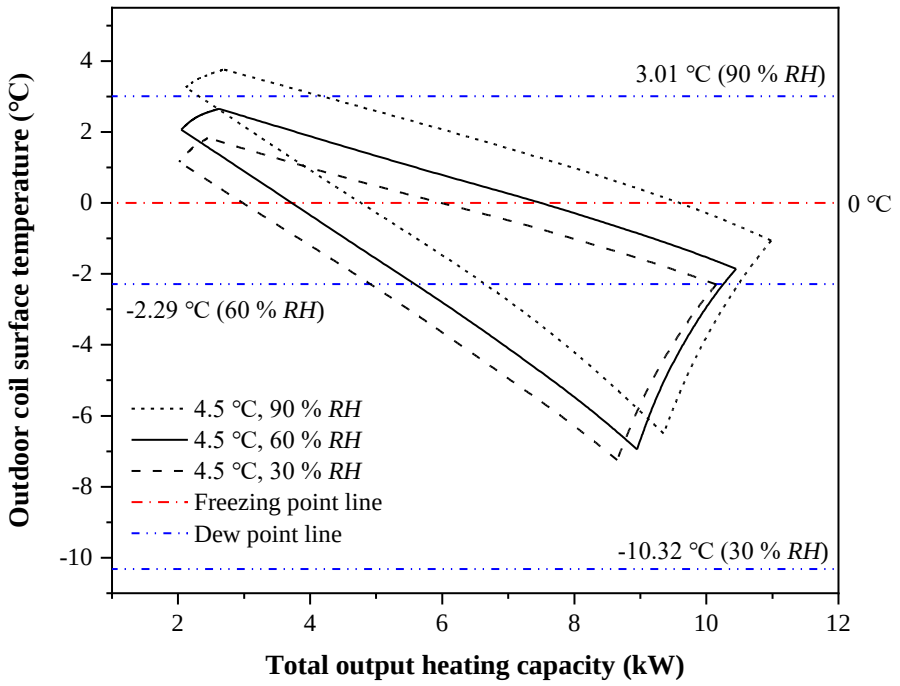

(b) Study Case II–3

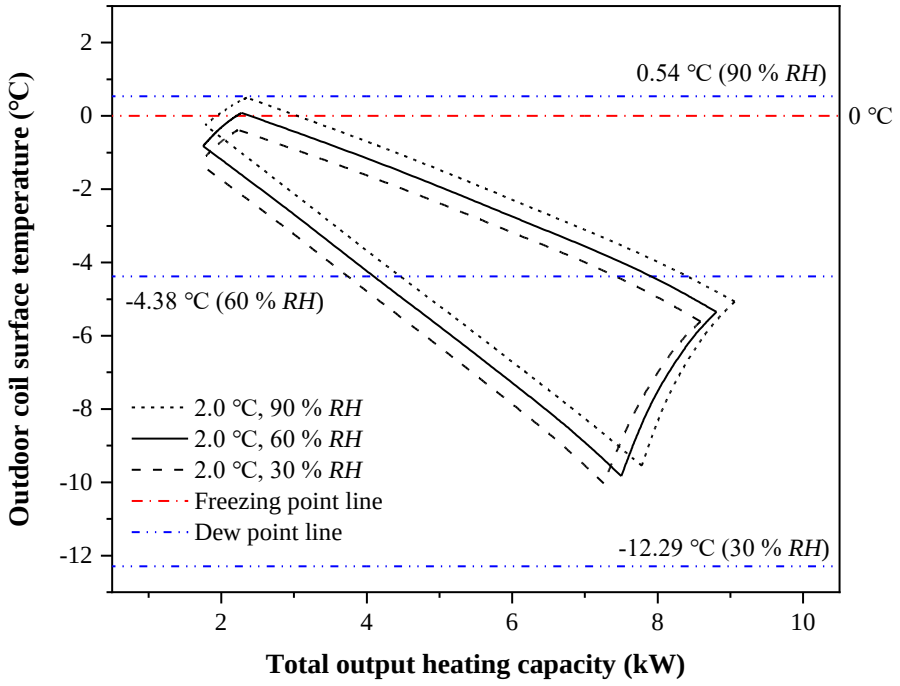

(c) Study Case II–4

Fig. 6.12 Predicted condensing-frosting performance maps for the experimental VS ASHP unit at different outdoor ambient air relative humidity

In addition to the simulation results discussed above, Tables 6.4 and 6.5 list the evaporating and condensing pressures of the experimental VS ASHP unit operated at the four special boundary speed combinations in Study Cases II–1 and II–2, respectively. The effect of the changes in compressor and outdoor air fan speeds on the evaporating and condensing pressures was consistent with that described in Section 6.4.1. With regards to the operating ambient conditions, a higher outdoor air temperature at a fixed outdoor air relative humidity would result in higher evaporating and condensing pressures of the experimental VS ASHP unit. In contrast, a relative drier operating ambient environment at a fixed outdoor air temperature would result in slightly lower evaporating and condensing pressures. By referring to the obtained condensing-frosting performance maps, the effects of outdoor air temperature and

relative humidity on the evaporating pressure and condensing pressure were consistent with those on the outdoor coil surface temperature and the total output heating capacity. Furthermore, in Study Cases II–3 and II–4, the variation trends in the evaporating and condensing pressures were similar to those in Study Case II–2, and are therefore not repeated here.

Table 6.4 Evaporating and condensing pressures in Study Case II–1 (90 %*RH* & 100 % *F*)

CS & FS	Varying operating parameters	Evaporating pressure (kPa)	Condensing pressure (kPa)
80 Hz & 100 %	$T_{a,d}$ – 7 ℃	799.24	2326.50
	$T_{a,d}$ – 4.5 ℃	765.25	2208.62
	$T_{a,d}$ – 2 ℃	670.62	2079.79
80 Hz & 25 %	$T_{a,d}$ – 7 ℃	659.74	2175.80
	$T_{a,d}$ – 4.5 ℃	638.71	2050.65
	$T_{a,d}$ – 2 ℃	574.63	1939.93
20 Hz & 100 %	$T_{a,d}$ – 7 ℃	955.69	1791.72
	$T_{a,d}$ – 4.5 ℃	890.68	1735.65
	$T_{a,d}$ – 2 ℃	803.56	1700.01
20 Hz & 25 %	$T_{a,d}$ – 7 ℃	937.49	1720.07
	$T_{a,d}$ – 4.5 ℃	877.25	1698.52
	$T_{a,d}$ – 2 ℃	782.21	1655.24

Table 6.5 Evaporating and condensing pressures in Study Case II–2 (7 ℃ & 100 % *F*)

CS & FS	Varying operating parameters	Evaporating pressure (kPa)	Condensing pressure (kPa)
80 Hz & 100 %	*RH* – 90 %	799.24	2326.50
	RH – 60 %	788.52	2305.35
	RH – 30 %	779.11	2294.21
80 Hz & 25 %	*RH* – 90 %	659.74	2175.80
	RH – 60 %	653.50	2164.92
	RH – 30 %	650.88	2154.04
20 Hz & 100 %	*RH* – 90 %	955.69	1791.72
	RH – 60 %	925.35	1784.25
	RH – 30 %	906.69	1772.14
20 Hz & 25 %	*RH* – 90 %	937.49	1720.07
	RH – 60 %	899.52	1711.84
	RH – 30 %	862.31	1703.61

6.5 Conclusions

In this Chapter, a mathematical model for the experimental VS ASHP unit was developed and validated. The validated model was further used in a follow-up modeling study to obtain condensing-frosting performance maps for the experimental VS ASHP unit with different outdoor coil surface areas and at different outdoor operating ambient conditions. The conclusions of this Chapter are as follows:

1) A mathematical model for the experimental VS ASHP unit has been developed, and there were two different sub-models for the outdoor coil, one for frost-free operations and the other for frosting operations. The experimental validation results showed that the average relative errors between the measured and predicted

total output heating capacity and COP were both within 4.0 %, and the average error between the measured and predicted outdoor coil surface temperature at 0.2 °C. This developed model could be used to obtain the condensing-frosting performance map with acceptable accuracy for predicting the operational characteristics of a VS ASHP unit.

2) Increasing the outdoor coil surface area of the experimental VS ASHP unit by three folds, its outdoor coil surface temperature and total output heating capacity on average were increased by more than 1.37 °C and 11.07 %, respectively, and the area of frost-free region in the performance map was enlarged. However, although improved frosting suppression and heating performances of the experimental VS ASHP unit by increasing its outdoor coil surface area can be resulted in as the operating ambient condition was deteriorated, a higher initial manufacturing cost should be expected.

3) Increasing the inlet outdoor air temperature from 2 °C to 7 °C at a fixed outdoor relative humidity, the variation range of outdoor coil surface temperature and the total output heating capacity from the experimental VS ASHP unit were increased by 1.29 °C and 32.55 %, respectively. A higher inlet outdoor air temperature would provide a more favorable operating environment for a higher total output heating capacity and better frost-suppression for an ASHP unit.

4) Reducing the inlet outdoor air relative humidity by 30 % at a fixed outdoor air temperature, the outdoor coil surface temperature and the total output heating capacity from the experimental VS ASHP unit were decreased by more than

0.34 °C and 1.96 %, respectively. However, a larger frost-free region in the performance map was obtained, which was conducive to improved frost-free operation for ASHP unit.

As mentioned earlier, further modifications may become necessary when applying the developed model to other types of VS ASHP units operated at different outdoor conditions. However, since the model was developed based on the fundamentals of thermodynamics and hence general in nature, the required modifications were expected to be minimum. Therefore, the model can be a very useful tool in studying the operating characteristics of VS ASHP units during both frosting and frosting-free operations, for guiding the design and control of ASHPs for their efficient and reliable operations.

The mathematical model presented in this Chapter, and the experimental study presented in Chapter 5, can provide comprehensive coverage of condensing-frosting performance maps for the experimental VS ASHP unit at both experimental and non-experimental unit configurations and operating ambient conditions. These performance maps can be used as a basis to provide guidance for an efficient and yet reliable operation of an ASHP through developing a novel control strategy for the experimental VS ASHP unit. This is reported in Chapter 7.

Chapter 7

Developing a novel control strategy for frosting suppression based on condensing-frosting performance maps for the experimental VS ASHP unit

7.1 Introduction

The experimental study reported in Chapter 5 has suggested that changing the speeds of the compressor and outdoor air fan in the experimental VS ASHP unit could change its outdoor coil surface temperature, thus its frosting suppression performance would be changed, but different heating performances in terms of output heating capacity may also result in. In order to comprehensively evaluate the frosting suppression performance and heating performance of the experimental VS ASHP unit at different speed combinations of its compressor and outdoor air fan, condensing-frosting performance maps were developed experimentally. To facilitate obtaining more condensing-frosting performance maps at other non-experimental unit configurations and non-experimental ambient conditions, a physics-based mathematical model for the experimental VS ASHP unit was developed and used for a further modeling study, as reported in Chapter 6. It was understandable that the developed performance maps could help the designers / operators of ASHPs to easily determine suitable speed combinations from frost-free operation, and may therefore be used as the basis for developing a novel control strategy for VS ASHPs for effective frosting suppression.

Therefore, in this Chapter, a novel control strategy for frosting suppression based on the condensing-frosting performance maps has been proposed and experimentally studied by using the experimental setup reported in Chapter 4, and the study results

are reported. Firstly, the novel control strategy is detailed. This is followed by describing experimental procedures and conditions. Thirdly, the experimental results and related discussions are presented. Finally, a conclusion is given.

7.2 Details of the developed novel control strategy based on condensing-frosting performance maps

7.2.1 Condensing-frosting performance maps obtained by the previous related experimental and modeling studies

As discussed in Chapters 5 and 6, condensing-frosting performance maps for the experimental VS ASHP unit at different operating ambient air conditions and configurations obtained in the experimental and modeling studies may be used to comprehensively evaluate both the heating and frosting suppression performances of the unit under different speed combinations of its compressor and outdoor air fan. Fig. 7.1 presents, as an example, the condensing-frosting performance maps for the experimental VS ASHP unit at two typical ambient air conditions of 2.0 ^{o}C ($T_{a,\,d}$) / 1.0 ^{o}C ($T_{a,\,w}$) and 4.5 ^{o}C ($T_{a,\,d}$) / 3.0 ^{o}C ($T_{a,\,w}$), respectively, which were obtained by using the validated mathematical model reported in Chapter 6.

The performance data on the condensing-frosting performance maps, for example those shown in Fig. 7.1 were obtained when the experimental VS ASHP unit was operated at steady-state conditions. As mentioned in Section 5.2, as the steady-state operation went by for a period of time of about 30 minutes, however, these data may no longer hold, as a result of gradually increased frost thickness and reduced air flow

rate. When the frost thickness actually exceeded a critical value, the air flow rate and the outdoor coil surface temperature would be greatly reduced, suggesting the need for defrosting.

Furthermore, as seen from the condensing-frosting performance maps shown in Fig. 7.1, at a required output heating capacity, an ASHP unit may have to operate at frosting conditions. This was particularly true when ambient air temperature was low, or the required heating capacity was high. However, to reduce the severity of frosting, it was highly desirable to select speed combinations that were closer to the frosting line, provided that the output heating capacity requirement can be met.

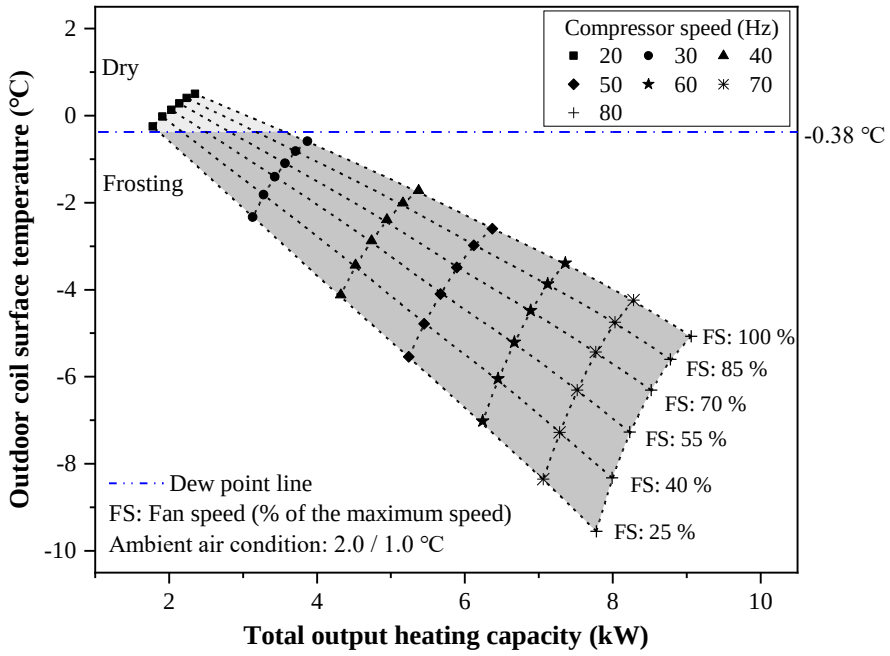

(a) at ambient air condition of 2.0 ºC ($T_{a,\,d}$) /1.0 ºC ($T_{a,\,w}$)

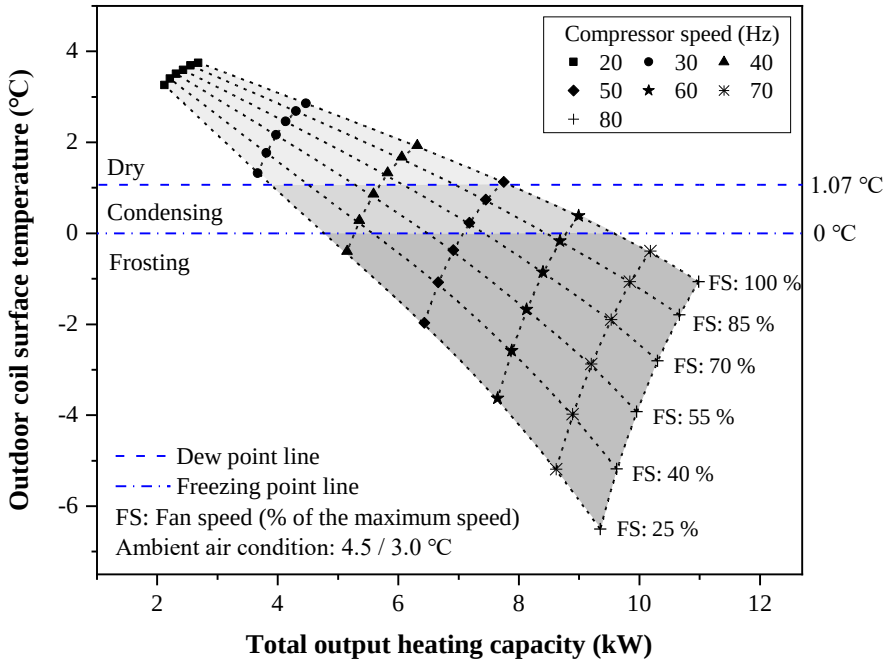

(b) at ambient air condition of 4.5 ºC ($T_{a,\,d}$) / 3.0 ºC ($T_{a,\,w}$)

Fig. 7.1 Condensing-frosting performance maps for the experimental VS ASHP unit at two typical ambient conditions

7.2.2 Control rules

To ensure that a VS ASHP unit can not only meet the required heating demand at the highest possible operating efficiency but also achieve the maximum level of frosting suppression, there were three control rules incorporated in the developed novel control strategy, as follows:

Firstly, the required output heating capacity should be the primary consideration as it was the objective of providing space heating using a VS ASHP unit. According to the appropriate design and testing standards [MIIT China, 2018; AHRI, 2008], the output

heating capacity from the VS ASHP unit during heating period should not be less than 90 % of the required space heating capacity.

Secondly, when the first rule was satisfied, the VS ASHP unit should be operated in a non-frosting region on a performance map as far as possible. If, however, the required heating capacity can only be provided when operating in the frosting region, the VS ASHP unit should be firstly operated at a speed combination point with a higher output heating capacity and a high COP value whenever possible.

Thirdly, as mentioned in Chapter 5, after the VS ASHP unit was operated at steady state for a period of time in the frosting region, as the frost layer became thicker, its operating performance would deteriorate, and the actual outdoor coil surface temperature may deviate from those shown on the performance maps. In this situation, in order to further delay the starting of defrosting thus further extending the heating operating of the VS ASHP, the speed combination can be further changed to a new one with a higher outdoor coil surface temperature. However, the implementation of such changes should also satisfy the first rule.

As mentioned above, when the unit had to operate in the frosting region, its speed combination would be changed during the heating operation to suppress frosting and enable an extended heating operation. However, the new speed combination that led to a better frosting suppression performance, i.e., a higher outdoor coil surface temperature, may result in a slightly lower output heating capacity and COP value. Since the initial speed combination was set with a higher output heating capacity and a high COP value whenever possible, it was expected that the average output heating

capacity and COP values over the entire heating duration would not be significantly affected.

7.2.3 Zoning of the condensing-frosting performance maps

According to the above mentioned three control rules, a condensing-frosting performance map may be divided into several zones to actually use it as the basis for the novel control strategy for frosting suppression for a VS ASHP unit. In this Chapter, the two condensing-frosting performance maps for the experimental VS ASHP unit shown in Fig. 7.1 were used, as examples, to specifically illustrate their zonings when developing the novel control strategy, as shown in Fig. 7.2. As seen, according to the speed combinations of the compressor and outdoor air fan and the output heating capacity from the experimental VS ASHP unit, each performance map was divided into 16 zones, i.e., Zones I-XVI. Since the relative differences of the output heating capacity between the compressor speeds of 20 Hz and 40 Hz were large, the data for the compressor speeds of 25 Hz and 35 Hz, obtained by the previously reported mathematical model, were added to the zoned performance maps. Furthermore, the speed combination with the highest COP in each zone was along the line for the outdoor air fan speed of 70 % in the experimental VS ASHP unit.

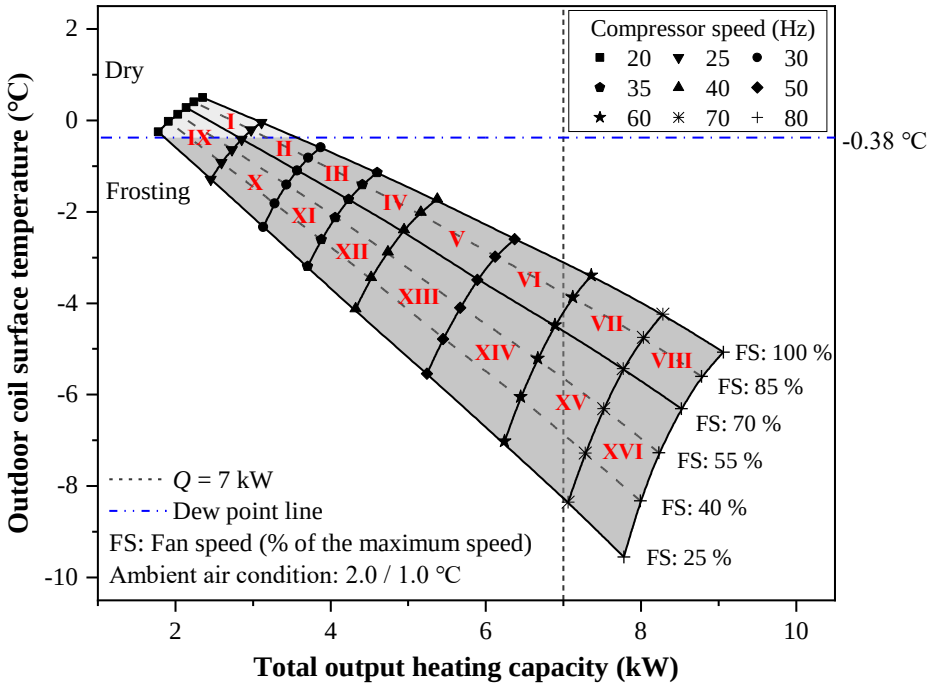

(a) at ambient air condition of 2.0 ºC ($T_{a,d}$) and 1.0 ºC ($T_{a,w}$)

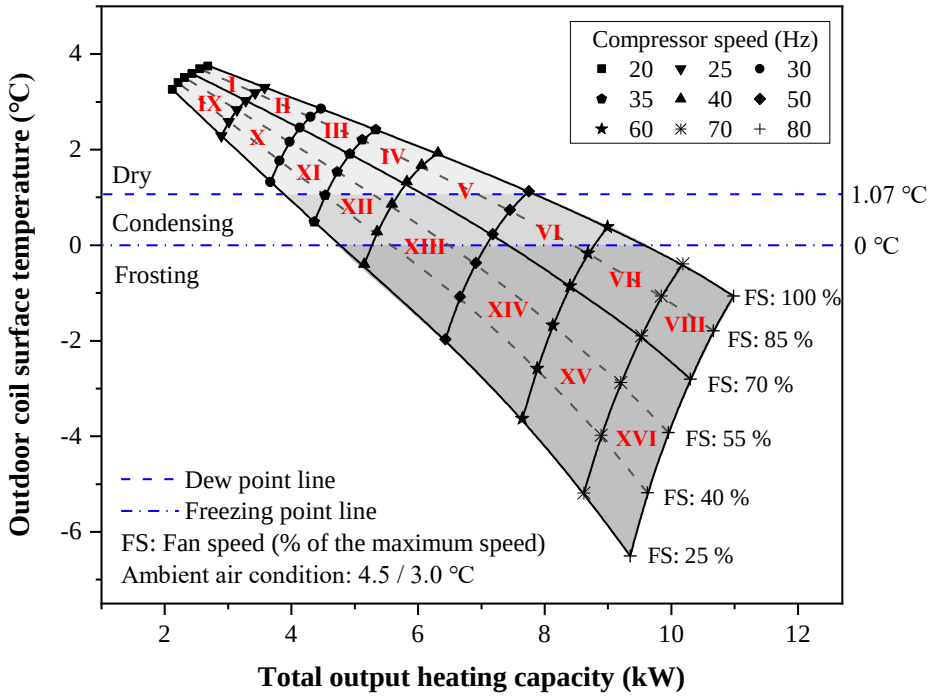

(b) at ambient air condition of 4.5 ºC ($T_{a,d}$) and 3.0 ºC ($T_{a,w}$)

Fig. 7.2 The zoned condensing-frosting performance maps used in the proposed novel control strategy

As seen from Fig. 7.2, when determining the operating speed combination of the experimental VS ASHP unit in a zoned performance map according to the first rule, i.e., to satisfy the required output heating capacity, the speed combination that satisfied the first rule may fall within between 1 and 3 zones. For example, as shown in Fig. 7.2 (a), if the required output heating capacity was 7 kW, the speed combinations may fall in Zones VI, VII and XV, respectively. Therefore, detailed procedures for locating an appropriate operating zone and speed combination in the zoned performance map can be explained in accordance with the three control rules, as follows:

Firstly, one of the Zones I-XVI, where the operating speed combinations for the VS ASHP unit would fall in, should be determined, using the following two steps:

1) The priority to assign an operating zone was given to Zones I-VIII, because the outdoor coil surface temperatures in these zones were higher than those in Zones IX-XVI, which was inducive to better frosting suppression.

2) As shown in Fig. 7.3, to ensure that the required output heating capacity could be met, the total output heating capacity value on the lower right corner point of the boundary for a candidate zone, i.e., Point C in Fig. 7.3, was designated as the critical maximum required output heating capacity for this zone. Then, if the actual required output heating capacity was not greater than the critical maximum value of the zone, this candidate zone may be selected. Otherwise, the zone (shaded zone on Fig. 7.3) on the right-hand side of the candidate zone may be considered as a new candidate zone instead.

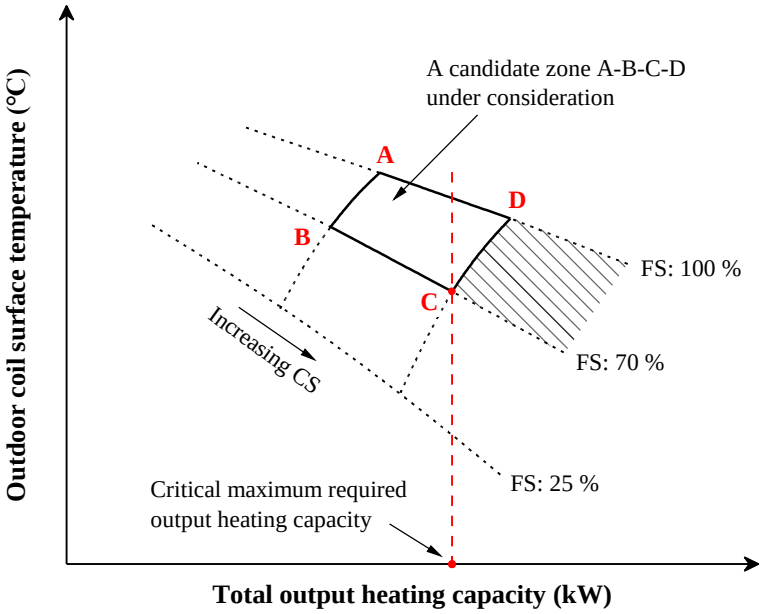

Fig. 7.3 Schematics of operating zone determination

Secondly, the operating speed combination within the selected zone should be determined, at the following two different operating conditions:

1) If there was an operating speed combination point in a non-frosting region on the performance map, with the output heating capacity at that point being not less than 90 % of the required heating capacity, this speed combination should be chosen as the operating point for the VS ASHP unit.

2) Otherwise, an operating point with a higher output heating capacity and the highest possible COP in the selected zone should be chosen as an initial operating speed combination point, and this point should be on the right-hand side boundary line of the selected zone, i.e., Line CD on Fig. 7.3. Since the critical maximum required output heating capacity was at Point C, the output heating capacity at this initial operating speed combination point would therefore be greater than the required output heating

capacity. On the other hand, the highest COP would also occur along 70% fan speed line where Point C lay. Therefore, to consider both the required output heat capacity and the highest possible efficiency, point C was normally selected.

With this initially assigned speed combination, the experimental VS ASHP unit can be operated at steady state for a period of the time. However, as discussed in Section 7.2.1, after the steady-state operation, when the actually measured outdoor coil surface temperature deviated from those shown in the performance map, to further extend the heating operation before defrosting initiation, the initially assigned speed combination would have to be changed to a new speed combination point that can lead to a higher surface temperature, within the selected zone. In general, the new speed combination point was located at up-left corner with the highest outdoor coil surface temperature in the selected operating zone, i.e., Point A in Fig. 7.3, but the output heating capacity at this operating point was in general lower than that at the initial operating point. However, based on the zoning of the condensing-frosting performance map and the selection procedures of the operating speed combination, the output heating capacity during the extended heating period could still meet at least 90 % of the output heating capacity requirements.

7.2.4 Flow chart of the novel control strategy

Fig. 7.4 shows the flow chart of the novel control strategy based on condensing-frosting performance maps for a VS ASHP unit. As seen, the ambient air conditions ($T_{a,\,d}$ and $T_{a,\,w}$) and the required output heating capacity (Q setting) were designated as the input parameters. This was because the ambient air conditions could

significantly affect the frosting suppression and heating performances of a VS ASHP unit, resulting in varying condensing-frosting performance map. On the other hand, the required output heating capacity was the objective for operating the ASHP unit. Then, following the control rules and the procedures in selecting operating zone, as detailed in Sections 7.2.2 and 7.2.3, the operating zone in the performance map was determined. Then, this was followed by judging whether the ASHP unit could be operated only in the frosting region to meet the required output heating capacity. If not, the unit was operated at the speed combination in the selected operating zone in a frost-free region. If yes, the ASHP unit was firstly operated at the initial speed combination in the selected operating zone, normally Point C as shown in Fig. 7.3, and its outdoor coil surface temperature was real-time measured and monitored during the operation. Considering the measurement errors and normal level of fluctuation in operating parameters, once the measured outdoor coil surface temperature was 1.5 °C lower than that at the steady state shown on a performance map, the speed combination would be changed to the new speed combination within selected operating zone, i.e., Point A in Fig. 7.3, to increase the outdoor coil surface temperature for better frosting suppression. Afterwards, the ASHP unit was operated at the new speed combination until defrosting was initiated. When defrosting was completed, the next heating-defrosting cycle began.

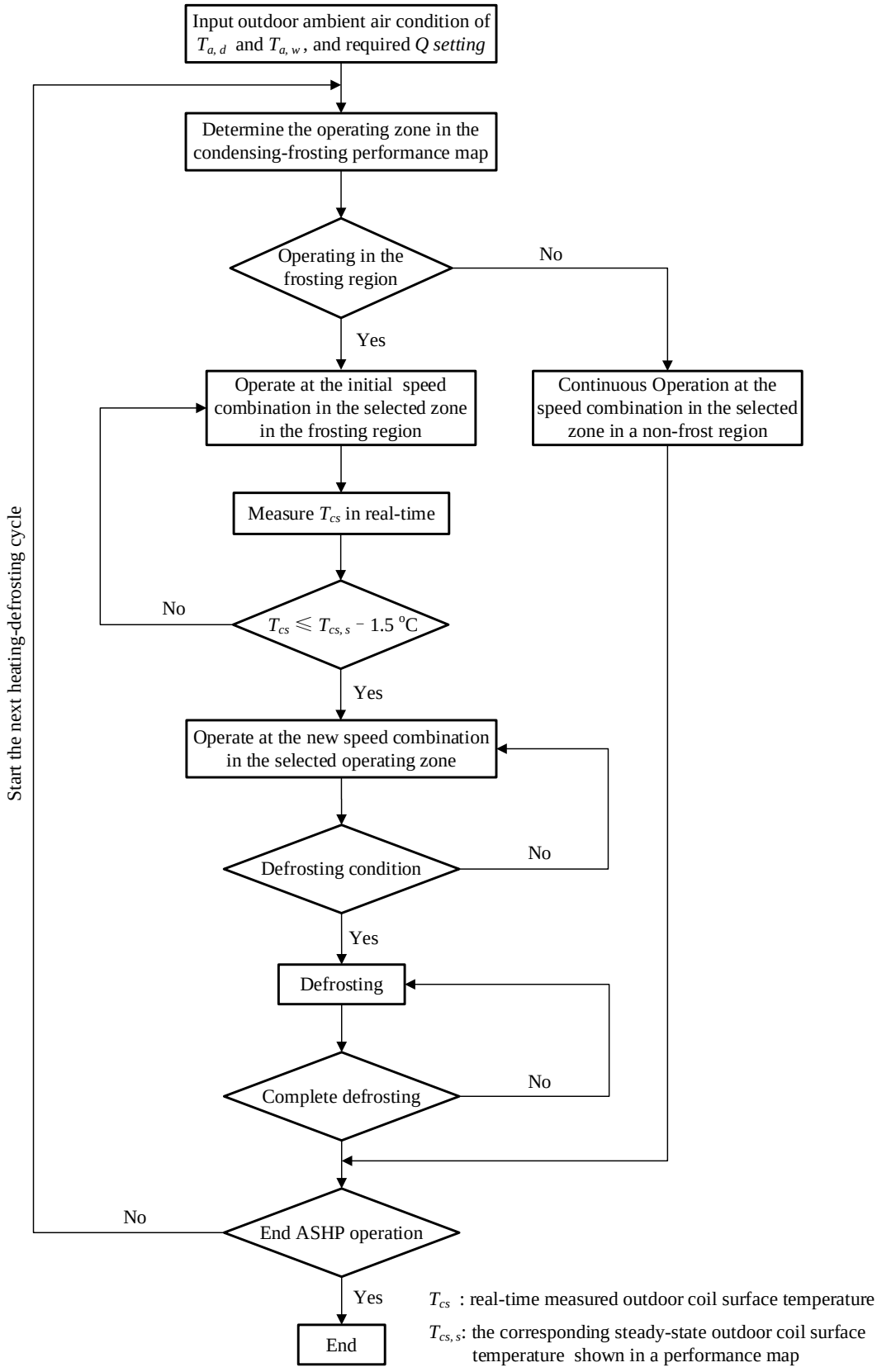

Fig. 7.4 The flow chart of the novel control strategy for frosting suppression based on condensing-frosting performance maps for a VS ASHP unit

7.3 Controllability test conditions and procedures

To examine and demonstrate the controllability of the proposed novel control strategy, controllability tests were carried out at different ambient conditions by using the experimental setup reported in Chapter 4. Although an ASHP unit may be operated at different ambient conditions, in this Chapter, the selection of test ambient conditions was based on the fact that condensing-frosting performance maps should be available at selected ambient conditions. Hence, with reference to the zoned performance maps shown in Fig. 7.2, two typical ambient air conditions were selected as shown in Table 7.1. Test ambient condition 1 was the standard frosting operation condition for ASHPs specified by the Chinese National Standard [MIIT China, 2018], and the typical winter ambient air condition with a mild ambient air temperature but a high air humidity.

Three sets of controllability tests were carried out at each of the two selected ambient air conditions. The details of the three test sets are given in Table 7.2. For each test set, a required output heating capacity from the experimental VS ASHP unit was designated. Therefore, three different output heating capacity settings were designated, and they were within the ranges of the output heating capacities specified in the condensing-frosting performance maps, as shown in Fig. 7.2. In each test set, there were two controllability test cases. One was under the proposed novel control strategy (Cases A-1, B-1 and C-1). The other was a baseline test case (Cases A-2, B-2 and C-2), to provide a comparison base, to demonstrate the effectives and advantages of the proposed novel control strategy. In a baseline test case, the experimental VS ASHP unit was operated at a constant compressor speed to provide the required output heating capacity, and a fixed outdoor air fan speed of 70 % of the maximum speed,

which was the rated fan speed in the experimental ASHP unit. As mentioned earlier, the COP in the baseline test case was highest in the selected operating zone, as the outdoor air fan operated at 70 % of the maximum speed. In all tests, the air temperature in the simulated indoor heated space was maintained at 20.0±0.5 °C.

Table 7.1 Two selected ambient air conditions used in the controllability tests

Ambient air condition	$T_{a,\,d}$	$T_{a,\,w}$	RH
1	2.0 ± 0.2 ℃	1.0 ± 0.2 ℃	83.9 ± 3.0 %
2	4.5 ± 0.2 ℃	3.0 ± 0.2 ℃	78.4 ± 3.0 %

Table 7.2 Details of controllability test conditions

Test Set	Case	Required Q	Mode	Ambient air condition
A	A-1	5.50 kW	Under Novel control strategy	1
	A-2		Baseline	1
B	B-1	7.50 kW	Under Novel control strategy	1
	B-2		Baseline	1
C	C-1	9.00 kW	Under Novel control strategy	2
	C-2		Baseline	2

On the other hand, conventional reverse-cycle defrosting [Qu et al., 2010] was used in all tests. When the outdoor coil surface temperature reached -15.0 ^{o}C, defrosting for the experimental VS ASHP unit was initiated. After completing defrosting, a new operating cycle for the ASHP unit was started. In all controllability tests, a defrosting duration was specified as the time period from the start of defrosting operation to the

resumption of a heating operation in the next operation cycle, and a heating duration as that from the start to the end of a heating operation within an operation cycle.

The instantaneous output heating capacity and COP of the experimental VS ASHP unit reported in this Chapter can be evaluated by Eqs. (5.1) and (5.2), respectively.

7.4 Experimental results and discussions

7.4.1 Experimental results in Test Set A

Figs. 7.5 - 7.8 show the experimental results of the key operating parameters in Test Set A. In Case A-1, the experimental VS ASHP unit was operated under the proposed novel control strategy. Its operating speed combination point was located within Zone V in the condensing-frosting performance map under the ambient air condition 1, i.e., Fig. 7.2 (a), and a given required output heating capacity of 5.50 kW. The experimental VS ASHP unit was first operated at an assigned initial speed combination of 50 Hz for the compressor and 70 % for the outdoor air fan. After 2310 s, its real-time measured outdoor coil surface temperature was 1.5 °C lower than that shown in the performance map, and then the operating speed combination was changed to a new speed combination of 40 Hz for the compressor and 100 % for the outdoor air fan, which was at the up-left corner of Zone V. Thereafter, the experimental VS ASHP unit was operated at the new speed combination until defrosting was initiated at 9560 s. In Case A-2, the experimental VS ASHP unit was operated at the baseline speed combination of 50 Hz for the compressor and 70 % for the outdoor air fan over the entire heating duration. In this case, the operating performances of the experimental VS ASHP unit

deteriorated quickly after 2310 s, and defrosting was initiated at 3710 s. Therefore, the heating duration in one heating-defrosting cycle in Case A-1 under the novel control strategy was 157.68 % longer than that in the baseline Case A-2.

The measured output heating capacity during one heating-defrosting cycle in both Cases A-1 and A-2 are shown in Fig. 7.5 (a). As seen, for both cases, prior to 2310 s, the output heating capacities were the same since the experimental VS ASHP unit was operated at the same speed combination. However, in Case A-1, as the new operating speed combination was used as from 2310 s, a lower output heating capacity was resulted in. The average output heating capacity over the heating duration of 9560 s was at 5.46 kW, which can still meet the required output heating capacity. On the other hand, in Case A-2, since no speed change was implemented as from 2310 s, although the average output heating capacity over the heating duration of 3710 s was higher at 5.72 kW, the experimental VS ASHP unit's operating performance quickly deteriorated, leading to the need for defrosting.

Fig. 7.5 (b) shows the experimental results of COP in Test Set A. As seen, the COP value in Case A-1 was slightly reduced after changing the speed combination, but the average COP over the heating duration of 9560 s was still at 3.50, which was only 0.85 % lower than that at 3.53 in Case A-2.

Fig. 7.5 (c) shows the experimental results of the variations in the measured outdoor coil surface temperature in Test Set A. In Case A-2, the outdoor coil surface temperature began to fall quickly at 2310 s, leading to faster frosting and defrosting

condition soon arrived at 3710 s. In Case A-1, however, the outdoor coil surface temperature soon after 2310 s was actually increased to the value corresponding to the new speed combination after speed change, and remained steadily for quite a long time. Overall, the average rate of reduction in outdoor coil surface temperature in Case A-1 was 0.11 ^{o}C/min, which was 61.87 % lower than that at 0.28 ^{o}C/min in Case A-2. In Fig. 7.5 (c), defrosting durations in Test Set A are also shown. As seen, defrosting duration in Case A-1 was longer than that in Case A-2, as a longer heating operation duration would result in more frost built-up, leading to a longer defrosting duration.

In Fig. 7.5 (d), the experimental results of the variations in air pressure difference across the outdoor coil in Test Set A are shown. In Case A-1, the sudden increase in pressure difference soon after 2310 s was due to the increase in fan speed, resulting in a higher air velocity thus high pressure drop. However, afterwards, the rate of the change in air pressure difference was smaller than that in Case A-2 after 2310 s. In general, the average rate of increase in air pressure difference in Case A-1 was 0.44 Pa/min, which was 36.35 % lower than that at 0.69 Pa/min in Case A-2. This suggested that under the novel control strategy, the growth rate of the frost layer on the outdoor coil surface was lowered, for effective frosting suppression. Furthermore, in Case A-1, the mass of melted frost collected was 2.25 kg after defrosting. This was greater than that in Case A-2 at 1.25 kg.

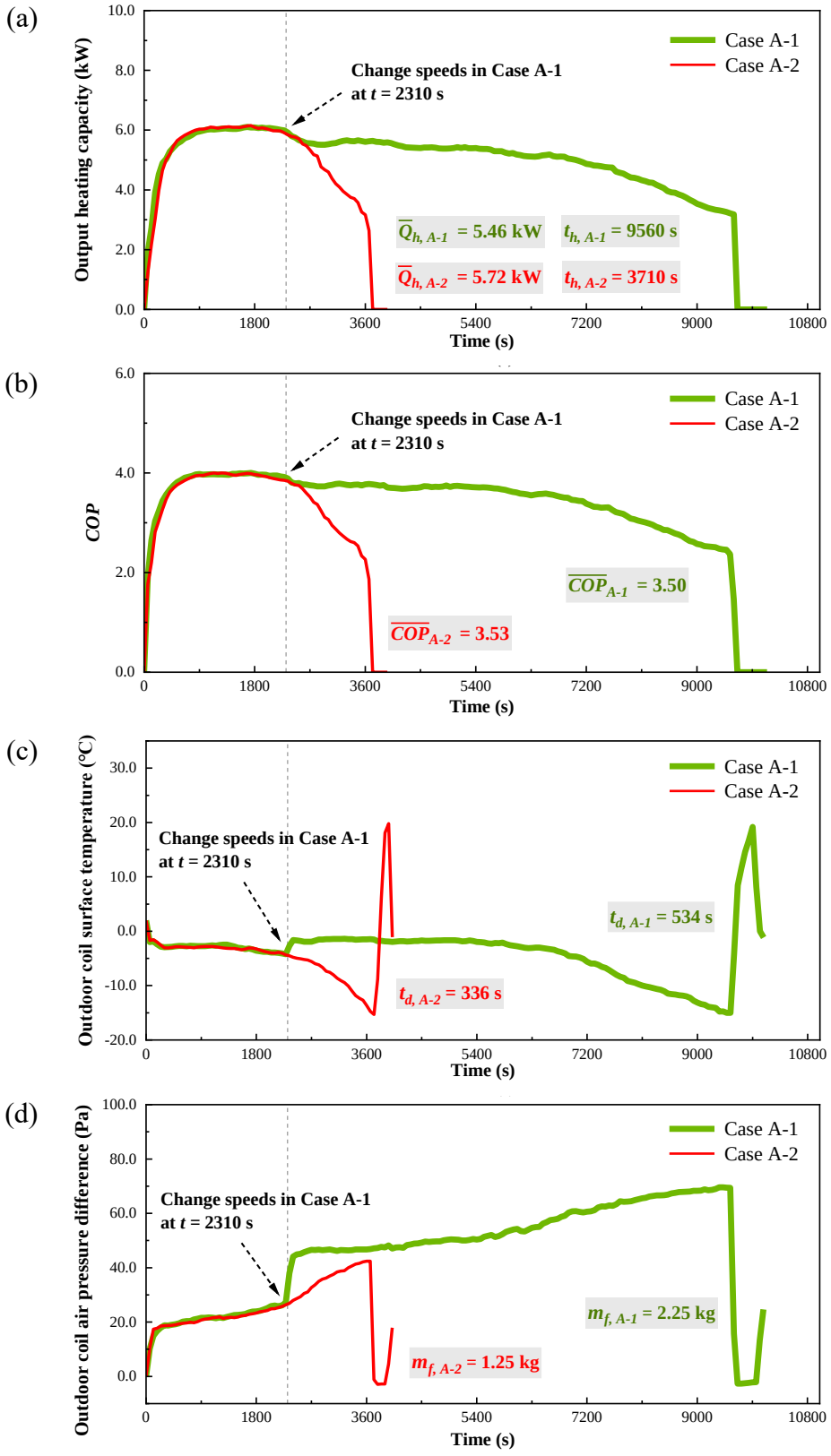

Fig. 7.5 Experimental results of the key operating parameters during one heating-defrosting cycle in Test Set A

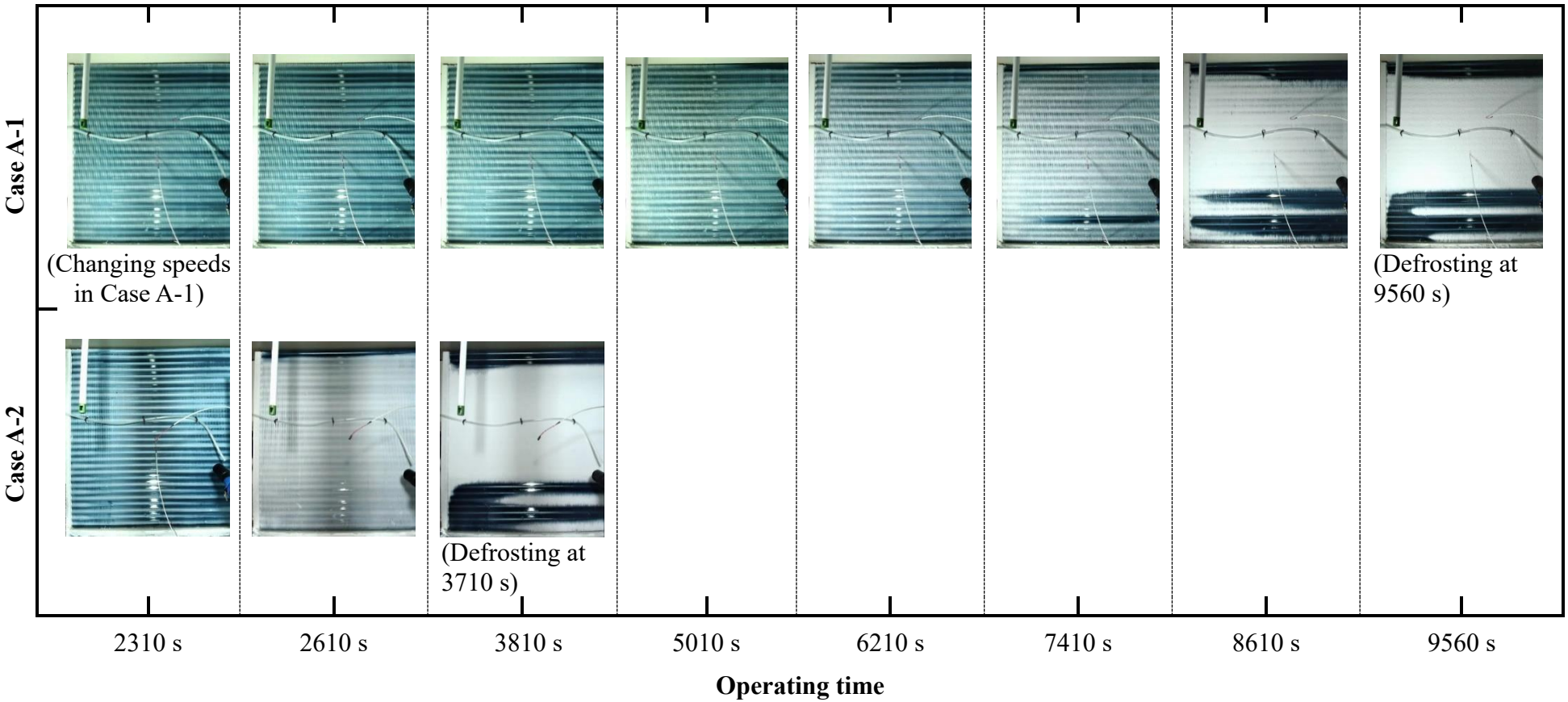

Fig. 7.6 Photo images of frosting on the windward side of the outdoor coil of the experimental ASHP unit in Test Set A

In addition, the photo images of frosting status on the windward side of the outdoor coil in the experimental ASHP unit in Test Set A are shown in Fig. 7.6. As seen, prior to 2310 s, the surface statuses for both cases were similar. However, after 2310 s, when speed changes were implemented in Case A-1, significant difference in surface frosting status for both cases were demonstrated. For example, at 2610 s, much more frost build-up was visible in Case A-2 than in Case A-1.

On the other hand, the daily average operating performances of the experimental VS ASHP unit in Test Set A were also experimentally evaluated, when the unit was operated for a total of 24 hours, as shown in Figs. 7.7 and 7.8, respectively. As seen in Fig. 7.7, for Case A-1, the unit underwent only 9 numbers of defrosting operating in 24 h, which was 59.09 % less than that at 22 number in Case A-2. The total daily defrosting operating duration was 76.18 min in Case A-1, which was 36.30 % lower than that at 119.58 min in Case A-2. Furthermore, the total daily output heating energy, daily defrosting energy consumption and daily average COP are shown in Fig. 7.8. In both cases, the total daily output heating energy was 446.79 MJ and 453.17 MJ, respectively, with a difference between the two only at 1.40 %. The total daily defrosting energy consumption was at 5.89 MJ in Case A-1, which was 31.59 % less than that at 8.61 MJ in Case A-2. In addition, the daily average COP was 3.32 in Case A-1, same as that in Case A-2.

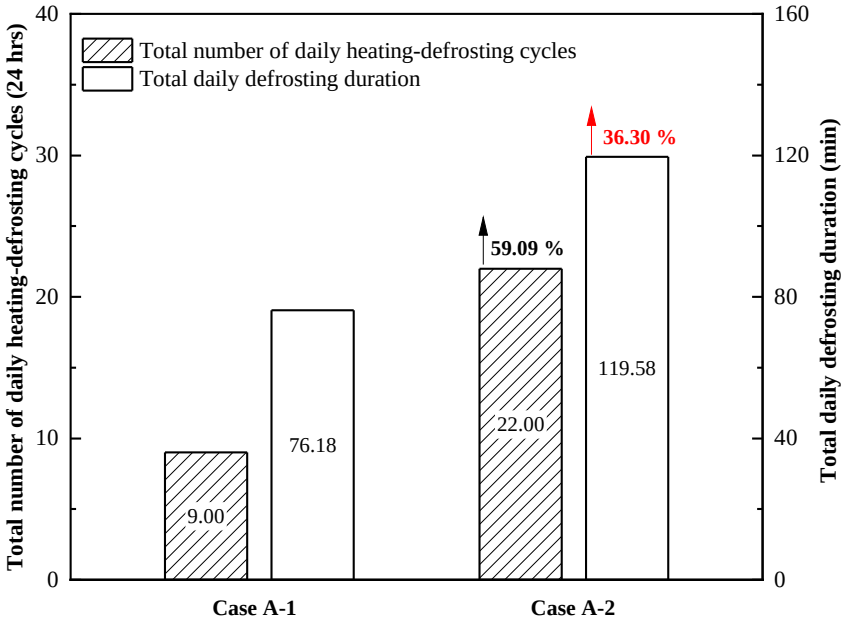

Fig. 7.7 Comparisons of the total number of daily heating-defrosting cycles and total daily defrosting duration in the two cases in Test Set A

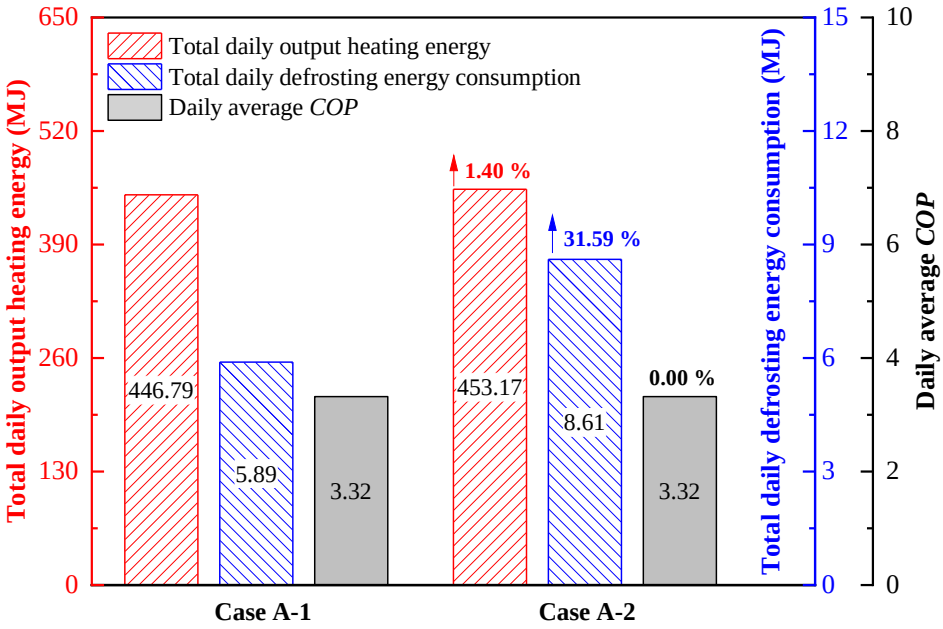

Fig. 7.8 Comparisons of the total daily output heating energy, total daily defrosting energy consumption and daily average COP in the two cases in Test Set A

7.4.2 Experimental results in Test Set B

Figs. 7.9-7.12 show the experimental results of the key operating parameters in Test Set B. Given the fact that the experimental results in Test Set B were similar to those in Test Set A, they are briefly described in this section. In Case B-1, the experimental VS ASHP unit was operated under the proposed novel control strategy. Its operating speed combination point was located within Zone VII in the condensing-frosting performance map under the ambient air condition 1 as shown in Fig. 7.2 (a), and a given required output heating capacity of 7.50 kW. The experimental VS ASHP unit was first operated at an assigned initial speed combination of 70 Hz for the compressor and 70 % for the outdoor air fan. After 1570 s' operation, its real-time measured outdoor coil surface temperature was 1.5 °C lower than that shown in the performance map, then the operating speed combination was changed to a new speed combination of 60 Hz for the compressor and 100 % for the outdoor air fan, which was at the up-left corner of Zone VII. Thereafter, the experimental VS ASHP unit was operated at the new speed combination until defrosting initiation at 5064 s. In Case B-2, to meet the required heating capacity, the experimental VS ASHP unit was operated at the baseline speed combination of 70 Hz for the compressor and 70 % for the outdoor air fan over the entire heating duration. In this case, the operating performances of the experimental VS ASHP unit deteriorated quickly after 1570 s' operation, and defrosting was initiated at 2430 s. Therefore, the heating duration in one heating-defrosting cycle in Case B-1 under the novel control strategy was 108.40 % longer than that in the baseline Case B-2.

As seen in Fig. 7.9 (a), the average output heating capacities over their respective heating durations in Cases B-1 and B-2 were 7.36 kW and 7.64 kW, both meeting the required output heating capacity. The average COP over the heating duration, as shown in Fig. 7.9 (b), in Case B-1 was at 3.46, only 1.14 % lower than that at 3.50 in Case B-2. Fig. 7.9 (c) shows the experimental results of the variations in the measured outdoor coil surface temperature in Test Set B. In Case B-2, the outdoor coil surface temperature began to fall at 1570 s and defrosting condition was reached at 2430 s. In Case B-1, however, since changing the operating speed combination at 1570 s, the outdoor coil surface temperature was rather increased, leading to effective frosting suppression and extending further the heating operation duration. Furthermore, the rate of change in air pressure difference across the outdoor coil in Case B-1, as shown in Fig. 7.9 (d), was smaller than that in Case B-2 after 1570 s. This suggested that under the novel control strategy, the growth rate of the frost layer on the outdoor coil surface in Case B-1 was lowered. In Case B-1, the defrosting duration at 402 s was longer, and the mass of melted frost at 1.95 kg greater than their counterparts in Case B-2, respectively, because a longer heating operation duration would result in more frost built-up. In addition, Fig. 7.10 shows the photo images of frosting status on the windward side of the outdoor coil in the experimental ASHP unit in Test Set B. It can be seen that after 1570 s, the frost growth rate in Case B-1 was much slower than that in Case B-2 at the same operating time points.

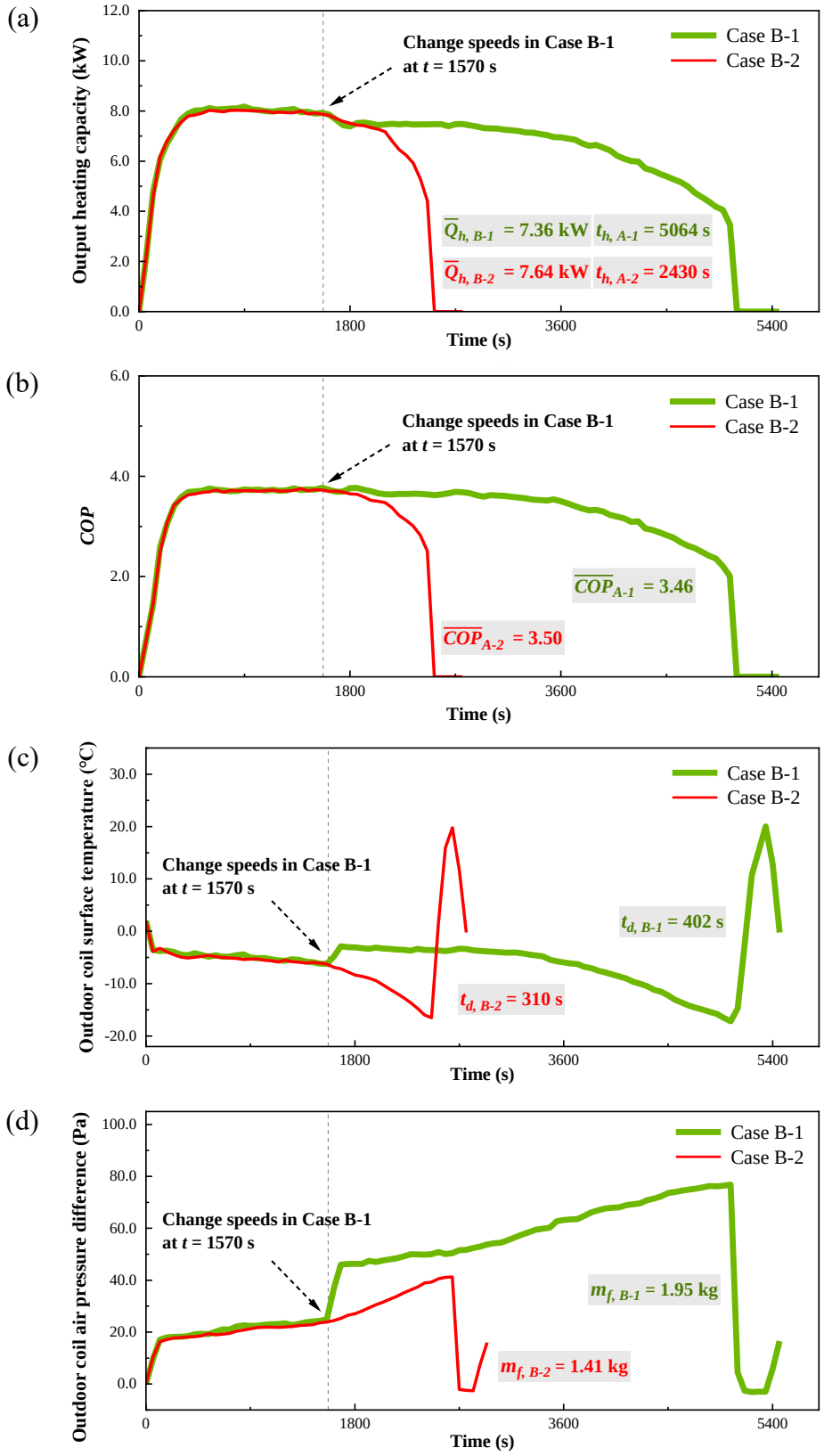

Fig. 7.9 Experimental results of the key operating parameters during one heating-defrosting cycle in Test Set B

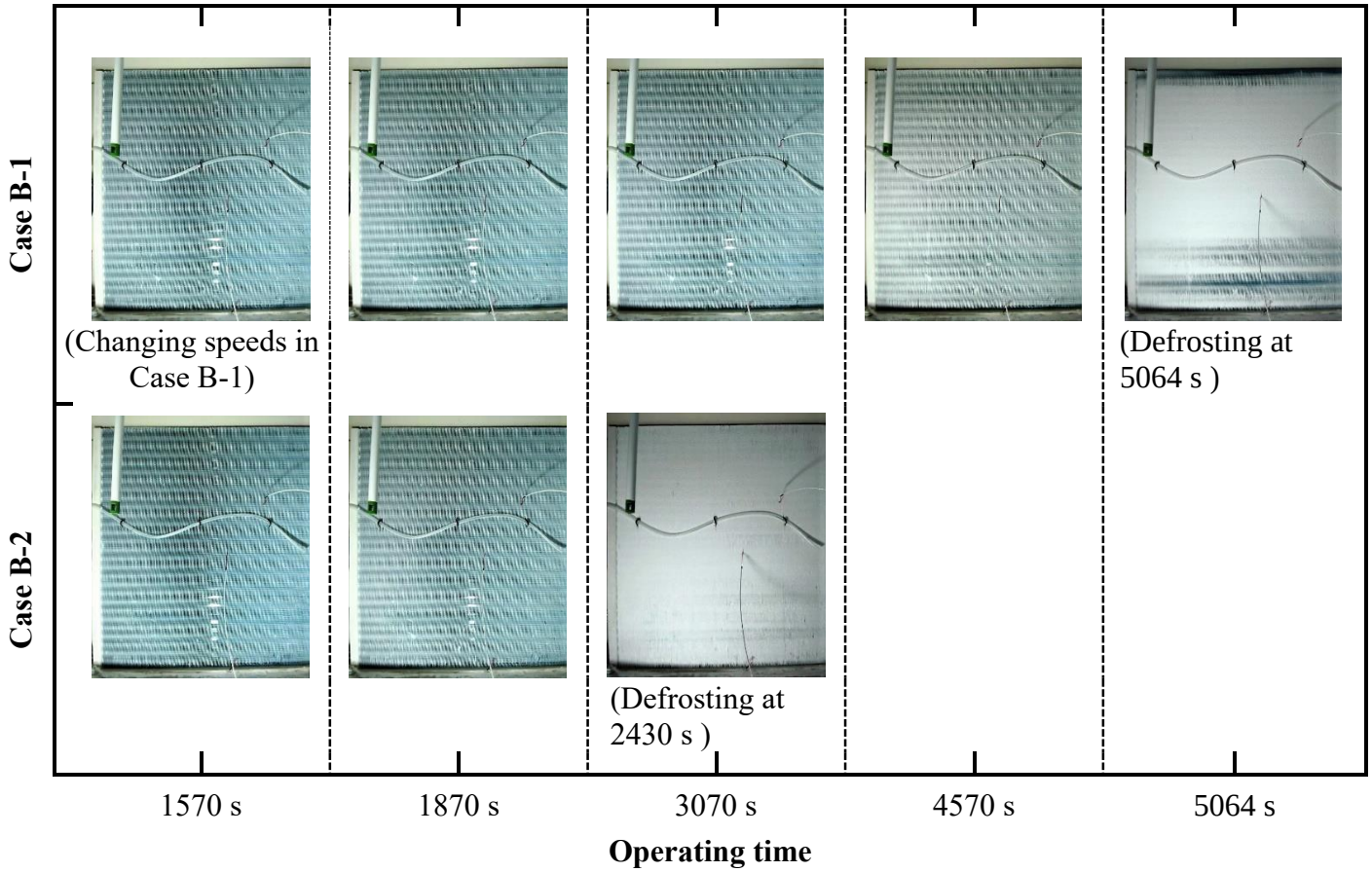

Fig. 7.10 Photo images of frosting on the windward side of the outdoor coil of the experimental ASHP unit in Test Set B

On the other hand, Figs 7.11 and 7.12 show the experimental results of the daily operating performances of the experimental VS ASHP unit in Test Set B. As seen, the number of total daily defrosting operation at 16 in Case B-1 was 50 % less than that at 32 in Case B-2. The total daily defrosting operating duration was 105.91 min in Case B-1, which was 35 % less than that at 162.92 min in Case B-2. The total daily output heating energy at 588.22 MJ in Case B-1 was 0.44 % higher than that at 585.61 MJ in Case B-2, and the total daily defrosting energy consumption at 8.39 MJ in Case B-1 was 32.96 % less than that in Case B-2. Finally, the daily average COP was at 3.28 in Case B-1, same as that in Case B-2.

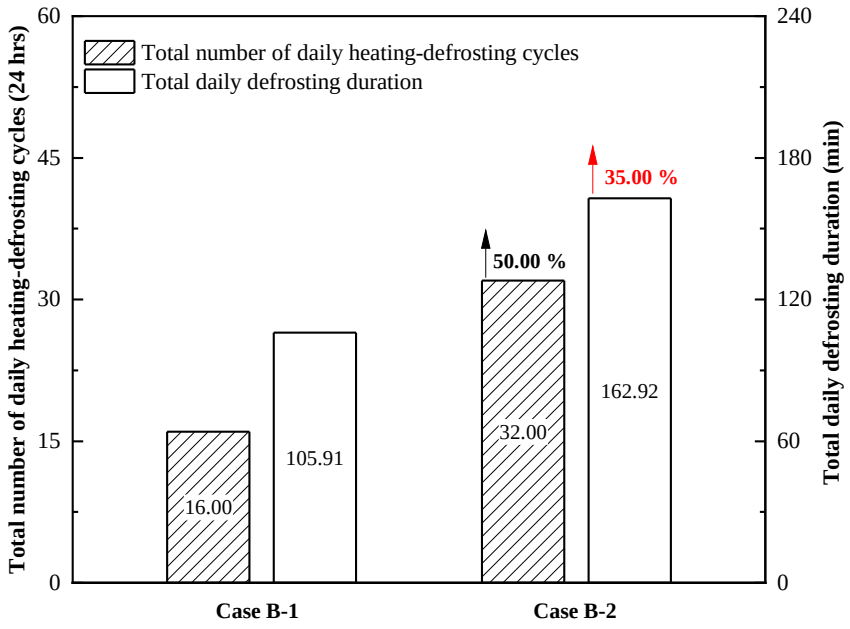

Fig. 7.11 Comparisons of the total number of daily heating-defrosting cycles and total daily defrosting duration in the two cases in Test Set B

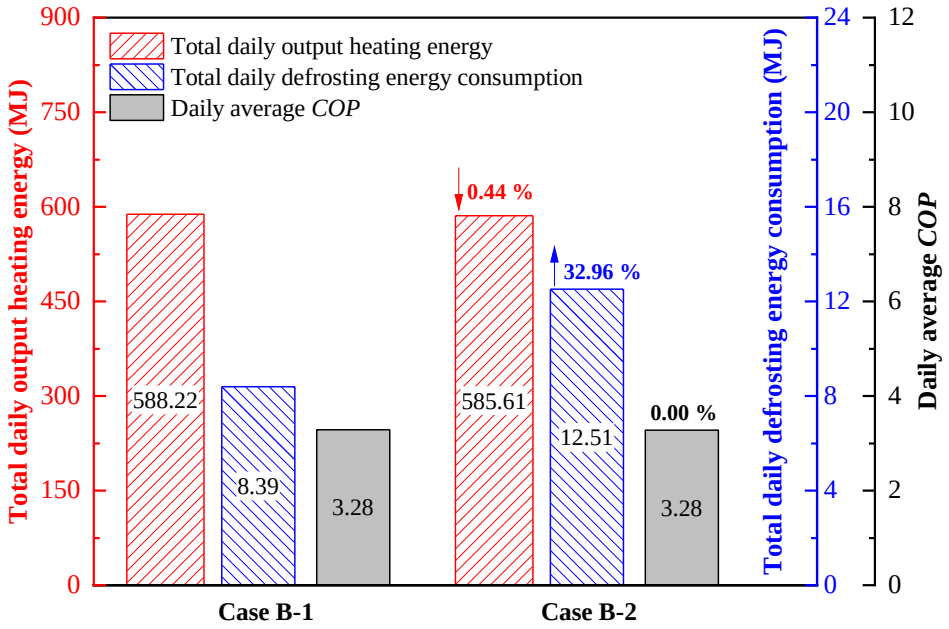

Fig. 7.12 Comparisons of the total daily output heating energy, total daily defrosting energy consumption and daily average COP in the two cases in Test Set B

7.4.3 Experimental results in Test Set C

Figs. 7.13-7.16 show the experimental results of the key operating parameters in Test Set C. In Case C-1, the experimental VS ASHP unit was operated under the proposed novel control strategy. Its operating speed combination point was located within Zone VII in the condensing-frosting performance map under the ambient air condition 2, i.e., Fig. 7.2 (b), and a given required output heating capacity of 9.00 kW. Since the up-left corner point of this selected zone was located in a non-frost region and its output heating capacity could also meet the heating requirement, the experimental VS ASHP unit was operated continuously at this point in Case C-1, at the speed combination of 60 Hz for the compressor and 100 % for the outdoor air fan. Although the measured outdoor coil surface temperature of the unit was the same as that shown in the performance map, with no visible frost accumulation on the outdoor coil surface,

in the earlier operating stage, frost became visible in the later stage, probably because the operating point was close to the freezing line on the performance map and the surface temperature can be uneven. Therefore, in Case C-1, defrosting was initiated after the experimental VS ASHP unit was operated for 8375 s. In Case C-2, to meet the required output heating capacity, the experimental VS ASHP unit was operated at the baseline speed combination of 70 Hz for the compressor and 70 % for the outdoor air fan until defrosting was initiated at 4044 s. Therefore, the heating duration in one heating-defrosting cycle in Case C-1 under the novel control strategy was 107.10 % longer than that in the baseline Case C-2.

The measured output heating capacity during one heating-defrosting cycle in both Cases C-1 and C-2 are shown in Fig. 7.13 (a). As seen, the operating speed combination of the experimental VS ASHP unit in Case C-1 was in a non-frost region on the performance map, leading to a stable operating performance of the unit for a long time. With the occurrence of frosting in the later operating stage due possibly to uneven surface temperature, defrosting was still initiated after 8375 s' operation. The average output heating capacity over the heating duration was at 8.87 kW, only 1.44 % below the required output heating capacity, and within an acceptable difference range. In Case C-2, although the average output heating capacity over the heating duration was at 9.20 kW, higher than that in Case C-1, the operating performance of the unit deteriorated quickly due to severe frosting, and defrosting was initiated at 4044 s.

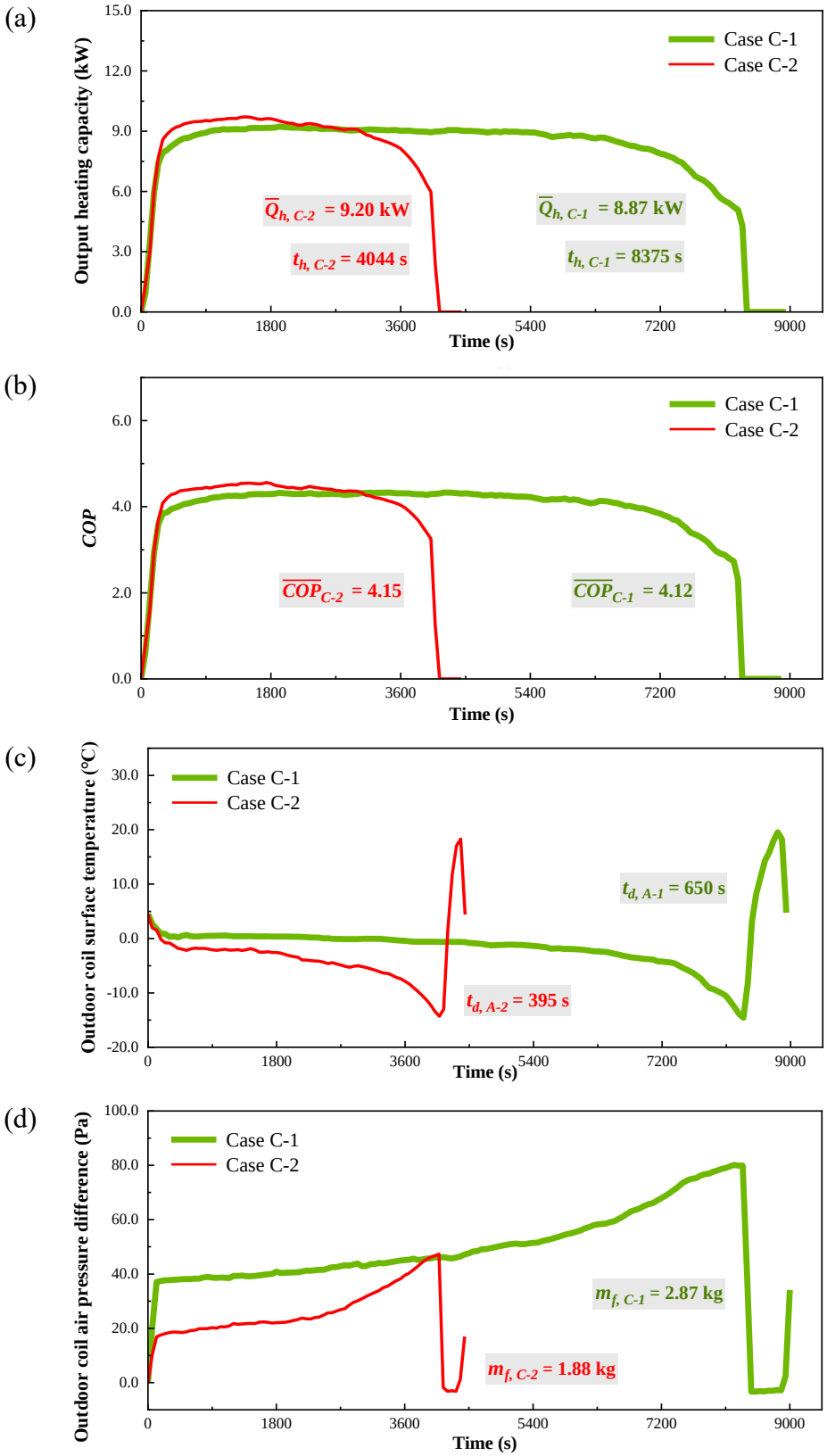

Fig. 7.13 Experimental results of the key operating parameters during one heating-defrosting cycle in Test Set C

Fig. 7.13 (b) shows the experimental results of COP in Test Set C. As seen, in both cases, the variation trends of the COP were similar to those of the output heating capacity. Although the average COP over the heating duration in Case C-2 was at 4.15, higher than that at 4.12 in Case C-1, the relative difference between the two was only 0.26 %.

Fig. 7.13 (c) shows the experimental results of the variations in the measured outdoor coil surface temperature in Test Set C. It was obvious that the outdoor coil surface temperature in Case C-2 was lower than both that in Case C-1 and freezing point, and began to fall quickly until reaching the defrosting condition at 4044 s. In contrast, in Case C-1, the outdoor coil surface temperature was higher than freezing point in the early operating stage. In Case C-1, the operating point was very close to the frosting line and surface temperature may not be even, as the operation went by, after a long time, some frost growth appeared. Surface temperature became gradually lower than the freezing point, and finally reached the defrosting condition. Overall, the average rate of reduction in outdoor coil surface temperature in Case C-1 was 0.12 ^{o}C/min, which was 51.00 % lower than that at 0.24 ^{o}C/min in Case C-2. In Fig. 7.13 (c), defrosting durations in Test Set C are also shown. As seen, defrosting duration in Case C-1 was longer than that in Case C-2.

The experimental results of the variations in air pressure difference across the outdoor coil in Test Set C are shown in Fig. 7.13 (d). As shown, the air pressure difference in Case C-1 was higher than that in Case C-2, due to the fact that the outdoor air fan speed in Case C-1 was higher than that in Case C-2, resulting a higher air velocity and

a higher air pressure difference. Before 4044 s, however, the rate of change in pressure difference in Case C-1 was significantly lower than that in Case C-2. In general, the average rate of increase in air pressure difference in Case C-1 was 0.57 Pa/min, which was 20.43 % lower than that at 0.71 Pa/min in Case C-2. This suggested that under the novel control strategy, the frost growth rate on the outdoor coil surface of the experimental VS ASHP unit was reduced. The final mass of melted frost collected in Case C-1 was greater than that in Case C-2, at 2.87 kg and 1.88 kg, respectively, due to a longer heating duration in Case C-1 than that in Case C-2.

In addition, the photo images of frosting status on the windward side of the outdoor coil in the experimental ASHP unit in Test Set C are shown in Fig. 7.14. As seen at 1200 s, no frost was visible on the outdoor coil in Case C-1, but frost accumulation may be clearly observed in Case C-2. Although frosting took place at the later stage in Case C-1, the frost growth rate was significantly slower than that in Case C-2.

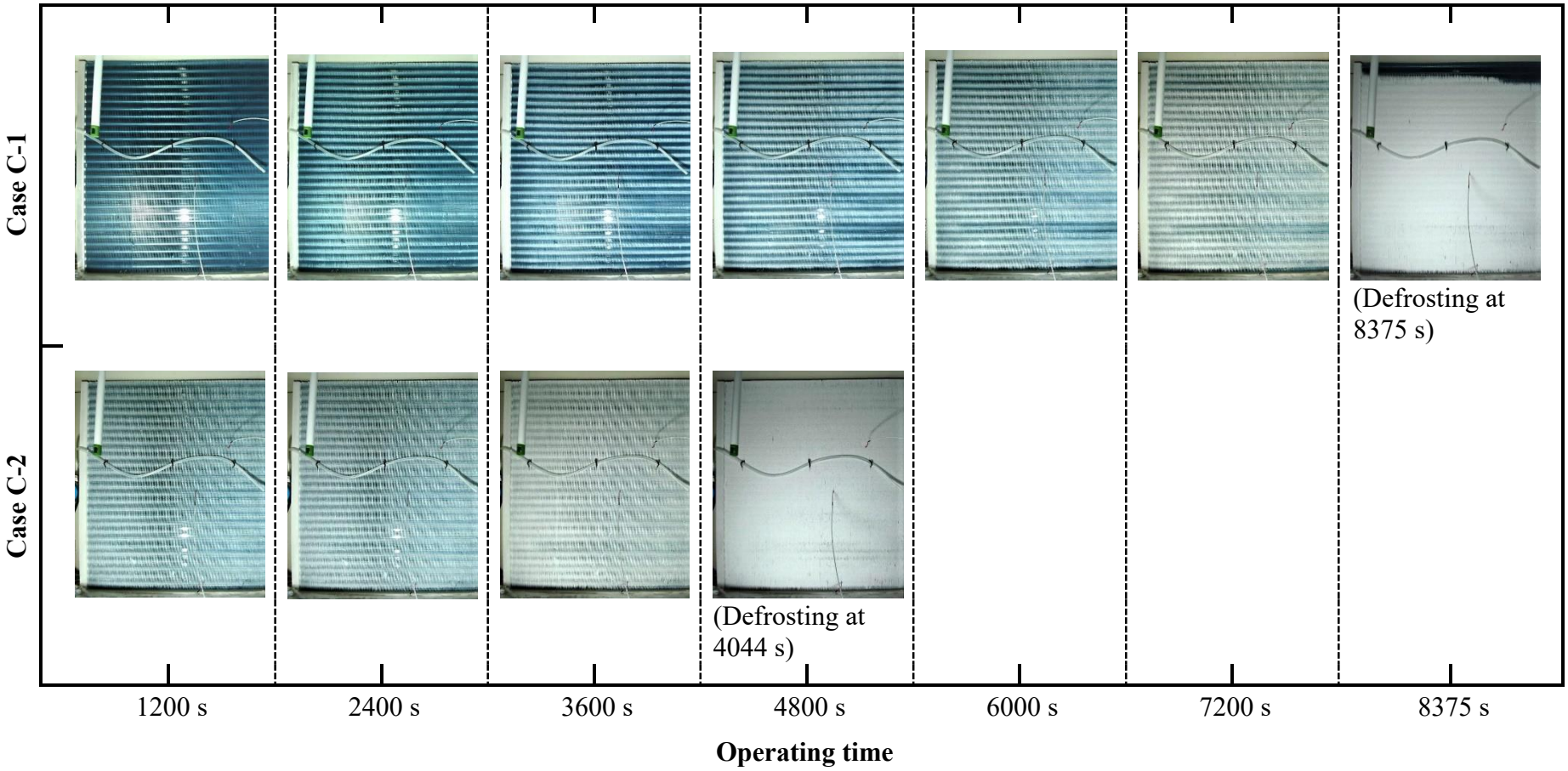

Fig. 7.14 Photo images of frosting on the windward side of the outdoor coil of the experimental ASHP unit in Test Set C

On the other hand, the daily average operating performances of the experimental VS ASHP unit in Test Set C are shown in Figs. 7.15 and 7.16, respectively. It can be seen that the number of total daily heating-defrosting cycle in Cases C-1 and C-2 was 10 and 20, respectively. Accordingly, the total daily defrosting operating duration was 103.71 min in Case C-1, 19.06 % less than that at 128.14 min in Case C-2. Furthermore, the total daily output heating energy in Case C-1 at 711.17 MJ was close to that at 724.15 MJ in Case C-2, with a relative difference of 1.79 %. The total daily defrosting energy consumption in Case C-1 was at 8.40 MJ, 20.82 % less than that at 10.61 MJ in Case C-2. Finally, the daily average COP was 3.93 in Case C-1, close to that at 3.92 in Case C-2.

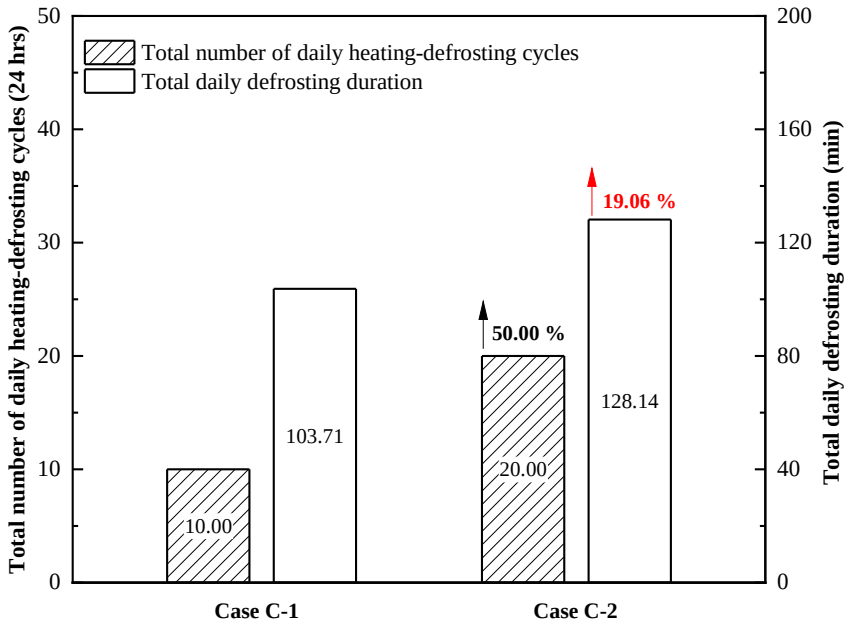

Fig. 7.15 Comparisons of the total number of daily heating-defrosting cycles and total daily defrosting duration in the two cases in Test Set C

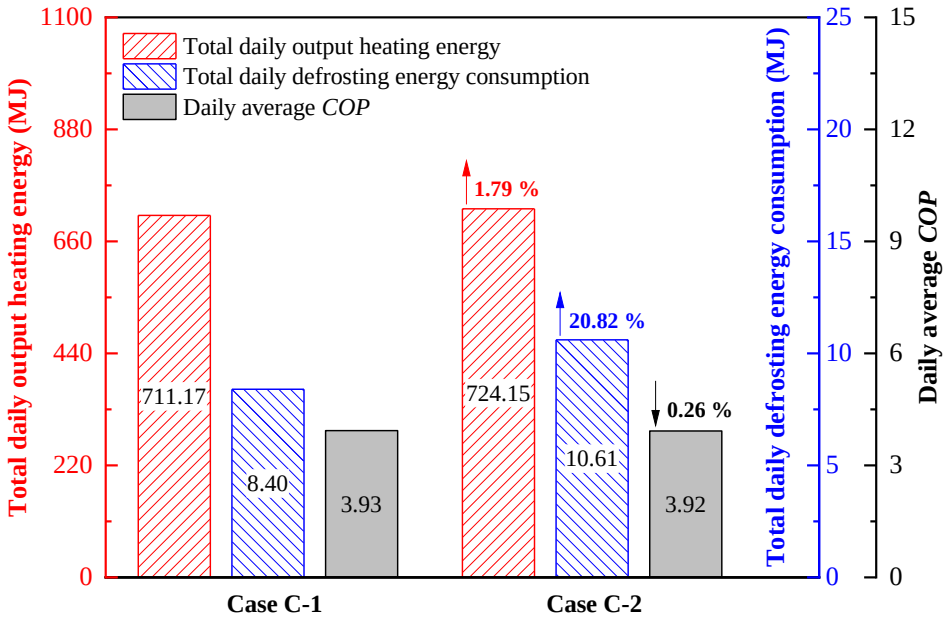

Fig. 7.16 Comparisons of the total daily output heating energy, total daily defrosting energy consumption and daily average COP in the two cases in Test Set C

7.4.4 Discussions

To examine the effectiveness of the proposed novel control strategy for frosting suppression, three sets of controllability tests were designed. As reported, the experimental VS ASHP unit under the novel control strategy was operated in a frosting region on the condensing-frosting performance maps in Cases A-1 and B-1, but in a non-frosting region in Case C-1.

Therefore, in both Cases A-1 and B-1, the unit was first operated at an initial speed combination, with a higher output heating capacity than the required and the highest possible COP value in the selected operating zone. This initial speed combination was not changed until the actual measured outdoor coil surface temperature was 1.5 oC lower than that shown on the performance map, when a new speed combination, which

was located at the up-left corner with the highest outdoor coil surface temperature in the selected operating zone, was used up to defrosting initiation. For the novel control strategy, the use of the new speed combination was to increase the outdoor coil surface temperature and thus achieve effective frosting suppression at the expenses of losing a small fraction of the output heating capacity. This was because a better frost suppression performance of an ASHP unit was usually achieved at a lower output heating capacity. Furthermore, a slightly lower COP may also result in. However, with the selected operating zone, due to the high COP value when the unit was operated at the initial speed combination, and a lower frost growth rate over the entire heating duration, the experimental results in Cases A-1 and B-1 under the novel control strategy suggested that their actual COP values were close to those in their respective matching baseline cases, having the highest COP values in the selected operating zones. Furthermore, in Case C-1, the experimental VS ASHP unit was continuously operated at a speed combination in a non-frosting region on the performance map up to defrosting initiation. Although frosting eventually occurred on the outdoor coil surface due possibly to the unevenness of the surface temperature, it had been operated under non-frosting condition steadily for a long time. Compared with the experimental results in the baseline case, i.e., Case C-2, although the output heating capacity in Case C-1 under the novel control strategy was slightly lower, the frost growth rate was reduced, resulting in a longer heating duration and a COP that was same as or slightly higher than that in Case C-2.

Furthermore, in Cases A-1, B-1 and C-1, the average rates of the reduction in outdoor coil surface temperature and that of the increase in air pressure difference cross the outdoor coil of the experimental VS ASHP unit were lower than those of the baseline

test cases. On one hand, a lower rate of reduction in outdoor coil surface temperature meant that the outdoor coil surface temperature can be maintained at a relatively higher value for a longer duration, which was not conducive to frost growth, and that the experimental VS ASHP unit was operated in a more stable condition. On the other hand, a lower rate of increase in air pressure difference cross the outdoor coil reflected a lower rate of frost growth. Therefore, the experimental results adequately indicated that using the developed novel control strategy can help achieve the effective frost suppression for the experimental VS ASHP unit.

Accordingly, from the experimental results, it can be seen that the novel control strategy can select an appropriate operating zone, depending on the required output heating capacity. Whenever possible, a non-frosting operation was given a priority in selecting the speed combination. When a frosting operation was inevitable by using a new speed within the selected zone, effective frosting suppression and thus a longer heating operation can be achieved. In addition, the COP values over an entire heating duration were not compromised.

On the other hand, it can also be seen from the experimental results that the heating duration of the experimental VS ASHP unit under the novel control strategy in a single heating-defrosting cycle was significantly increased due to effective frost suppression. Although the defrosting duration in a single heating-defrosting cycle may increase, its rate of increase was far smaller than that in the heating duration. Thus, a smaller number of heating-defrosting cycles over an operation of fixed duration may be resulted in, suggesting that the number of defrosting operation and the total defrosting duration were reduced. This would in turn reducing the energy consumption and the

duration of a poor level of indoor thermal comfort due to defrosting. Meanwhile, the average COP values over an entire operating period can be increased.

7.5 Conclusions

In this Chapter, a novel control strategy for frosting suppression based on the condensing-frosting performance map for the experimental VS ASHP unit was proposed. The condensing-frosting performance maps at two typical ambient air conditions were used as examples to illustrate the development of the novel control strategy. The performance maps were divided to 16 different operating zones where operating speed combination may fall in, depending on the required output heating capacity. The proposed control strategy was tested using the experimental VS ASHP unit, and three sets of controllability tests carried out at the two selected ambient air conditions under which the zoned performance maps were available. In each test set, there were two controllability test cases, one under the proposed novel control strategy and the other a baseline test case. The main conclusions are as follows:

1) When the experimental VS ASHP unit was under the proposed novel control strategy, the average rate of reduction in its outdoor coil surface temperature and the average rate of increase in air pressure difference cross the outdoor coil were lowered by up to 61.87 % and 36.35 %, respectively, so that effective frosting suppression may be achieved.

2) Compared with the results from the baseline test cases, the duration of heating operation under the proposed control strategy for the experimental VS ASHP unit in a single heating-defrosting cycle could be increased by up to 157.68 %.

3) With a total operating duration of 24 hours, when the experimental VS ASHP unit was under the proposed control strategy, the number of defrosting operation, the total daily defrosting duration and the total daily defrosting energy consumption were reduced by up to 59.09 %, 36.30 % and 32.96 %, respectively, as compared with those of the baseline test cases.

4) The novel control strategy was developed based on the condensing-frosting performance maps obtained experimentally and by modeling. Therefore, by locating speed combination in an appropriate operating zone based on the required output heating capacity, effective frosting suppression may be achieved. At the same time, a high operating COP may also be possible since the initial speed combination assigned was at those with the highest operating COP, as determined in previous experimental studies.

The proposed novel control strategy for frosting suppression based on condensing-frosting performance maps for a VS ASHP unit was straightforward and simple to implement, and could contribute to the development of frosting suppression measures for ASHPs.

Chapter 8

Conclusions and future work

8.1 Conclusions

A research project on developing condensing-frosting performance maps for the experimental VS ASHP unit to comprehensively evaluate its frosting suppression and heating performances under different speed combinations of its compressor and outdoor air fan by experimental and modeling studies, and on developing a novel control strategy based on the developed performance maps to achieve effective frosting suppression while still providing the required heating outputs, has been successfully carried out and is reported in this Thesis. The conclusions of this Thesis are as follows:

1) An experimental study on the detailed relationships between the outdoor coil surface temperatures and the total output heating capacities of the experimental VS ASHP unit under different speed combinations of its compressor and outdoor air fan was carried out and the study results are reported in Chapter 5. The study results demonstrated that for the experimental VS ASHP unit, changing the speeds of its compressor and outdoor air fan would result in different outdoor coil surface temperatures, thus leading to different frosting suppression performances, as well as different total output heating capacities. Based on the experimental data, condensing-frosting performance maps for the experimental VS ASHP unit at different outdoor operating ambient conditions were developed to comprehensively evaluate its frosting suppression and heating performances under different speed

combinations of the compressor and outdoor air fan. The developed performance maps suggested that for the experimental ASHP unit, a better frosting suppression performance may be achieved, at however the expense of losing some output heating capacity. In addition, further comparative experimental results suggested that when the experimental ASHP unit was operated at different speed combinations that can lead to the same or similar total output heating capacities, its operating characteristics in terms of outdoor coil surface statuses can be significantly different.

2) A modeling study on developing a physical-based mathematical model for the experimental VS ASHP unit is reported in Chapter 6. The model was developed by referring to previously published mathematical sub-models for VS A/C systems and ASHPs, and experimentally validated using the experimental data reported in Chapter 5, with an acceptable accuracy for predicting the operational characteristics of the experimental VS ASHP unit. The validated model was further used in a follow-up modeling study to obtain condensing-frosting performance maps for the experimental VS ASHP unit at non-experimental configurations and non-experimental outdoor operating ambient conditions. The modeling study results demonstrated that i) a larger outdoor coil surface area could result in both better heating and frosting suppression performance of the experimental VS ASHP unit, but at a higher initial manufacturing cost; ii) the maximum total output heating capacity of the unit under frost-free operation was significantly increased as the outdoor air dry-bulb temperature was increased; and iii) a lower outdoor air relative humidity could result in a reduction in both the outdoor coil surface temperature and the total output heating capacity, but a lager frost-free region on the

condensing-frosting performance map, due mainly to the change in outdoor air dew point temperature.

3) The development of a novel control strategy based on the developed condensing-frosting performance maps for the experimental VS ASHP unit for frosting suppression is reported in Chapter 7. The developed novel control strategy was experimentally tested using the experimental VS ASHP unit, and the test results suggested that the experimental VS ASHP unit under the novel control strategy could not only achieve effective frosting suppression, but also output the required heating capacity at high COP values whenever possible. Furthermore, by using the novel control strategy, the heating duration in one frosting-defrosting cycle of the experiment unit could be increased by up to 157.68 %, while the daily defrosting frequency, duration, and energy consumption were reduced by up to 59.09 %, 36.30 % and 32.96 %, respectively.

The successful carrying out of the research project reported in this Thesis has made important contributions to the development of frosting suppression measures for ASHPs. The developed condensing-frosting performance maps could be used to provide detailed guidance for the design, operation and control of ASHPs for frosting suppression to improve their operating performances and reduce energy consumptions. It was expected that the developed performance maps can be included as part of the product inventory for ASHPs. Therefore, it is believed that the research results reported in this Thesis can help encourage wider use of ASHPs as a renewable energy source technology, and contributing significantly to energy conservation and sustainable development worldwide.

8.2 Proposed further work

Based on the successful completion of the research project reported in this Thesis, a number of possible future studies are proposed as follows:

1) The experimental and modeling studies reported in Chapters 5 and 6 illustrated that the developed condensing-frosting performance maps could clearly reveal the relationships between the frosting suppression and heating performances for the experimental VS ASHP unit under different speed combinations of its compressor and outdoor air fan. Different unit configurations and operating conditions could result in different sizes and locations of the performance maps, which reflected the changes in frosting suppression and heating performances. Therefore, the developed condensing-frosting performance maps for ASHPs could be used as the basis for not only frosting suppression, but also for the design and selection of the configuration of ASHPs. For example, selecting a large outdoor coil surface area would benefit frosting suppression but at a higher initial cost. Therefore, it may still be cost-effective to design an outdoor coil with a larger surface area in climates where a standard space heating ASHP unit is normally operated at frosting region.

2) The developed physical-based mathematical model for the experimental VS ASHP unit was experimentally validated with an acceptable predicting accuracy, as reported in Chapter 6. The model included actually two outdoor coil sub-models, i.e., a steady-state sub-model under frost-free conditions and a quasi-steady-state sub-model under frosting conditions. Nonetheless, a full dynamic model for an ASHP unit to simulate the transient responses should be further developed, which

can be used to predict both its steady and transient operating performances for control purpose.

3) The development of the novel control strategy for the experimental VS ASHP unit and its controllability test results reported in Chapter 7 demonstrated that the developed condensing-frosting performance maps could be used as the basis for achieving frosting suppression while still providing the required output heating capacity. In the future, it is possible to digitalize those performance maps which can be directly used for integration with any computerized control schemes for achieving frosting suppression while still meeting space heating requirements.

Appendix

Photo images of the experimental setup

Photo 1 The VS outdoor air fan of the experimental VS ASHP unit

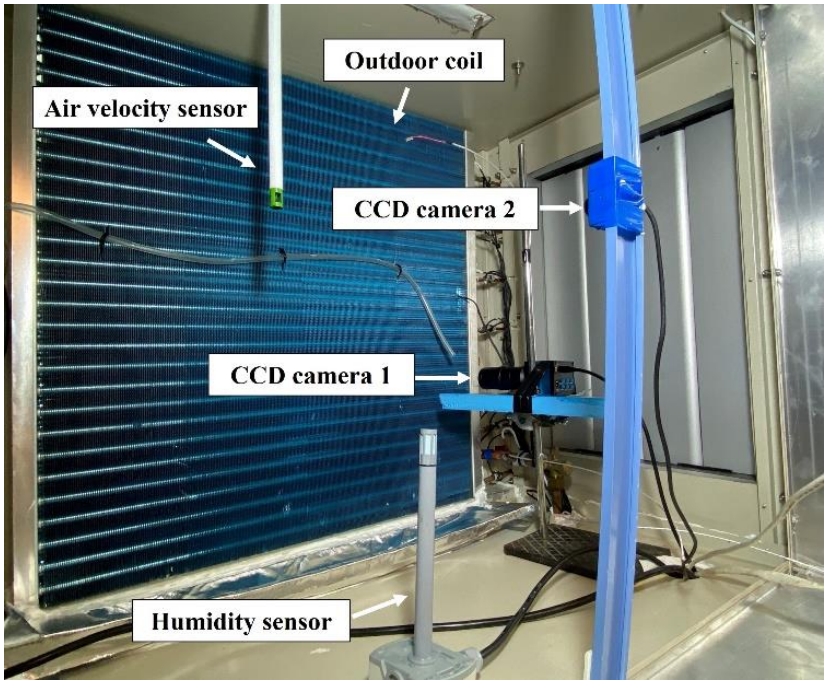

Photo 2 The windward side of the outdoor coil of the experimental VS ASHP unit

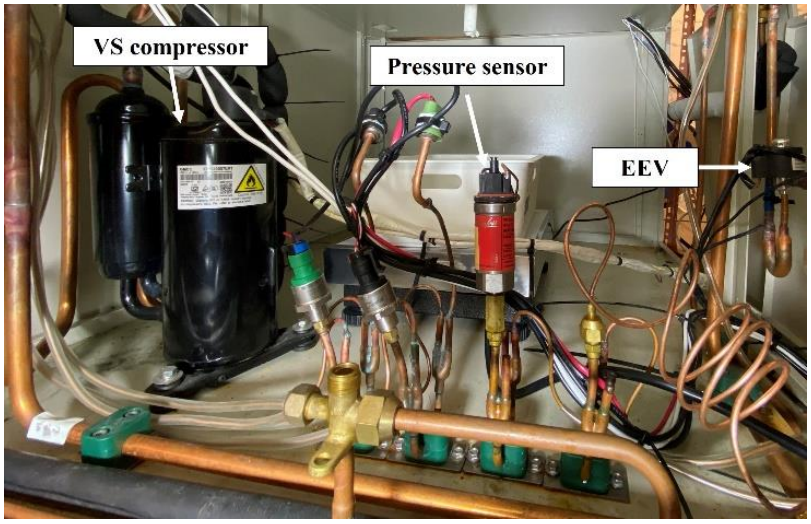

Photo 3 The refrigeration plant in the experimental VS ASHP unit

Photo 4 The existing environmental chamber

References

1. Amirirad et al. 2018
   Amirirad, A., Kumar, R., Fung, A. S. and Leong, W. H.
   Experimental and simulation studies on air source heat pump water heater for year-round applications in Canada. Energy and Buildings, 165 (2018): 141-149.

2. Adachi et al. 1998
   Adachi, K., Saiki, K. and Sato, H.
   Suppression of frosting on a metal surface using ultrasonic vibrations. In 1998 IEEE Ultrasonics Symposium. Proceedings (Cat. No. 98CH36102). IEEE, (1998): 759-762.

3. AHRI 2008
   Air-Conditioning, Heating, and Refrigeration Institute (AHRI).
   AHRI Standard 210/240-2008, Performance Rating of Unitary Air-Conditioning & Air-Source Heat Pump Equipment.

4. ASHRAE 2009
   ASHRAE Handbook Fundamentals.
   American Society of Heating, Refrigerating and Air-Conditioning Engineers. Atlanta, GA, USA.

5. Barrow 1985
   Barrow, H.
   A note on frosting of heat pump evaporator surfaces. Heat Recovery System, Vol . 5, No. 3, pp. 195-201 (1985)

6. Babakin and Elykin 1985
   Babakin, B. C. and Elykin, M. A.
   Frost formation on the surface of refrigeration apparatus under electric fields. Journal of Refrigeration, 2 (1985): 239-245.

7. Bensafi et al. 1997
Bensafi, A., Borg, S. and Parent, D.
CYRANO: a computational model for the detailed design of plate-fin-and-tube heat exchangers using pure and mixed refrigerants. International Journal of Refrigeration, 20 (1997): 218-228.

8. Brown 2003
Brown, G. O.
The history of the Darcy-Weisbach equation for pipe flow resistance. Environmental and water resources history, 2003: 34-43.

9. Carroll et al. 2020
Carroll, P., Chesser, M. and Lyons, P.
Air Source Heat Pumps field studies: A systematic literature review. Renewable and Sustainable Energy Reviews, 134 (2020): 110275.

10. Chesser et al. 2021
Chesser, M., Lyons, P., O'Reilly, P. and Carroll, P.
Air source heat pump in-situ performance. Energy and Buildings, 251 (2021): 111365.

11. China 2015
Guidance Manual for Incorporating Air Thermal Energy into the Scope of Renewable Energy. (2015). Science and Technology Development Promotion Center of the Ministry of Housing and Urban-Rural Development.
Cheng et al. 2001

12. Cheng, C. H. and Cheng, Y. C.
Predictions of frost growth on a cold plate in atmospheric air. International Communications in Heat and Mass Transfer, 28 (2001): 953-962.

13. Cheng et al. 2006
Cheng, W., Yao Y. and Ma, Z.

Influence of Structural Parameters of Air-side Heat Exchanger of Air Source Heat Pump on Frosting Characteristics. Journal of Shenyang Jianzhu University: Natural Science Edition, 22 (2006): 458-461. [in Chinese]

14. Chung et al. 2019
Chung, Y., Yoo, J. W., Kim, G. T. and Kim, M. S.
Prediction of the frost growth and performance change of air source heat pump system under various frosting conditions. Applied Thermal Engineering, 147 (2019):410-420.

15. Chuah et al. 1998
Chuah Y.K., Hung C.C. and Tseng P.C.
Experiments on the dehumidification performance of a finned tube heat exchanger. HVAC&R Research, 4 (1998): 167-178.

16. Chen et al. 2018
Chen, W., Chan, M., Deng, S., Yan, H. and Weng, W.
A direct expansion based enhanced dehumidification air conditioning system for improved year-round indoor humidity control in hot and humid climates. Building and Environment, 139 (2018): 95-109.

17. Choi and Kim 2003
Choi, J. and Kim, Y.
Capacity modulation of an inverter-driven multi-air conditioner using electronic expansion valves. Energy, 28 (2003): 141-155.

18. Chen et al. 2000
Chen, H., Thomas, L. and Besant, R. W.
Modeling frost characteristics on heat exchanger fins: Part I, numerical model/Discussion. ASHRAE Transactions, 106 (2000): 357.

19. Cui et al. 2011
Cui, J., Li, W. Z., Liu, Y. and Zhao, Y. S.

A new model for predicting performance of fin-and-tube heat exchanger under frost condition. International Journal of Heat and Fluid Flow, 32 (2011): 249-260

20. Chinese National Standard 2016
Water chilling (heat pump) packages using the vapor compression cycle. Part 2: Water chilling (heat pump) packages for household and similar application: GB/T 18430. 2-2016. Beijing: Standard Press of China. [In Chinese]

21. Chinese National Standard 2012
Design code for heating ventilation and air conditioning of civil buildings: GB 50736-2012. Beijing: China Architecture & Building Press. [In Chinese]

22. Da Silva et al. 2011
Da Silva, D. L., Hermes, C. J. and Melo, C.
Experimental study of frost accumulation on fan-supplied tube-fin evaporators. Applied Thermal Engineering, 31 (2011): 1013-1020.

23. Dong et al. 2012
Dong, J., Deng, S., Jiang, Y., Xia, L. and Yao, Y.
An experimental study on defrosting heat supplies and energy consumptions during a reverse cycle defrost operation for an air source heat pump. Applied Thermal Engineering, 37 (2012): 380-387.

24. Diaz et al. 1999
Diaz G., Sen M., Yang K. and McClain R.L.
Simulation of heat exchanger performance by artificial neural networks. Hvac&R Research, 5 (1999): 195-208.

25. Ding 2007
Ding G.l.
Recent developments in simulation techniques for vapour-compression refrigeration systems. International Journal of Refrigeration, 30 (2007): 1119-1133.

26. Deng 2000
Deng, S.
A dynamic mathematical model of a direct expansion (DX) water-cooled air-conditioning plant. Building and Environment, 35 (2000): 603-613.

27. Domanski 1991
Domanski, P. A.
Simulation of an evaporator with nonuniform one-dimensional air distribution.(1991)

28. Damasceno et al. 1990
Damasceno, G., Goldschmidt, V. and Rooke, S.
Comparison of three steady-state heat pump computer models. ASHRAE Transactions, 96 (1990).

29. European Union 2009
Commission E. Directive 2009/28/EC of the European Parliament and of the Council of 23 April 2009 on the Promotion of the Use of Energy from Renewable Sources and Amending and Subsequently Repealing Directives 2001/77/EC and 2003/30/EC. Official Journal of the European Union.

30. Elmahdy et al. 1977
Elmahdy, A., AH, E. and GP, M.
A simple model for cooling and dehumidifying coils for use in calculating energy requirements for buildings. (1977).

31. Fletcher and Hasted 1971
Fletcher, N.H. and Hasted, J.B.
The chemical physics of ice. Phys. Today 24 (6) 4 9-4 9. (1971)

32. Guo et al. 2008
Guo, X. M., Chen, Y. G, Wang, W. H. and Chen, C. Z.
Experimental study on frost growth and dynamic performance of air source heat pump system. Applied Thermal Engineering, 28 (2008): 2267-2278.

33. Guo et al. 2011
Guo, X., Wang, S., Wang, W. and Chen, C.
Effects of Environmental Parameters on Surface Frost Layer of Air Source Heat Pump Evaporator. Journal of Xi'an Jiaotong University, 45 (2011): 30-34.

34. Gong et al. 2010
Gong J, Yuan X and Lv B.
Effect of airflow on the performance of middle - large sized air source heat pump system under frosting conditions. Fluid Machinery, 138 (2010): 58-61

35. Guo et al. 2012
Guo, X., Wang, D., Chen, Y., et al.
Effects of face velocity of outdoor heat exchanger on frosting characteristics of air source heat pump system. CIESC Journal, 63 (2012): 32-37.

36. Gu et al. 2001
Gu, B., Tian, S., Sun, T. and Tan, L.
Research on frosting characteristics of air-cooled heat pump units. Heating Ventilation and Air Conditioning, 31 (2001): 81-82. [in Chinese]

37. Gou et al. 2009
Gou, Y., Liu, Z., Liu, Y., Huang, L. and Zhang, M.
Experimental study on the effect of magnetic field on the frosting process on cold surfaces. Journal of Engineering Thermophysics, 3 (2009): 465-467. [in Chinese]

38. Huang 2011
Huang Lingyan
Research on the influence of surface characteristics on the frosting process of cold wall. PhD. Thesis, Beijing University of Technology, (2011)

39. Hayashi et al. 1977
Hayashi Y., Aoki A., Adachi S. and Hori K.

Study of frost properties correlating with frost formation types. Journal of Heat Transfer, 99 (1977): 239-245

40. Hassan et al. 2010
Hassan, M. F., Lee, H. P. and Lim, S. P.
The variation of ice adhesion strength with substrate surface roughness. Measurement Science and Technology, 21 (2010): 075701.

41. Hosoda and Uzuhashi 1967
Hosoda, T. and Uzuhashi, H.
Effects of frost on the heat transfer coefficient. Hitachi Review, Vol. 16, No. 6, pp. 254-259 (1967)

42. Huang et al. 2008
Huang, J.M, Hsieh, W.C., Ke, X.J. and Wang, C.C.
The effects of frost thickness on the heat transfer of finned tube heat exchanger subject to the combined influence of fan types. Applied Thermal Engineering, 28 (2008): 728-737.

43. Huang et al. 2007
Huang, D., He, Z.L. and Y uan, X.L.
Dynamic characteristics of an air-to-water heat pump under frosting/defrosting conditions. Applied Thermal Engineering, 27 (2007): 1996-2002

44. Highgate et al. 1989
Highgate, D., Knight, C. and Probert, S. D.
Anomalous ‘Freezing’ of water in hydrophilic polymeric structures. Applied Energy, 34 (1989): 243-259.

45. Hermes et al. 2014
Hermes, C. J., Loyola, F. R. and Nascimento Jr, V. S.
A semi-empirical correlation for the frost density. International journal of refrigeration, 46 (2014): 100-104.

46. Iragorry et al. 2004
Iragorry, J., Tao, Y. X. and Jia, S.
A critical review of properties and models for frost formation analysis. HVAC&R Research, 10 (2004): 393-420.

47. Ismail et al. 1999
Ismail, K. A. R. and Salinas, C. S.
Modeling of frost formation over parallel cold plates. International Journal of Refrigeration, 22 (1999): 425-441

48. Jhee et al. 2002
Jhee, S., Lee, K. S. and Kim, W. S.
Effect of surface treatments on the frosting/defrosting behavior of a fin-tube heat exchanger. International Journal of Refrigeration, 25(2002), 1047-1053.

49. Jacobi and Goldschmidt 1990
Jacobi, A.M. and Goldschmidt, V.
Low Reynolds number heat and mass transfer measurements of an overall counterflow, baffled, finned-tube, condensing heat exchanger. International Journal of Heat and Mass Transfer, 33 (1990): 755-765.

50. Jia et al. 1995
Jia X., Tso C., Chia P. and Jolly P.
A distributed model for prediction of the transient response of an evaporator. International Journal of Refrigeration, 18 (1995): 336-342.

51. Kim et al. 2017
Kim, M.H., Kim, H., Lee, K.S. and Kim, D.R.
Frosting characteristics on hydrophobic and superhydrophobic surfaces: a review. Energy Convers. Manag. (2017) 138, 1–11.

52. Kobayashi 1958
Kobayashi, T.

On the habit of snow crystals artificially produced at low pressures. Journal of the Meteorological Society of Japan. Ser. II, 36 (1958): 193-208.

53. Kandula 2011
Kandula, M.
Frost growth and densification in laminar flow over flat surfaces. International Journal of Heat & Mass Transfer, 54 (2011): 3719 - 3731.

54. Kondepudi and O'Neal 1991
Kondepudi, S. N. and O'Neal, D. L.
Frosting performance of tube fin heat exchangers with wavy and corrugated fins. Experimental Thermal and Fluid Science, 4 (1991): 613-618.

55. Kim et al. 2013
Kim K., Kim D. R. and Lee K.
Local frosting behavior of a plated-fin and tube heat exchanger according to the refrigerant flow direction and surface treatment. International Journal of Heat and Mass Transfer, 64 (2013): 751-758.

56. Kim and Lee 2013
Kim K. and Lee K.
Frosting and defrosting characteristics of surface-treated louvered-fin heat exchangers: Effects of fin pitch and experimental conditions. International Journal of Heat and Mass Transfer, 60 (2013): 505-511.

57. Kwak and Bai 2010
Kwak, K. and Bai, C.
A study on the performance enhancement of heat pump using electric heater under the frosting condition: Heat pump under frosting condition. Applied Thermal Engineering, 30 (2010): 539–543.

58. Kragh et al. 2005
Kragh, J., Jørgen, R. and Svend, S.

Mechanical ventilation with heat recovery in cold climates. Proceedings of the seventh Nordic symposium on building physics in Nordic countries. Technical University of Denmark, 1 (2005).

59. Kondepudi et al. 1995
Kondepudi, S., Murali, K., Lorsch, H. and Bhalerao, A.
Avoiding heat pump evaporator frosting through the use of desiccants (No. CONF-950336-). American Society of Mechanical Engineers, New York, NY (United States), (1995).

60. Kinsara et al. 1996
Kinsara, A. A., Elsayed, M. M. and Al-Rabghi, O. M.
Proposed energy-efficient air-conditioning system using liquid desiccant. Applied Thermal Engineering, 16 (1996): 791-806.

61. Kim et al. 2016
Kim, H., Kim, D., Jang, H., Kim, D.R. and Lee, K.S.
Microscopic observation of frost behaviors at the early stage of frost formation on hydrophobic surfaces. International Journal of Heat and Mass Transfer, 97 (2016): 861-867.

62. Kim and Lee 2011
Kim, K. and Lee, K. S.
Frosting and defrosting characteristics of a fin according to surface contact angle. International Journal of Heat and Mass Transfer, 54 (2011): 2758-2764.

63. Kim and Lee 2012
Kim, K. and Lee, K. S.
Characteristics and performance evaluation of surface-treated louvered-fin heat exchangers under frosting and wet conditions. International journal of heat and mass transfer, 55 (2012): 6676-6681.

64. Kim and Lee 2013
Kim, K. and Lee, K. S

Frosting and defrosting characteristics of surface-treated louvered-fin heat exchangers: effects of fin pitch and experimental conditions. International Journal of Heat and Mass Transfer, 60 (2013): 505-511.

65. Khattar et al. 1987
Khattar M.K., Swami M.V. and Ramanan, N.
Another aspect of duty cycling: effects on indoor humidity. ASHARE Transaction, 93 (1987): 1678-1687.

66. Khattar and Handerson 1999
Khattar M.K. and Henderson H.I.
Impact of HVAC control improvements on supermarket humidity levels. ASHRAE Transactions, 105 (1999): 521-532.

67. Krakow et al. 1995
Krakow, K. I., Lin, S. and Zeng, Z. S.
Temperature and humidity control during cooling and dehumidifying by compressor and evaporator fan speed variation. ASHRAE Transactions, 101 (1995): 292-304.

68. Kondepudi and O'Neal 1993
Kondepudi, S. N., and O'Neal, D. L
Performance of finned-tube heat exchangers under frosting conditions: I. Simulation model. International Journal of Refrigeration, 16 (1993): 175-180.

69. Liang 1993
Liang, J.
Phase Diagrams and Phase Structures: Theory, Practice and Applications of Phase Diagrams. Science Press, (1993). [in Chinese]

70. Liu et al. 2007
Liu, D., Zhao, F. and Tang, G.
Frosting of heat pump with heat recovery facility. Renewable Energy, 32 (2007): 1228-1242.

71. Lee and Ro 2001
Lee, Y. B. and Ro, S. T.
An experimental study of frost formation on a horizontal cylinder under cross flow. International journal of refrigeration, 24 (2001): 468-474.

72. Liu and Yang 2004
Liu B and Yang Y.
Analysis of a frosting model and its affecting factors. Journal of Refrigeration. 4 (2004): 40-42.

73. Lee et al. 2003
Lee, K. S., Jhee, S. and Yang, D. K.
Prediction of the frost formation on a cold flat surface. International journal of heat and mass transfer, 46 (2003), 3789-3796.

74. Lee et al. 2010
Lee, M., Kim, Y., Lee, H. and Kim, Y.
Air-side heat transfer characteristics of flat plate finned-tube heat exchangers with large fin pitches under frosting conditions. International Journal of Heat and Mass Transfer, 53 (2010): 2655-2661.

75. Lee et al. 2004
Lee, H., Shin, J., Ha, S., Choi, B. and Lee, J.
Frost formation on a plate with different surface hydrophilicity. International Journal of Heat and Mass Transfer, 47 (2004): 4881-4893.

76. Li et al. 2014a
Li, L., Wang, W., Sun, Y., Feng, Y., Lu, W., Zhu, J. and Ge, Y.
Investigation of defrosting water retention on the surface of evaporator impacting the performance of air source heat pump during periodic frosting–defrosting cycles. Applied energy, 135 (2014): 98-107.

77. Li et al. 2010
Li, D., Chen, Z. and Shi, M.

Effect of ultrasound on frost formation on a cold flat surface in atmospheric air flow. Experimental Thermal and Fluid Science, 34 (2010): 1247-1252.

78. Li and Chen 2014
Li, D. and Chen, Z.
Experimental study on instantaneously shedding frozen water droplets from cold vertical surface by ultrasonic vibration. Experimental thermal and fluid science, 53 (2014): 17-25.

79. Liu et al. 2018
Liu, S., Li, H., Song, M., Dai, B. and Sun, Z.
Impacts on the solidification of water on plate surface for cold energy storage using ice slurry. Applied Energy, 227 (2018): 284-293.

80. Li and Deng 2007a
Li Z. and Deng S.M.
An experimental study on the inherent operational characteristics of a direct expansion (DX) air conditioning (A/C) unit. Building and Environment, 42 (2007): 1-10.

81. Li and Deng 2007b
Li Z. and Deng S.M.
A DDC-based capacity controller of a direct expansion (DX) air conditioning (A/C) unit for simultaneous indoor air temperature and humidity control–Part I: control algorithms and preliminary controllability tests. International Journal of Refrigeration, 30 (2007): 113-123.

82. Li and Deng 2007c
Li Z. and Deng S.M.
A DDC-based capacity controller of a direct expansion (DX) air conditioning (A/C) unit for simultaneous indoor air temperature and humidity control–Part II: further development of the controller to improve control sensitivity. International Journal of Refrigeration, 30 (2007): 124-133.

83. Li et al. 2014b
Li, Z., Xu, X., Deng, S. and Pan, D.
Further study on the inherent operating characteristics of a variable speed direct expansion air conditioning system. Applied Thermal Engineering, 66 (2014): 206-215.

84. Li et al. 2017
Li, Z., Chen, J., Yu, H. and Cui, L.
The development and experimental performance evaluation on a novel household variable refrigerant flow based temperature humidity independently controlled radiant air conditioning system. Applied Thermal Engineering, 122 (2017): 245-252.

85. Li et al. 2018
Li, Z., Chen, J., Wang, F., Cui, L. and Qu, M.
A simulation study for evaluating the performances of different types of household radiant air conditioning systems. Applied Thermal Engineering, 131 (2018): 553-564.

86. Liang et al. 2020
Liang, S., Wang, W., Sun, Y., Li, Z., Zhao, J., Lin, Y. and Deng, S.
A novel characteristic index for frosting suppression based on the configuration and operation of air source heat pumps. International Journal of Refrigeration, 109 (2020): 161-171.

87. Lu 2003
Lu, J.
Numerical simulation of air-cooled heat pump chiller and hot water unit in heating mode and theoretical research on gas-liquid separator with heat exchanger.MA Thesis. Xi'an Jiao Tong University, (2003). [in Chinese]

88. Li 2013a
Li W.

Simplified steady-state modeling for variable speed compressor. Applied thermal engineering, 50 (2013): 318-326.

89. Lee et al. 1997
Lee, K. S., Kim, W. S. and Lee, T. H.
A one-dimensional model for frost formation on a cold flat surface. International Journal of Heat and Mass Transfer, 40 (1997): 4359-4365.

90. Li 2013b
Li W.
Simplified modeling analysis of mass flow characteristics in electronic expansion valve. Applied Thermal Engineering, 53 (2013): 8-12.

91. Lemmon et al. 2013
Lemmon, E., Huber, M. and McLinden, M.
NIST Standard Reference Database 23: Reference Fluid Thermodynamic and Transport Properties-REFPROP, Version 9.1. (2013). National Institute of Standards and Technology, Standard Reference Data Program, Gaithersburg.

92. Min 1982
Min N.
The physical basis of crystal growth. Published by Shanghai Science and Technology Press, (1982).

93. Memon et al. 2020
Memon, H., Liu, J., De Focatiis, D. S., Choi, K. S. and Hou, X.
Intrinsic dependence of ice adhesion strength on surface roughness. Surface and Coatings Technology, 385 (2020): 125382.

94. Machielsen and Kerschbaumer 1989
Machielsen, C. H. M. and Kerschbaumer, H. G.
Influence of frost formation and defrosting on the performance of air coolers: standards and dimensionless coefficients for the system designer. International Journal of Refrigeration, 12 (1989): 283-290.

95. Maybank and BARTHAKUR 1967
Maybank, J. and BARTHAKUR, N. N.
Growth and destruction of ice filaments in an electric field. Nature, 216 (1967): 50-52.

96. Ma and Peterson 1995
Ma, H. B. and Peterson, G. P.
Thermodynamic analysis of the influence of electric fields on frost formation. Journal of thermophysics and heat transfer, 9 (1995): 562-564.

97. MacArthur 1984
MacArthur, J.W.
Transient heat pump behaviour: a theoretical investigation. International Journal of Refrigeration, 7 (1984): 123-132.

98. MacArthur and Grald 1987
MacArthur, J. and Grald, E.
Prediction of cyclic heat pump performance with a fully distributed model and a comparison with experimental data. ASHRAE Transactions, 93 (1987).

99. Mei and Levermore 2002
Mei L. and Levermore G.
Simulation and validation of a VAV system with an ANN fan model and a non-linear VAV box model. Building and Environment, 37 (2002): 277-284.

100. MIIT China 2018
Low ambient temperature air source heat pump air heaters: JB/T 13573-2018. Beijing: Standard Press of China. [In Chinese]

101. Na and Webb 2003
Na, B. and Webb, R. L.
A fundamental understanding of factors affecting frost nucleation. International Journal of Heat and Mass Transfer, 46.20 (2003): 3797-3808.

102. Nasr et al. 2014
Nasr, M. R., Fauchoux, M., Besant, R. W. and Simonson, C. J.
A review of frosting in air-to-air energy exchangers. Renewable and Sustainable Energy Reviews, 30 (2014):538-554.

103. Niederer 1976
Niederer, D. H.
Frosting and defrosting effects on coil heat transfer. ASHRAE Transactions, 82 (1976): 467-473.

104. Ndiaye and Bernier 2010
Ndiaye, D. and Bernier, M.
Dynamic model of a hermetic reciprocating compressor in on–off cycling operation (Abbreviation: Compressor dynamic model). Applied Thermal Engineering, 30 (2010): 792-799.

105. Nascimento et al. 2015
Nascimento Jr, V. S., Loyola, F. R. and Hermes, C. J.
A study of frost build-up on parallel plate channels. Experimental Thermal and Fluid Science, 60 (2015): 328-336.

106. Na and Webb 2004
Na, B. and Webb, R. L.
New model for frost growth rate. International Journal of Heat and Mass Transfer, 47 (2004): 925-936.

107. Ozbay et al. 2015
Ozbay, S., Yuceel, C. and Erbil, H. Y.
Improved icephobic properties on surfaces with a hydrophilic lubricating liquid. ACS applied materials & interfaces, 7 (2015): 22067-22077.

108. O'neal and Tree 1985
O'neal, D. L. and Tree, D. R.

A review of frost formation in simple geometries. ASHRAE Transactions, 91 (1985): 267-281

109. Oskarsson 1990
Oskarsson, S. P.
Evaporator models for operation with dry, wet, and frosted finned surfaces. ASHRAE Trans, 96 (1990): 373-380.

110. Oskarsson et al. 1990
Oskarsson, S. P., Krakow, K. I. and Lin, S.
Evaporator Models for Operation with Dry, Wet, and Frosted Finned Surfaces, Part II: Evaporator Models and Verification. ASHRAE Transactions, 96 (1990): 381-392.

111. Park et al. 2016
Park, J. S., Kim, D. R. and Lee, K. S.
Frosting behaviors and thermal performance of louvered fins with unequal louver pitch. International Journal of Heat and Mass Transfer, 95 (2016): 499-505.

112. Pacheco-Vega et al. 2001
Pacheco-Vega A., Sen M., Yang K. and McClain R.L.
Neural network analysis of fin-tube refrigerating heat exchanger with limited experimental data. International Journal of Heat and Mass Transfer, 44 (2001): 763-770.

113. Park et al. 2007
Park, C., Cho, H., Lee, Y. and Kim, Y.
Mass flow characteristics and empirical modeling of R22 and R410A flowing through electronic expansion valves. International Journal of Refrigeration, 30 (2007): 1401-1407.

114. Pan et al. 2012
Pan, Y., Xu, X., Xia, L. and Deng, S.

A modeling study on the effects of refrigerant pipeline length on the operational performance of a dual-evaporator air conditioning system. Applied Thermal Engineering, 39 (2012): 15-25.

115. Qin et al. 2014
Qin, H., Li, W., Dong, B., Zhao, Z. and Zhu, W.
Experimental study of the characteristic of frosting on low-temperature air cooler. Experimental thermal and fluid science, 55 (2014): 106-114.

116. Qiao et al. 2017
Qiao, H., Aute, V. and Radermacher, R.
Dynamic modeling and characteristic analysis of a two-stage vapor injection heat pump system under frosting conditions. International Journal of Refrigeration, 84 (2017): 181-197.

117. Qi and Deng 2009
Qi, Q. and Deng, S.
Multivariable control of indoor air temperature and humidity in a direct expansion (DX) air conditioning (A/C) system. Building and Environment, 44 (2009): 1659-1667.

118. Qu et al. 2010
Qu, M., Xia, L., Deng, S. and Jiang, Y.
Improved indoor thermal comfort during defrost with a novel reverse-cycle defrosting method for air source heat pumps. Building and Environment, 45.11 (2010): 2354-2361.

119. Rahman and Jacobi 2012
Rahman, M. A. and Jacobi, A. M.
Drainage of frost melt water from vertical brass surfaces with parallel microgrooves. International Journal of Heat and Mass Transfer, 55 (2012): 1596-1605.

120. Rahman and Jacobi 2013
Rahman, M. A. and Jacobi, A. M.
Condensation, frost formation, and frost melt-water retention characteristics on microgrooved brass surfaces under natural convection. Heat transfer engineering, 34 (2013): 1147-1155.

121. Rahman and Jacobi 2014
Rahman, M. A. and Jacobi, A. M.
Study of frost properties and frost melt water drainage on microgrooved brass surfaces in multiple frost/defrost/refrost cycles. Applied thermal engineering, 64 (2014): 453-461.

122. Rasmussen and Alleyne 2004
Rasmussen B.P. and Alleyne A.G.
Control-oriented modeling of transcritical vapor compression systems. Journal of dynamic systems, measurement, and control, 126 (2004): 54-64.

123. Sanders 1974
Sanders, C.T.
Frost formation: the influence of frost formation and defrosting on the performance of air coolers. PhD. Thesis, Technische Hogeschool, Delft, The Netherlands (1974).

124. Sun et al. 1995
Sun Y., Wu G., Liu H., etc.
Research on the suppression of frost formation on the humid air side of heat exchangers. The Academic Conference on Heat and Mass Transfer of the Chinese Society of Engineering Thermophysics, (1995).

125. Song and Dang 2018
Song M. J. and Dang C. B.
Review on the measurement and calculation of frost characteristics. International Journal of Heat and Mass Transfer, 124 (2018): 586-614.

126. Sahin 2000
Sahin A. Z.
Effective thermal conductivity of frost during the crystal growth period. International Journal of Heat and Mass Transfer, 43 (2000): 539-553.

127. Senshu 1990
Senshu, T.
Heat pump performance under frosting conditions: partI-heat and mass transfer on cross-finned tube heat exchangers under frosting conditions. ASHRAE Transactions, 96(1), 324-329.

128. Shen et al. 2021
Pu, J., Shen, C., Zhang, C. and Liu, X.
A semi-experimental method for evaluating frosting performance of air source heat pumps. Renewable Energy, 173 (2021): 913-925.

129. Seker et al. 2004a
Seker, D., Karatas, H. and Egrican, N.
Frost formation on fin-and-tube heat exchangers. Part I—Modeling of frost formation on fin-and-tube heat exchangers. International Journal of Refrigeration. 27 (2004): 367-374.

130. Stoecker 1957
Stoecker, W.F.
How frost formation on coils affects refrigeration systems. Refrigeration Engineering, V ol. 65, Part 2, pp. 42-46 (1957)

131. Seker et al. 2004b
Seker, D., Kartas, H. and Egrican, N.
Frost formation on fin-and-tube heat exchangers, Part II: Experimental investigation of frost formation on fin-tube heat exchangers. International Journal of Refrigeration, V ol. 27, No. 4, pp. 375-377 (2004)

132. Song 2010
Song, M.
Experimental research on air source heat pump supercooled energy storage defrosting system. Harbin Institute of Technology, MA thesis. (2010).

133. Song et al. 2018
Song, M., Deng, S., Dang, C., Mao, N. and Wang, Z.
Review on improvement for air source heat pump units during frosting and defrosting. Applied energy, 211 (2018): 1150-1170.

134. Song 2014
Song, M.
An experimental and numerical study on improving defrosting performances for an air source heat pump unit having a multi-circuit outdoor coil. PhD. Thesis, The Hong Kong Polytechnic University, (2014).

135. Sommers et al. 2016
Sommers, A. D., Truster, N. L., Napora, A. C., Riechman, A. C. and Caraballo, E. J.
Densification of frost on hydrophilic and hydrophobic substrates–Examining the effect of surface wettability. Experimental Thermal and Fluid Science, 75 (2016): 25-34.

136. Sheng et al. 2017
Sheng, W., Liu, P., Dang, C. and Liu, G.
Review of restraint frost method on cold surface. Renewable and Sustainable Energy Reviews, 79 (2017): 806-813.

137. Sonobe et al. 2015
Sonobe, N., Fukiba, K., Sato, S. and Yoshimura, Y.
Method for defrosting heat exchangers using an air-particle jet. International journal of refrigeration, 60 (2015): 261-269.

138. Sami 1993
Sami, S.
Dynamic performance of heat pumps using refrigerant R-134a. ASHRAE Transactions, 99 (1993): 41-47.

139. Sami and Zhou 1995
Sami, S. and Zhou, Y.
Numerical prediction of heat pump dynamic behaviour using ternary non-azeotropic refrigerant mixtures. International Journal of Energy Research, 19 (1995): 19-35.

140. Singh et al. 2006
Singh J., Singh N. and Sharma J.
Fuzzy modeling and control of HVAC systems–A review. (2006).

141. Turaga et al. 1988
Turaga, M., Lin, S. and Fazio, P. P.
Correlations for heat transfer and pressure drop factors for direct expansion air cooling and dehumidifying coils. ASHRAE Transactions, 94 (1988): 616-630.

142. Tao 1993
Tao Y. X.
Characteristics of frost growth on a flat plate during the early growth period. ASHRAE Transactions, (1993).

143. Tan et al. 2014
Tan, H., Tao, T., Xu, G., Zhang, S., Wang, D. and Luo, X.
Experimental study on defrosting mechanism of intermittent ultrasonic resonance for a finned-tube evaporator. Experimental thermal and fluid science, 52 (2014): 308-317.

144. Tan et al. 2015
Tan, H., Xu, G., Tao, T., Sun, X. and Yao, W.

Experimental investigation on the defrosting performance of a finned-tube evaporator using intermittent ultrasonic vibration. Applied Energy, 158 (2015): 220-232.

145. Vocale et al. 2014
Vocale, P., Morini, G. L. and Spiga, M.
Influence of outdoor air conditions on the air source heat pumps performance. Energy Procedia, 45 (2014): 653-662.

146. Votsis et al. 1989
Votsis, P.P ., Tassou, S.A., Wilson, D.R. and Marquand, C.J.
Investigation of the performance of a heat pump under frosting and defrosting conditions. Heat Recovery System and CHP, 9 (1989): 399-406

147. Van Dyke et al. 2015
Van Dyke, A. S., Collard, D., Derby, M. M. and Betz, A. R.
Droplet coalescence and freezing on hydrophilic, hydrophobic, and biphilic surfaces. Applied Physics Letters, 107 (2015): 141602.

148. Vargas and Parise 1995
Vargas, J. and Parise, J.
Simulation in transient regime of a heat pump with closed-loop and on-off control. International Journal of Refrigeration, 18 (1995): 235-243.

149. Wang et al. 2018a
Wang, F., Liang, C. and Zhang, X.
Experimental study on frost suppression for ASHP combining superhydrophobic heat exchanger and air flow. Applied Thermal Engineering, 136 (2018): 666-673.

150. Wang et al. 2010
Wang, W., Zhang F., Zhao, Y., Xiao, J. and Guo, Q.

Experimental study on the effect of cold surface temperature on frost layer characteristics during dynamic frosting process. Journal of Engineering Thermophysics, 4 (2010), 663-666. [in Chinese]

151. Wang et al. 2006
Wang, Y., Jiang, H. and Ma, Z.
Experiment and analysis of delaying frost of air-source heat pump water chiller-heater units by increasing the evaporator area. Heating Ventilating & Air Conditioning. 36 (2006): 83-87. [In Chinese]

152. Wang et al. 2011
Wang, W., Xiao, J., Guo, Q. C., Lu, W. P. and Feng, Y. C.
Field test investigation of the characteristics for the air source heat pump under two typical mal-defrost phenomena. Applied Energy, 88 (2011): 4470-4480.

153. Wang et al. 2013
Wang, W., Feng, Y. C., Zhu, J. H., Li, L. T., Guo, Q. C. and Lu, W. P.
Performances of air source heat pump system for a kind of mal-defrost phenomenon appearing in moderate climate conditions. Applied Energy, 112 (2013): 1138-1145.

154. Wang and Liu 2005
Wang, S. and Liu, Z.
A new method for preventing HP from frosting. Renewable Energy. 30.5 (2005): 753-761.

155. Wang et al. 2018b
Wang F, Liang C and Zhang X.
Research of anti-frosting technology in refrigeration and air conditioning fields: A review. Renewable and Sustainable Energy Reviews, 81 (2018): 707-722

156. Wang et al. 2015
Wang, Z. J., Kwon, D. J., DeVries, K. L. and Park, J. M.

Frost formation and anti-icing performance of a hydrophobic coating on aluminum. Experimental Thermal and Fluid Science, 60 (2015): 132-137.

157. Wu and Webb 2001
Wu, X. M. and Webb, R. L.
Investigation of the possibility of frost release from a cold surface. Experimental Thermal and Fluid Science, 24 (2001): 151-156.

158. Watters et al. 2002
Watters, R. J., O'Neal, D. L. and Yang, J.
Frost/defrost performance of a three-row fin staged heat pump evaporator. ASHRAE Transactions, 108 (2002): 318.

159. Wang et al. 2004
Wang, C. C., Huang, R. T., Sheu, W. J. and Chang, Y. J.
Some observations of the frost formation in free convection: with and without the presence of electric field. International Journal of Heat and Mass Transfer, 47 (2004): 3491-3505.

160. Wang et al. 2012
Wang, D., Tao, T., Xu, G., Luo, A. and Kang, S.
Experimental study on frosting suppression for a finned-tube evaporator using ultrasonic vibration. Experimental thermal and fluid science, 36 (2012):1-11.

161. Wei et al. 2020
Wei, W., Ni, L., Li, S., Wang, W., Yao, Y., Xu, L. and Yang, Y.
A new frosting map of variable-frequency air source heat pump in severe cold region considering the variation of heating load. Renewable Energy, 161 (2020):184-199.

162. Wang and Touber 1991
Wang, H., and Touber, S.
Distributed and non-steady-state modelling of an air cooler. International Journal of Refrigeration, 14 (1991): 98-111.

163. Xu et al. 2020
Xu, X., Fang, Z. and Wang, Z.
Climatic division based on frosting characteristics of air source heat pumps. Energy and Buildings, 224 (2020): 110219.

164. Xu 2004
Xu W. F.
Experimental studies on mechanism of frost formation on cold surfaces and its control. Tsinghua University, (2004).

165. Xu et al. 2010
Xu, X., Xia, L., Chan, M. and Deng, S.
Inherent correlation between the total output cooling capacity and equipment sensible heat ratio of a direct expansion air conditioning system under variable-speed operation (XXG SMD SHR DX AC unit). Applied Thermal Engineering, 30 (2010): 1601-1607.

166. Xia et al. 2019
Xia, Y., Ding, Q., Jiangzhou, S., Zhang, X. and Deng, S.
A simulation study on the operational stability of an EEV-controlled direct expansion air conditioning system under variable speed operation. International Journal of Refrigeration, 103 (2019): 115-125.

167. Xue et al. 2008
Xue, Z., Lin, S. and Ou, H.
Refrigerant flow characteristics of electronic expansion valve based on thermodynamic analysis and experiment. Applied Thermal Engineering, 28 (2008): 238-243.

168. Yan et al. 2003a
Yan, W. M., Li, H. Y., Wu, Y. J., Lin, J. Y. and Chang, W. R.
Performance of finned tube heat exchangers operating under frosting conditions. International Journal of Heat and Mass Transfer, 46 (2003): 871-877.

169. Yang et al. 2022
Yang, X., Liu, X., Dong, X., Meng, Y., Hou, Y. and Lai, T.
Numerical simulation on the frosting and heat transfer characteristics of plate-fin heat exchanger considering confinement effect. Energy Storage and Saving. (2022).

170. Yao et al. 2004
Yao, Y ., Jiang, Y .Q., Deng, S.M. and Ma, Z.L.
A study on the performance on the airside heat exchanger under frosting in air-source heat pump water heater/chiller unit. International Journal of Heat and Mass Transfer, 47 (2004): 3745-3756.

171. Yang et al. 2006
Yang, D. K., Lee, K. S. and Song, S.
Fin spacing optimization of a fin-tube heat exchanger under frosting conditions. International Journal of Heat and Mass Transfer, 49 (2006): 2619-2625.

172. Yan et al. 2003b
Yan, Q., Zhu, L., Yan, N., Zhang, M. E. and Hui, X.
Study on ultrasonic defrost technology of refrigeration fan. J Agric mach, 34 (2003): 74-5.

173. Yan et al. 2018
Yan, H., Xia, Y., Xu, X. and Deng, S.
Inherent operational characteristics aided fuzzy logic controller for a variable speed direct expansion air conditioning system for simultaneous indoor air temperature and humidity control. Energy and Buildings, 158 (2018): 558-568.

174. Yang et al. 2021
Yang, L., Deng, S., Fang, G. and Li, W.
Improved indoor air temperature and humidity control using a novel direct-expansion-based air conditioning system. Journal of Building Engineering, 43 (2021):102920.

175. Ye et al. 2007
Ye, Q., Chen, J. and Chen, Z.
Experimental investigation of R407C and R410A flow through electronic expansion valve. Energy Conversion & Management, 48 (2007): 1624-1630.

176. Yang et al. 2020
Yang, L., Weng, W. and Deng, S.
A modeling study on a direct expansion based air conditioner having a two-sectioned cooling coil. Applied Energy, 278 (2020): 115688.

177. Zhang et al. 2017
Zhang, Q., Zhang, L., Nie, J. and Li, Y.
Techno-economic analysis of air source heat pump applied for space heating in northern China. Applied Energy, 207 (2017): 533-542.

178. Zhu et al. 2015
Zhu J., Sun Y., Wang W., Ge Y., Li L. and Liu J.
A novel Temperature–Humidity–Time defrosting control method based on a frosting map for air-source heat pumps. International Journal of Refrigeration, 54 (2015): 45-54.

179. Zhang et al. 2018a
Zhang, L., Jiang, Y., Dong, J. and Yao, Y.
Advances in vapor compression air source heat pump system in cold regions: A review. Renewable and Sustainable Energy Reviews, 81 (2018): 353-365

180. Zhang et al. 2018b
Zhang, L., Guo, X. and Xue, J.
Experimental study on the growth characteristics of frost layer on the surface of finned tube heat exchanger. CIESC Journal, 69.S2 (2018): 186-192.

181. Zhao et al. 2022
Zhao, B., Bi, H., Wang, H. and Zhou, Y.

Experimental and numerical investigation on frosting of finned-tube heat exchanger considering droplet impingement. Applied Thermal Engineering, 216 (2022); 119134.

182. Zhang et al. 2019
Zhang, L., Jiang, Y., Dong, J., Yao, Y. and Deng, S.
A comparative study of frosting behavior on finned tube heat exchanger under different fan control modes. Applied Thermal Engineering, 160 (2019): 114063.

183. Zou et al. 2011
Zou, M., Beckford, S., Wei, R., Ellis, C., Hatton, G. and Miller, M. A.
Effects of surface roughness and energy on ice adhesion strength. Applied surface science, 257 (2011): 3786-3792.

184. Zhang et al. 2012a
Zhang, L., Fujinawa, T., Saikawa, M.
A new method for preventing air-source heat pump water heaters from frosting. International Journal of Refrigeration, 35 (2012): 1327-1334.

185. Zhang et al. 2010
Zhang, L., Dang, C. and Hihara, E.
Performance analysis of a no-frost hybrid air conditioning system with integrated liquid desiccant dehumidification. International journal of refrigeration, 33 (2010): 116-124.

186. Zhang et al. 2012b
Zhang, L., Hihara, E. and Saikawa, M.
Combination of air-source heat pumps with liquid desiccant dehumidification of air. Energy conversion and management, 57 (2012): 107-116.

187. Zhao et al. 2015
Zhao, H., Wang, L., Lai, Y., Han, J. and Li, W.

Effects of weak magnetic fields on frosting process on surface of copper tube. In Proceedings of the 24th IIR International congress of Refrigeration, Yokohama, Japan, (2015): 17-22.

188. Zhang 2021

Zhang, L.

A study on the characteristics of frost distribution and growth on finned tube heat exchangers. PhD. Thesis, The Hong Kong Polytechnic University, (2021).

189. Zhang et al. 2022

Zhang, L., Song, M., Hosseini, S. H., Shen, J. and Jiang, Y.

A modeling study of spatial and temporal frost growth on the edge of windward fins for a tube-finned heat exchanger. International Journal of Heat and Mass Transfer, 183 (2022): 122093.